THE INSTANTANEOUS LOCAL HEAT FLUX IN A SCRAPED-SURFACE HEAT EXCHANGER

THE INSTANTANEOUS LOCAL HEAT FLUX IN A SCRAPED-SURFACE HEAT EXCHANGER

By

JOHN YAMANIS, DIPL.CHEM.ENG.

A Thesis

Submitted to the School of Graduate Studies

in Partial Fulfilment of the Requirements

for the Degree

Master of Engineering

McMaster University

(October) 1970

MASTER OF ENGINEERING (1970) McMASTER UNIVERSITY
(Chemical) Hamilton, Ontario.

TITLE: The Instantaneous Local Heat Flux in a Scraped-Surface Heat Exchanger

AUTHOR: John Yamanis, Dipl.Chem.Eng. (National Technical University of Athens, Athens)

SUPERVISOR: Dr. T.W. Hoffman

NUMBER OF PAGES: x, 142

SCOPE AND CONTENTS:

The objective of this investigation was to examine the potential of the point heat-flux meter in studying the dynamic heat transfer process in a scraped-surface heat exchanger.

The heat-flux meters were an integral part of the copper heat exchanger which was steam-heated. Water was passed through the equipment as a thin film. The steam condensate was collected for measurement.

Mathematical analysis related the transient differential temperature of the detector with the transient applied heat flux. A mathematical model was found that would estimate the instantaneous heat flux from the heat-flux-meter experimental temperature difference.

Instantaneous and time-average local heat fluxes were measured by the heat-flux meter and the condensate respectively. The meter accuracy was -7000 Btu/hr sq ft.

The heat-flux meter can be used in studying dynamic heat transfer processes.

ACKNOWLEDGEMENTS

The author wishes to express his gratitude to Dr. T.W. Hoffman for suggesting the problem and for his guidance.

Sincere thanks are extended to Messrs. J. Newton and R. Dunn for their excellent craftsmanship and patience during the trials and tribulations of this work.

Miss E. Jones is gratefully acknowledged for her typing.

Feelings of deep appreciation are cherished for the patience and understanding that my wife has shown throughout this investigation.

TABLE OF CONTENTS

LIST OF FIGURES

LIST OF PLATES

1. INTRODUCTION

Fluid processing equipment in which the fluid is acted upon by an agitator that sweeps the entire volume of the vessel is called either a "Close Clearance" equipment or a "Mechanically-aided Thermal Processor". This is a collective term that embraces equipment used for heat transfer, mass transfer or chemical reaction. Equipment used in heat exchange is commonly called "Scraped-surface Heat Exchanger" while that in mass transfer is called a "Thin-film Evaporator". The liquid can either fill the entire vessel or flow as a thin film along the vessel surface. The flow is induced by gravity and centrifugal force as in liquid-full tapered units. The agitator edge may come very close to or actually scrape the wall.

Mechanically-aided thermal processors find extensive use in the chemical industry, for example in concentration, distillation, fractionation, stripping, crystallization and sterilization. Their main characteristics are:

(a) Short residence-time

(b) High heat and mass transfer rates

(c) Low liquid hold-up

(d) Effectiveness in processing highly viscous fluids.

Heat transfer in this kind of equipment is known to be an unsteady state phenomenon, and this is the reason for which such a system was chosen for investigating the potential of a point heat-flux meter as an instantaneous detector of heat flux.

The two types of scraped-surface heat exchangers, i.e., liquid-full and thin film are shown in Fig. 1-1.

In this thesis thin-film systems, without mass transfer or chemical reaction, are considered unless otherwise stated.

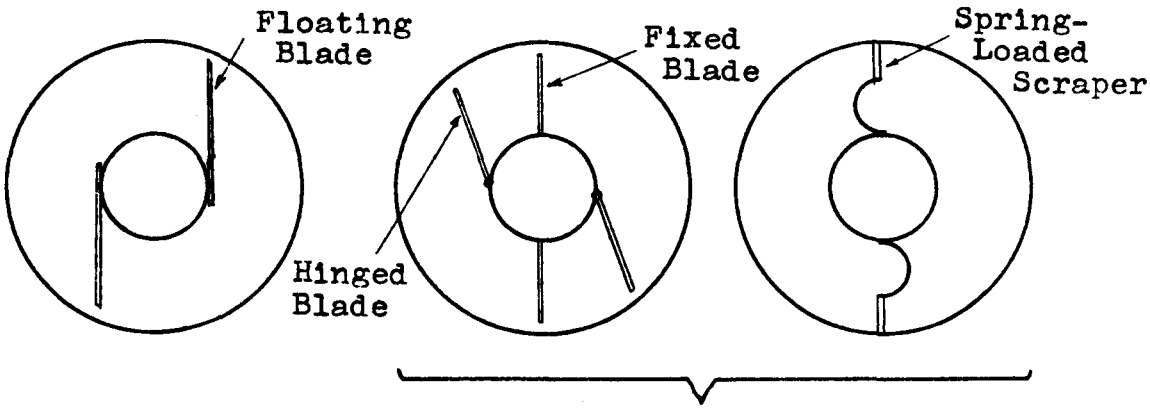

Fig. 1-1

Mechanically-Aided Thermal Processors

2. LITERATURE REVIEW

2.1 SCRAPED-SURFACE HEAT EXCHANGERS

Early research in mechanically-aided thermal processors was primarily aimed at obtaining operating data. It is in the last decade or so that research studies have taken a more fundamental approach. These studies have sought to elucidate the heat transfer and fluid mechanical phenomena occuring in this type of equipment. The phenomena are closely related to the flow conditions, backmixing and wetting of the thermal surface.

2.1.1 Heat Transfer Models

Kern and Karakas (K1) have attempted to analyse the case where process liquid flows down the exchanger isothermally. They noted that the liquid in its travel through the exchanger can follow four paths but, under the conditions usually encountered in practice, it flows as a thin film on the wall and exists as a "liquid fillet" on the downstream tip of the rotating blade. In their heat transfer model, they postulated that heat is transferred through the film by molecular conduction in the steady state. The inside heat transfer coefficient is then given by

$$\bar{h} = \frac{k}{\delta} \qquad (2\text{-}1)$$

where δ is the thickness of the wall film. They noted that this relationship will give conservative values if convection takes place. They pointed out that convection should not be too important in the thin film.

Kern et al. have neither verified their model experimentally nor given any experimental values of the inside coefficient for comparison with those predicted by their model. The significance of δ in equation (2-1) is not clear. No doubt, the coefficient is not infinite as δ approaches zero and does not tend to zero as the thickness increases. Obviously, equation (2-1) presents extrapolation problems. But even for thicknesses of 0.03 to 0.10 in., which are usual in thin film equipment, the predicted coefficients are much lower than those reported in the literature (M1, B1, G1). Moreover, heat transfer to isothermal thin films is likely to be affected by such a phenomenon as nucleate boiling (B2), in which case, the heat transfer coefficient would be greatly increased. Kern et al. have postulated no dependence of the inside coefficient on the rotational speed of the blades. This is in agreement with the pilot-plant data of Borg, Provost and Bawn (B1).

Jepson (J1) in an attempt to analyse the heat transfer process in extruders, which in some respects are similar to scraped-surface heat exchangers, suggested that heat is transferred to the polymer by molecular conduction in the unsteady state.

Kool (K2) has analysed the case where a liquid is being heated or cooled in a liquid-full exchanger. The liquid is considered to be so viscous that laminar flow regime exists. Kool visualized the action of the blade as follows: When the blade passes by a point, A, it wipes "hot" ("cold") liquid from the wall. This liquid is then transferred to the core of the liquid where it is assumed to be mixed by the turbulent mixing processes. At the same time, fresh "cold" ("hot") material at the local bulk temperature of the liquid replaces this liquid at point A. The latter is heated (cooled) by molecular conduction in the unsteady state until the following blade comes along to repeat the process. Kool suggested that it is this action of the blade which causes the increased heat transfer rates. It can be seen that this model is very similar to the penetration surface renewal models that have been suggested by Higbie (H1) and Dankwerts (D1). Moreover, since the time between successive scrapings is small, the thickness of liquid penetrated by the increased temperature is small. The process then, can be paralleled to unsteady state heat conduction to a semi-infinite solid with contact time the time between two consecutive blade passes. The analysis resulted in the following relationship for the inside heat transfer coefficient

$$\bar{h} = 1.24\ \bar{h}' S^{-1.03} \qquad (2\text{-}2)$$

where $\bar{h}$ = heat transfer coefficient from scraping plane

$\bar{h}'$ = heat transfer coefficient from jacket to scraping plane

$$S = \bar{h}' \left(\frac{\overset{*}{\theta}_c}{k C_p \rho} \right)^{\frac{1}{2}}$$

$\overset{*}{\theta}_c$ = contact time

Kool considered that there may be a thin film remaining on the wall the resistance of which should be taken into account. However, he did not suggest a way to predict this film thickness. Coefficients predicted by equation (2-2) should be the minimum expected, since any turbulence will increase heat transfer. In the case of small diameter vessels some of the "hot" ("cold") material scraped from the wall may immediately be returned to it, and as a result lower coefficients may be obtained.

Harriott (H2) made a similar analysis as Kool, but he considered that the scraping plane is the inside surface of the shell. He suggested that the local heat transfer coefficient be calculated from the relationship

$$h(T_W - T_B) = - k \left(\frac{dT}{dx} \right)_{x = 0} \qquad (2\text{-}3)$$

where the derivative is to be obtained from the solution of

$$\frac{\partial T}{\partial \theta} = \alpha \frac{\partial^2 T}{\partial x^2} \qquad (2\text{-}4)$$

as applied to the process liquid. The time-average local heat transfer coefficient is obtained by integrating

equation (2-3) over the contact time $\overset{*}{\theta}_c = \frac{1}{60nN}$ (same as that used by Kool). The result is

$$\bar{h} = 8.74\ (KC_p \rho nN)^{\frac{1}{2}} \qquad (2\text{-}5)$$

This model differs from Kool's in that the coefficient does not depend on the coefficient from the jacket to scraping plane and has a smaller dependence on the physical properties of the liquid, the rotational speed and the number of blades.

To test this model Harriott carried out experimental work in a Votator. It was found that the model agreed well with experimental data for water but predicted higher coefficients for viscous fluids. This discrepancy could be attributed to incomplete mixing of the fluid wiped from the wall with the bulk liquid, a situation that would be aggravated as the viscosity of the liquid was increased. Moreover, the effects of viscous dissipation have not been considered by any of these authors.

It is worth pointing out that the penetration theory models predict the instantaneous local heat transfer coefficient as infinite at the beginning of the cycle. Its value falls off rapidly for times greater than zero to $0.5\bar{h}$ at the end of the cycle. This is shown in Fig. 2-1. Undoubtedly this is a highly idealized picture. It takes no account of turbulence, incomplete mixing, viscous dissipation or thermal inertia of the heat transfer boundary. Nor does it consider channeling, a likely situation in thin-film equipment

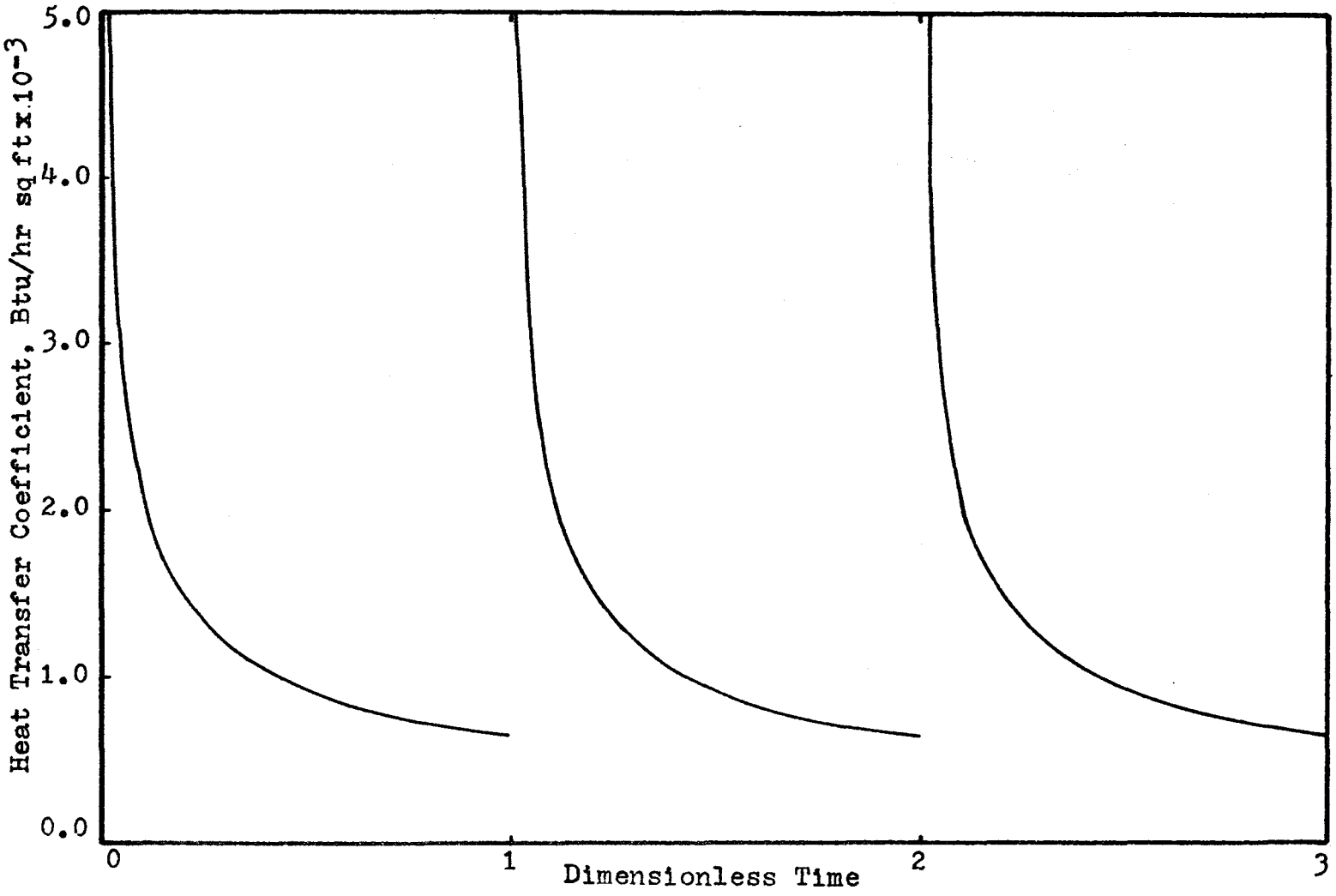

Fig. 2-1. Penetration-Theory Instantaneous Coefficient

operated at low rotational speeds. However, it does show that the local heat transfer coefficient is a function of time as one would expect.

In conventional mixing vessels the rotary Reynolds number ($Re_r = \frac{D_s^2 N \rho}{\mu}$) is used to characterize the flow regime in the vessel. The transition region between laminar and fully turbulent flow is defined by values of Re_r between 10 and 10,000 according to Green (G2), whereas according to Uhl (U1) it is between 100 and 1000. The former definition is to be used here.

Coefficients predicted by the penetration theory models are as high as 50% greater than the reported experimental values in the lower transition regime. In the turbulent regime, the predicted coefficients are 15% lower than experimental ones. In addition, the predicted values for the coefficients and the experimental ones converge as the rotary Reynolds number is increased. In the light of this experimental information, Kool's model comes closer to predicting heat transfer coefficients in the turbulent regime although it assumes a laminarly flowing liquid at least in the region of the wall. It should be pointed out that the penetration theory assumes a turbulent core of fluid whose interface is renewed by turbulent eddies from the core.

The complexity of the real problem and the shortcomings of the theoretical analyses necessitated empirical correlations which in turn introduce their own limitations.

Latinen (L1) has put the penetration model in the following dimensionless form:

$$Nu_x = C(Re_r Pr)_x^{\frac{1}{2}} \qquad (2\text{-}6)$$

where subscript x denotes time-average local values.

Skelland (S1) has come up with a correlation for the inside heat transfer coefficient in a liquid-full exchanger which shows the following dependence:

$$\bar{h} \propto \left(\frac{v^{0.40}}{L^{0.37}}\right)\left(k^{0.53} C_p^{0.47} \rho^{0.57}\right) N^{0.17} \qquad (2\text{-}7)$$

As Latinen has pointed out this relationship has the same functional dependence on K, C_p and ρ but N seems to have a very small effect on $\bar{h}$. Latinen suggested that this low dependence on N may be due to the conditions existing in the transition regime where Skelland's data were obtained. He also used Houlton's (H3) data to establish the coefficients and found $\bar{h}$ to be in effect dependent on

$$\bar{h} \propto \left(\frac{D_t}{L}\right)^{.4} (k C_p \rho N)^{\frac{1}{2}} \qquad (2\text{-}8)$$

Houlton's data were taken in the turbulent regime. Functionally, equation (2-8) is in very good agreement with the penetration model. Latinen suggested that the considerable effect of D_t and L in equations (2-7) and (2-8) may be attributed to entrance effects. He also noted that at high Reynolds numbers the heat transfer layer would be penetrated by eddies and therefore coefficients should be higher than

those predicted by the penetration theory.

Skelland et al. (S2) after a lengthy investigation in Votators reported another correlation which for viscous fluids shows in effect the following dependence for $\bar{h}$:

$$\bar{h} \propto \left(v^{.38} D_s^{.55}\right)\left(\frac{D_t - D_s}{D_t}\right)\left(k^{.04} C_p\, \rho\right) N^{.62} n^{.53} \qquad (2\text{-}9)$$

i.e., there is virtually no effect of the conductivity on $\bar{h}$, which is very unlikely. Moreover, the dependence of $\bar{h}$ on v is not substantiated by the work of other researchers. It is rather an effect of backmixing that shows up as flow rate dependence.

Research work aimed at obtaining a correlation for the inside heat transfer coefficient was carried out by Bott and Romero (B3). Their studies resulted in a correlation that shows the following dependence:

$$\bar{h} \propto \left(\tau^{.46}\right)\left(\frac{D_t^{.68}}{L^{.48}}\right)\left(\frac{1}{\mu^{.19}}\right)\left(k^{.13} C_p^{.87} \rho^{.6}\right) N^{.6} n^{.24} \qquad (2\text{-}10)$$

As pointed out by these authors, the experimental conditions were such that the thermal surface was not fully wetted. However, the entire area of the tube was used for the calculation of the coefficient. The dry condition of the wall depends strongly on the flow rate and the rotational speed of the scrapers. It appears likely that the pronounced dependence of $\bar{h}$ on the flow rate is an effect of the incomplete wetting of the wall that shows up through the flow rate dependence.

Azoory and Bott (A1) have carried out work with the objective of relating the time-average, local heat transfer coefficient to the penetration theory. They determined the point heat transfer through use of a plug heat-flux meter. They found that $\bar{h}$ had the same functional dependence on the physical properties of the process liquid, the rotational speed and the number of blades as shown in equation (2-5). However, the local inside coefficients were substantially lower than those predicted by the penetration theory. Their analysis showed that the time-average local heat transfer coefficients could be predicted by the penetration theory if a correction factor, f, was included, viz:

$$h = 8.74\ (kC_p \rho nN)^{\frac{1}{2}}\ \frac{1}{f} \qquad (2\text{-}11)$$

The correction factor is a function of Prandtl Number, namely

$$f = \frac{Pr}{500} + 3.50 \qquad (2\text{-}12)$$

It should be remarked that all the investigations carried out in mechanically-aided thermal processors but one, namely that of Azoory, have obtained the inside coefficient from over-all experimental measurements. This method tacitly assumes that the inside and over-all coefficients are constant over the entire exchanger. These observations also include end, wall conduction and backmixing effects. According to the penetration theory the inside coefficient varies little along the exchanger for moderate temperature changes. But

how well is the theory approaching reality? For example, if the thermal surface is not wiped clean a thin "stagnant" liquid film may remain at the wall. This increases the resistance to heat flow and results in lower actual coefficients. This point must be given due consideration by researchers. It also suggests that fabricating tolerances in scraped-surface equipment may be of great importance.

2.1.2 Fluid Flow

There has been no attempt to elucidate the fluid flow in liquid-full systems. This may well be due to the fact that the annular space of this equipment is full with liquid, thus presenting no obvious need for such a study. Should one view the exchanger as a peculiar mixing vessel, one could consider such a study important.

In thin-film equipment Kern et al. have attempted a theoretical analysis. They arbitrarily divided the flow field in two regions. One is the wall film and the other the fillet at the tip of the blade. By making suitable simplifying assumptions, they were able to use hydrodynamic equations from which they derived theoretical relationships for the liquid hold-up. The value of their hydrodynamic model is open to question, since it has not been tested experimentally.

Kern et al. have discussed the effects of blade clearance. They stress the importance of blade clearance

and suggest that equipment fitted with hydrodynamic blades* relax the requirement of tight tolerances that are necessary in equipment with fixed blades.

Bott et al. (B3) have conducted flow visualization studies in a clear plastic model of the exchanger and observed the fluid fillet at the leading edge of the rotating tip. Their examination indicated that a very large proportion of the liquid passed through the tube in the form of fillets, thus leaving most of the thermal surface dry. They noted that copper** and plastic material have different wetting characteristics, but they did interpret their "cold model" findings as indications that the flow down the actual wall of the exchanger is negligible relative to the flow in the fillets. Additional visual observations were carried out by Bott et al. (B5). Still pictures were taken. It was found that at low flow rates and low rotational speeds the liquid is held as roughly triangular fillets extending along the blade. As the speed is increased the fillet becomes more equilateral. At higher speeds the triangular fillet extends along the exchanger wall and at higher flow rates and high shaft speeds the liquid spreads over the entire surface of the tube.

---

*Blades that "float" in their holder; their equilibrium position is determined by the centrifugal force balancing the hydrodynamic one in the liquid film.

**Their actual exchanger was made of copper.

Bott and Sheikh (B4) have investigated the design of scrapers. They found that certain scrapers produce a larger wetted area thus increasing the effectiveness of the operation. They noted, however, that higher flow rates combined with flat blades could wet the entire area with the result of avoiding the dry condition of the thermal surface.

Mutzenburg (M1) studied the fluid flow in a model exchanger made of glass and fitted with fixed blades. He qualitatively described the flow field as made up of three zones. One is the "bow wave" or fillet at the tip of the blade (See Fig. 2-2); this is followed by a turbulent "squeeze" zone, which turns into a "tranquilizing" zone further upstream from the blade. He used the residence-time distribution technique to obtain more information about the flow. The experimental data show that the flow is similar to dispersed plug flow.* The data also exclude the possibility of channeling in the equipment.

Bott, Azoory and Porter (B6) investigated the liquid hold-up by means of the residence-time distribution technique. They found that for isothermal conditions the hold-up increases with flow rate and rotational speed and decreases with number of blades on the shaft. Their work resulted in the following correlation for the hold-up:

---

*The limited data presented were obtained in a commercial unit.

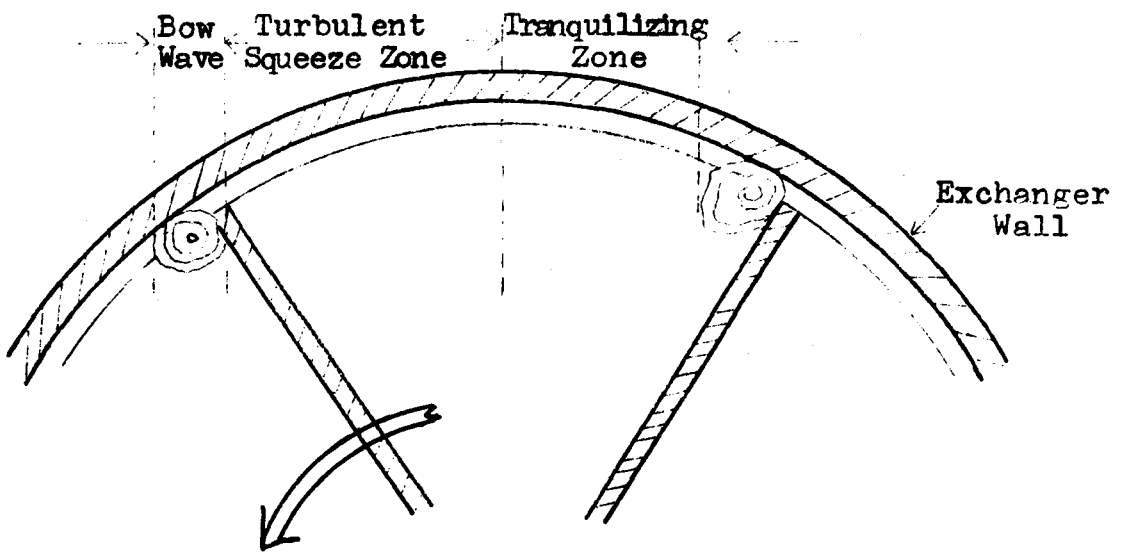

Fig. 2-2

Thin-Film Flow

$$H' = 0.425 \times 10^{-5}(N + \frac{s}{10}) + 0.196\ (w')^{0.86}(\frac{\mu}{\mu_w})^{0.3} \quad (2\text{-}13)$$

where H' = hold-up per unit length per blade (ft^2)

N = shaft speed (sec^{-1})

s = blade spacing ($=\pi D_b/n$) (ft)

w' = volumetric flow per blade ($= w/n$) (ft^3/sec blade)

2.1.3 Backmixing-Axial Dispersion Problems

Blaisdell and Zahradnik (B6) have investigated heat transfer in a Votator with the aim of obtaining axial liquid bulk temperature distributions. When they plotted the logarithm of the reduced temperature versus heat exchanger length, the resulted curves were not straight lines. This indicated that the assumption of plug flow in the derivation of the log-mean temperature difference (LMTD) was violated. They suggested that "a change in mixing effectiveness was a probable cause."

Uhl and Root (U2) in an investigation of the heat transfer to granular solids in agitated units have stressed the importance of the mixing action of the equipment.

Penney and Bell (P1) have noted that axial dispersion of heat resulting from backmixing will certainly affect the mean temperature difference (MTD). They went on to state some qualitative facts about axial dispersion.

> "1) Axial dispersion as a result of backmixing has an increasing effect on MTD as (a) axial flow rate decreases, (b) rotation speed increases,

and (c) equivalent diameter of the flow passage increases.

2) As a decreased flow rate will increase the effect of backmixing, thereby lowering the MTD, data reduced, using the LMTD, often show a false dependence of the heat transfer coefficient on the axial flow rate."

Penney et al. have remarked that the dependence of $\bar{h}$ on v in Skelland's correlations ((2-7) and (2-9)) must be due to the effect of backmixing.

One concludes on the basis of this evidence that backmixing effects are important in heat transfer equipment like the Votator.

Braginskii and Begachev (B8) agreeing with Penney's hypothesis have attempted to quantitavely evaluate the longitudinal mixing effects in Votators. They used the differential model for plug flow with axial dispersion of heat and the penetration model for the scraped heat transfer coefficient and obtained relationships that could successfully describe the heat transfer phenomena. The integrated form of the axial dispersion model is

$$T = A_1 \exp m_1 x + A_2 \exp m_2 x \qquad (2\text{-}14)$$

where m_1 and m_2 are functions of the Bodenstein Number ($Bo = \frac{vL}{\alpha t}$), the overall heat transfer coefficient, the radius and length of exchanger, the shaft radius, the density and heat capacity of the process liquid. The thermal diffusivity α_t, was correlated by the authors, with the geometrical

characteristics of the exchanger, namely, the radii of exchanger, shaft and mutator* and the angular velocity of the scrapers. The integration constants are functions of m_1, and m_2 and inlet, outlet and jacket temperatures. With inlet and jacket temperatures known, the outlet temperature could be obtained from a heat balance over the exchanger

$$\rho wc \left(T_{in} - T_{out}\right) = 2\pi RU \int_o^L (T - T_j)\, dx \qquad (2\text{-}15)$$

which would permit, along with the other known quantities, the evaluation of all the constants in equation (2-14) and consequently, the temperature profile in the exchanger.

The theoretical results of Braginskii et al. checked very well with Blaisdell's experimental data. Their theoretical analysis shows that backmixing can greatly reduce the heat transferred (20 to 40%). They remarked that total heat flux decreases with decreasing Bodenstein Number, that is decreasing axial velocity of the liquid, which is in agreement with observations.

Bott and co-workers (B9) employed the residence-time distribution technique to investigate axial dispersion. They also solved the axial dispersion model as proposed by Churchill and White (C1) (same as that used by Braginskii et al.) and pointed out the effects of axial dispersion on heat

---

*This is comprised of the shaft and the scrapers.

transfer. Their experimental findings showed that backmixing increases with mean axial velocity and rotational speed but decreases with number of blades. They empirically correlated the axial dispersion coefficient and concluded that backmixing effects can safely be ignored in thin film mechanically-aided thermal processors.

The experimental evidence of Bott et al. (B9) that axial dispersion increases with increasing axial velocity is in apparent antithesis to the statement by Penney et al. that the former increases with decreasing flow rate. However, since liquid hold-up, hence flow cross-sectional area, increases with flow rate it may be inferred that the effects of flow cross-section overshadow those of flow rate. In addition, the effects of backmixing are negligible according to Bott et al. (B9) contrary to the importance attributed to axial dispersion by Penney et al. and the findings of Braginskii et al. in liquid-full systems. It may be that the cross-sectional area of the flow is the controlling variable of the backmixing process in thin-film equipment, and since this is small the axial dispersion effects are not important. However, in view of the results of Braginskii et al. the question should be considered unresolved.

2.1.4 Wetting

In their flow visualizations studies Bott and co-workers have used models of their actual heat exchangers

made of plastic. Their observations led them to certain qualitative conclusions about the flow in the models. These conclusions were then assumed applicable to flow in their actual heat exchangers which were made of materials of different wetting characteristics. As a first approximation the method is entirely justified. But is it, really, adequate enough so that the information gathered can be used for the quantitative analysis of data? It is known that very thin liquid films break up by the action of capillary forces, and that the destruction of the film depends on the wetting characteristics of the solid surface. Could it not be possible, then, that flow in an actual heat exchanger, under conditions that leave the surface of the plastic model partially dry, be drastically different from that in the model? It is to be expected that once the entire surface is covered by a stable film the wetting characteristics of the solid will cease to have any effect on the flow. The flow in an actual exchanger, under conditions that allow a stable liquid film on the surface of the model, will form a continuous film over the entire thermal surface. Actually, since the metal wall has, for a number of liquids at least, better wetting characteristics than the plastic a stable liquid film in the actual exchanger would be expected to obtain under more stringent conditions.

Flow in thin liquid films is greatly affected by surface tension and viscosity. Experimental studies of thin-

film flow by gravity on vertical or inclined surfaces have revealed the existence of three regimes (L2):

(a) at Re (Re = $\frac{v\delta}{\nu}$) $<$ 30 the flow is laminar

(b) at Re $>$ 30 to 50 waves appear on the surface (wave regime)

(c) At Re $\approx$ 1500 flow is turbulent.

In laminar steady state flow the film thickness is uniform and capillary forces have no effect. In the wave regime capillary forces appear because of surface deformation and become important when they are of the order of magnitude of the gravity and viscosity forces. The capillary forces play a principal role in establishing the distribution in the wave regime. In the turbulent regime surface tension assures the stability of the surface and changes the velocity distribution near the surface. Capillary forces reduce the scale of turbulence and prevent liquid from splashing.

None of the research studies in thin-film equipment reported in the literature has considered even the existence of surface tension forces. In thin-film heat exchangers the liquid surface is not planar (e.g., fillet) and the film thickness is not uniform. Capillary forces play a role, important or otherwise. Their importance can only be ascertained by comparing their magnitude to those of the other forces in the system. This is an aspect of flow in thin-film equipment that might be worth looking into by future researchers.

2.2 HEAT FLUX METERS

Various devices are reported in the literature for measuring heat fluxes. They can be classified into two broad classes: (a) those that measure point temperatures in the device, and (b) those that directly measure the energy input to the device. In the former, one or two point temperatures are measured from which the heat flux to or from the device is calculated by using the functional relationship between the two. In the latter, the energy into the device is recorded over a period of time from which the heat flux from the meter is obtained.

A device that falls into the first category was first suggested by Gardon (G3). It is a cylindrical recess into a metal block (See Fig. 2-3).

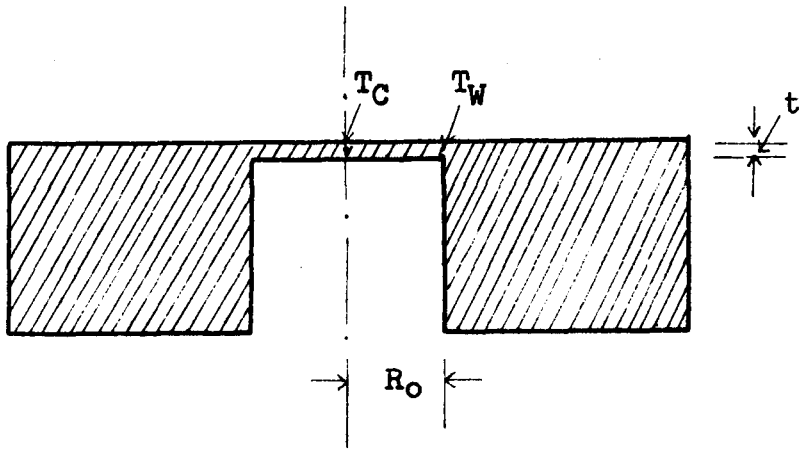

Fig. 2-3
Heat-Flux Meter

The thickness, t, of the disc is of the order of 0.010 in. to 0.030 in. and the radius is 1/8 to 1/4 in. When heat is transferred to or from the meter a hot or cold spot is

developed at the center of it. A two-dimensional, steady-state analysis, assuming constant heat flux density over the disc, shows that the temperature difference between the edge and the center of the meter is given by:

$$\Delta T = T_W - T_C = \frac{(q/A)R_o^2}{4kt} \qquad (2\text{-}16)$$

for heat transfer from the meter.

Dernedde (D2) used a similar meter to study the heat transfer to boiling liquid films. The mathematical analysis of the heat-flux meter was extended to three-dimensional steady and unsteady conduction in the device. In both cases analytical solutions were obtained that show spatial and time effects. In particular, the unsteady state solution was used to obtain the time constant of the device. This was found to be of the order of 7 msec for one of the copper meters used by Dernedde. It should be pointed out that the time constant, for the same material, increases with radius and thickness of disc. Dernedde in studying the boiling heat transfer, which is an unsteady state phenomenon, used the two dimensional steady state solution. To do so, he had to assume that the heat flux meter responded instantaneously, i.e., the time constant was assumed zero. Dernedde concluded that the meter can be used in boiling, but that its accuracy is limited due to the conduction along the thermocouple wire. It was recommended that the heat-flux meter be calibrated over a wide range of conditions and that the conduction error be minimized.

Despite the use of the meter for the study of an unsteady state process no mention was made about its potential as a tool in the study of dynamic processes in heat transfer work.

A heat-flux meter that comes under the second class was used by Azoory (A1). The meter consisted of a small rectangular copper plate at the back of which a 25 W heater element was placed. The face was machined so that it exactly fitted the inside curvature of a plastic tube, which consisted the shell of his scraped-surface heat exchanger. A D.C. input was fed to the heater. The voltage across and the current through the heater was measured, which provided a measure of the energy input to the device. From this and the heat losses to the environment, which were found to be very small and therefore ignored, the heat output was calculated which could be translated into heat flux. Azoory used these meters to obtain the time-average, local, heat-transfer coefficients in a scraped-surface heat exchanger made of plastic (except for the copper plug).

3. EXPERIMENTAL WORK

3.1 EXPERIMENTAL SET-UP

3.1.1 Equipment Lay-Out

The lay-out of experimental equipment is shown in Fig. 3-1. A positive displacement pump (1) (GEARCHEM model 70Y3, capacity 5 g.p.m.) pumped process liquid from either holding tank (2) or measuring tank (3) through a cooler (4) (ROSS type BCF heat exchanger) to the constant head tank (5). Liquid from the constant head tank flowed, under gravity, through a rotameter (6) (FISHER and PORTER, max. capacity 1.19 g.p.m.) into the scraped-surface heat exchanger (7). The fluid discharged from the exchanger into either the holding or measuring tank. The measuring tank was weighed by a scale (8) (AVERY, capacity 250 lb., scale division to 1 oz.). Vapour, if any, from the exchanger passed into a condenser (9). The scrapers in the exchanger were revolved by the motor (10) ($\frac{1}{4}$ HP) which was fitted with a variable speed hydraulic drive (CHEMINEER, INC. model ELB, max. r.p.m. 1100).

3.1.2 Scraped-Surface Heat Exchanger

The exchanger was made of a 19 in. long copper (99.99% Cu.) tube of which the inside diameter and wall thickness were 3.1 in. and 7/32 in. respectively. Another

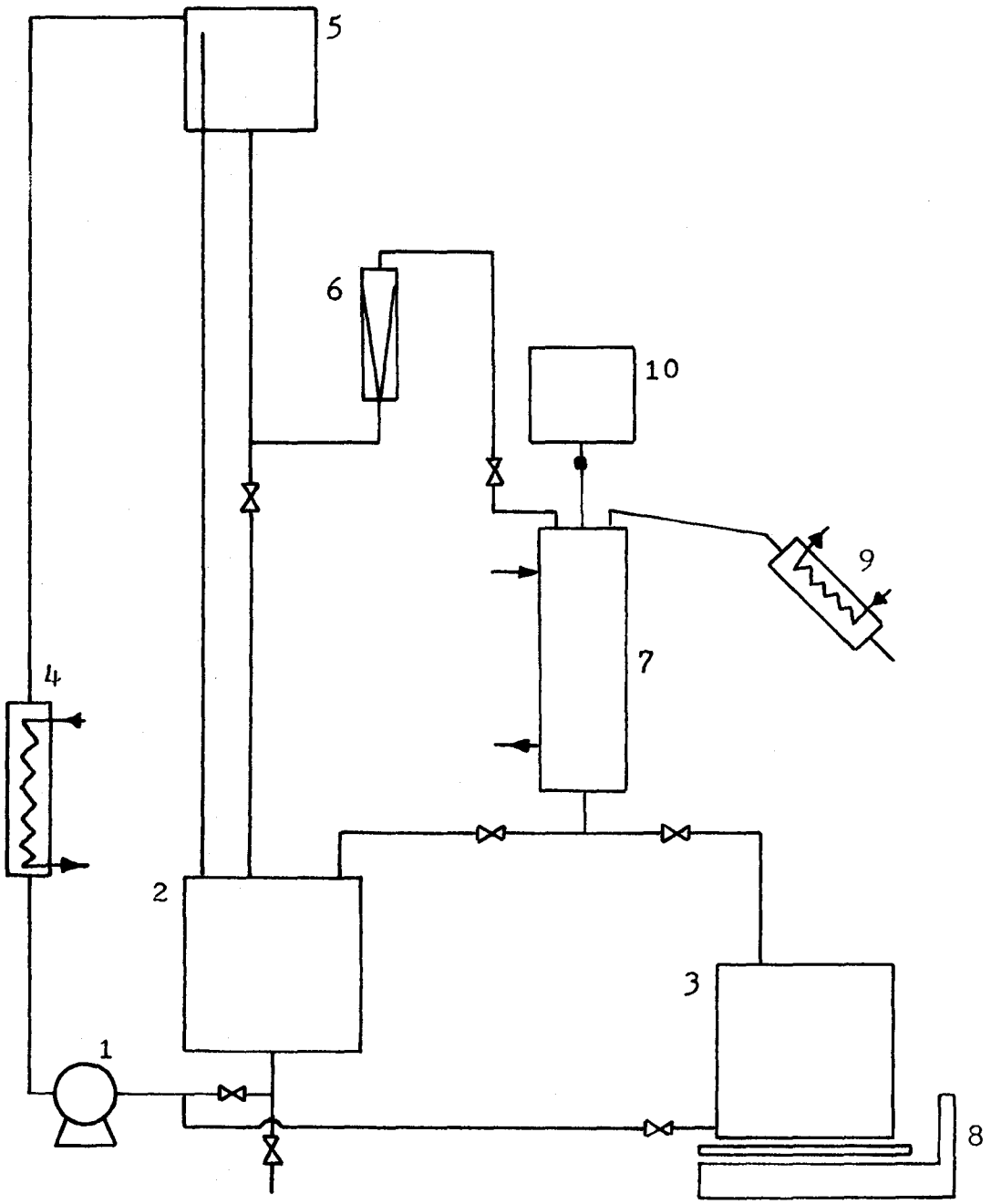

Fig. 3-1

Equipment Lay-Out

copper tube 18 in. I.D. and 1/8 in. wall formed the steam jacket of the exchanger. The end plates of the exchanger were made of yellow brass sheet. Fig. 3-2 shows how the heat exchanger was assembled. To prevent leakage, Klingerite gaskets were placed in between the metallic plates. Dimensions of the end-plates are given in the same figure. Screwed on the external face of the top end-plate was a housing made of brass inside which a ball bearing and an oil seal were located (See Fig. 3-3). On the inside face of the bottom end-plate a footstep bearing made of teflon was mounted by means of a brass housing.

The feed and vapour offtake system is shown in Plate 3-1. The incoming liquid stream was split in two by means of a Y-tube; each of these two streams was further split in two by means of short $\frac{1}{4}$ in. copper tubes. The process liquid coming out of these four channels fell onto the distributor plate which revolved with the scrapers. There the liquid was acted upon by centrifugal force and was thereby distributed as a thin liquid film on the wall of the exchanger. A copper-constantan thermocouple placed just before the junction of the first split of the incoming stream was used to measure the inlet temperature of the process liquid. Vapour, if any, was removed from the exchanger by two $\frac{1}{2}$ in. tubes connected to a condenser. A diagrammatic sketch of the distributor plate and the vapour chamber is shown in Fig. 3-4.

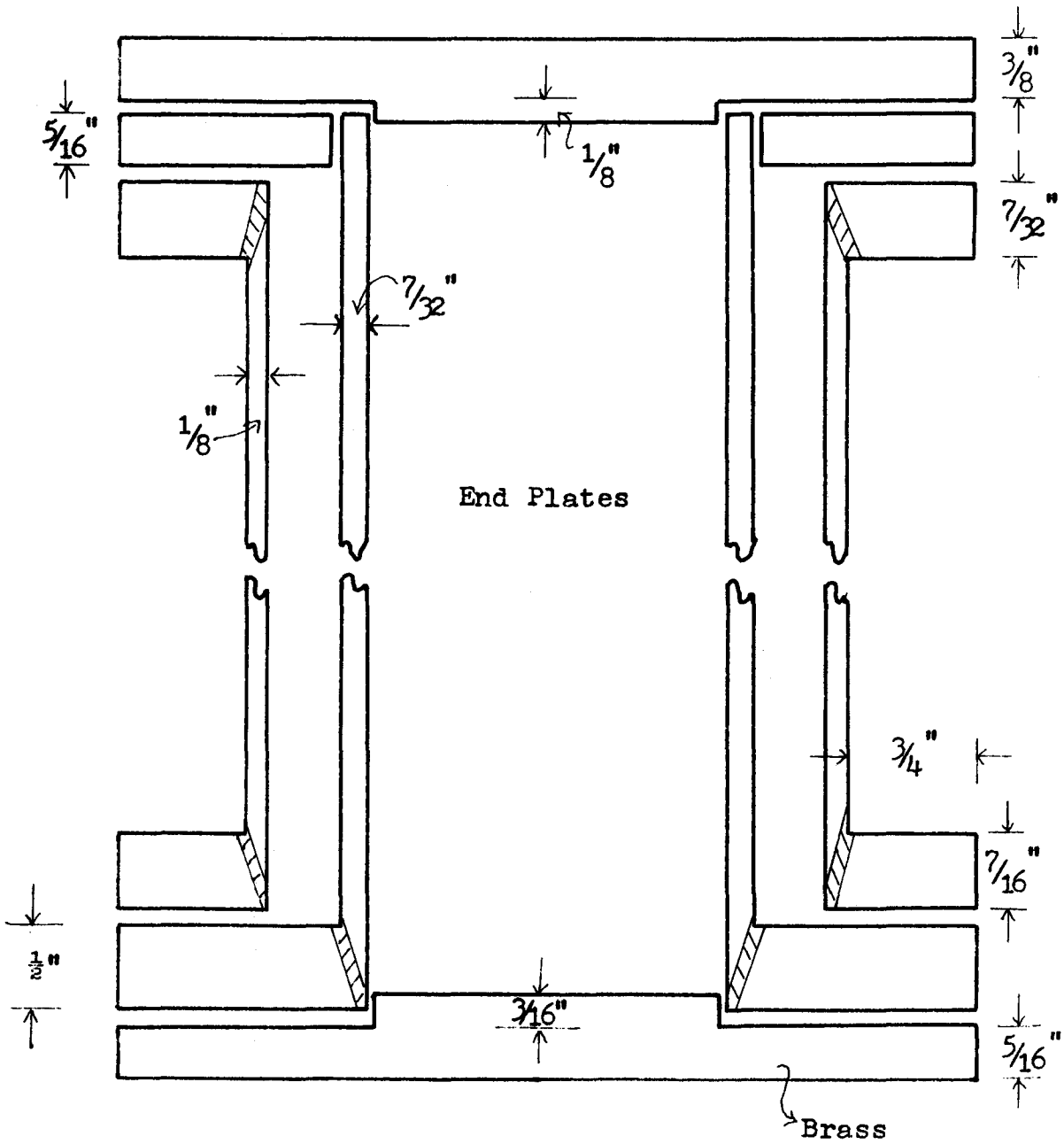

////// denotes soldering or brazing

Fig. 3-2

Heat Exchanger Assembly

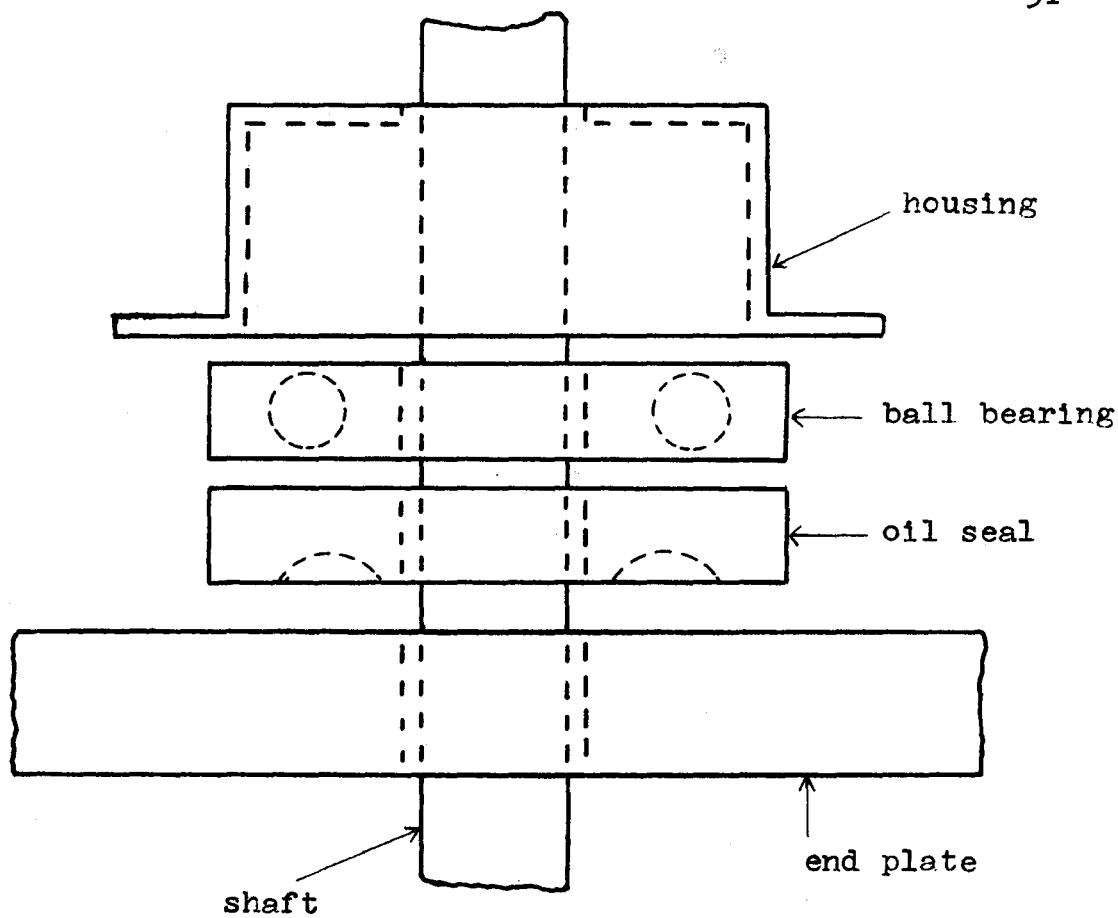

Fig. 3-3

Seal and Bearing

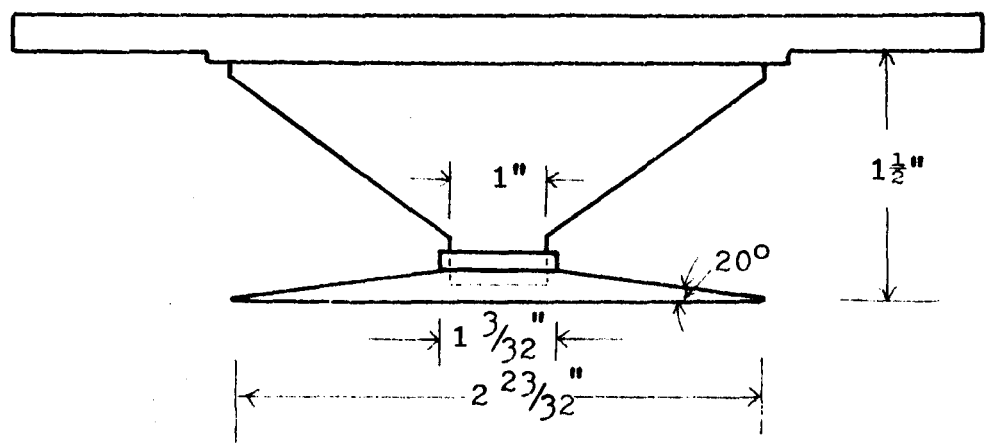

Fig. 3-4

Feed Distributor

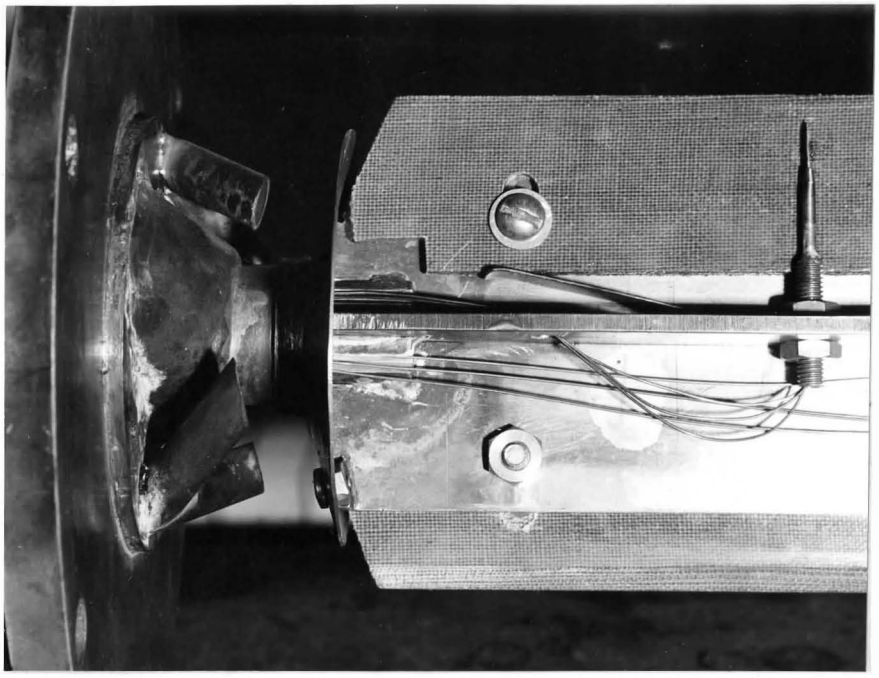

Plate 3-1. Feed Distributor

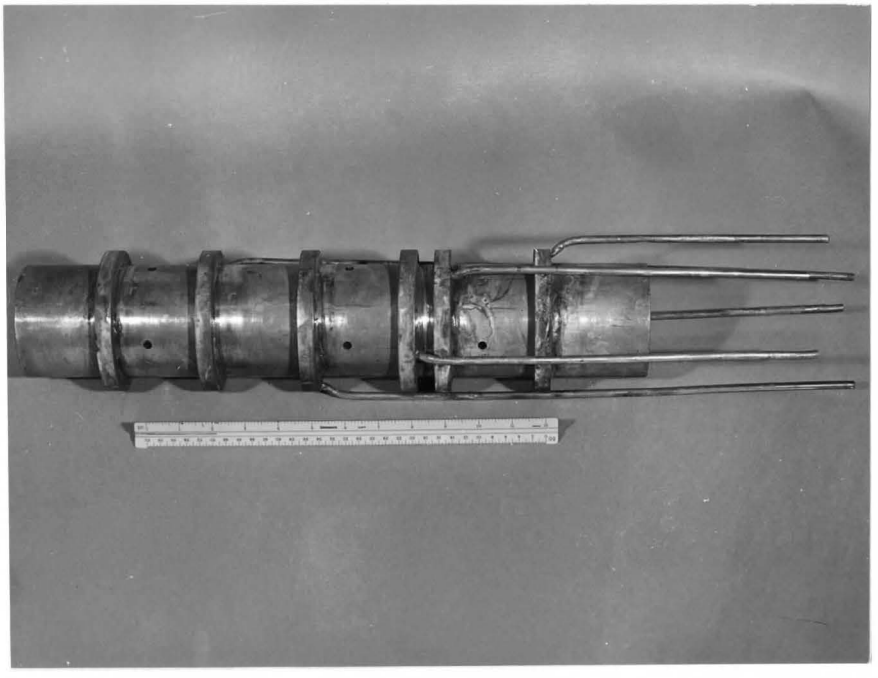

Plate 3-2. Heat Exchanger

The outlet of the exchanger, consisted of four short ½ in. copper tubes soldered onto the bottom end-plate as shown in Fig. 3-5. The tubes led to a small manifold made of copper tube, 3¼ in. I.D., 3½ in. O.D., 2 in. long. One-inch-diameter copper tubes took the liquid from the manifold to either the holding or measuring tank. A copper-constantan thermocouple was placed in the manifold and was used to measure the bulk temperature of the outgoing liquid.

The shell of the heat exchanger was externally divided into seven regions by circular troughs which acted as condensate collectors (See Plate 3-2). These were soldered directly onto the exchanger. Fig. 3-6.a diagrammatically shows the location of these rings while Fig. 3-6.b shows details of their construction. Copper tubes (¼ in. O.D.) soldered into the rings took the condensate as soon as it was formed out of the jacket for measurement. This arrangement is shown by tube D in Fig. 3-7. Tests indicated that the draining capacity of trough-and-tube was at least 500 cc/min before overflow occurred.

It should be mentioned here that the exchanger shell was machined true before the condensate rings were installed. These rings were fitted tightly. The different coefficients of expansion of yellow brass and copper resulted in stresses that caused some buckling of the tube at the locations of the rings. Although an attempt was made to remove this material the diameter could not be made completely uniform because the

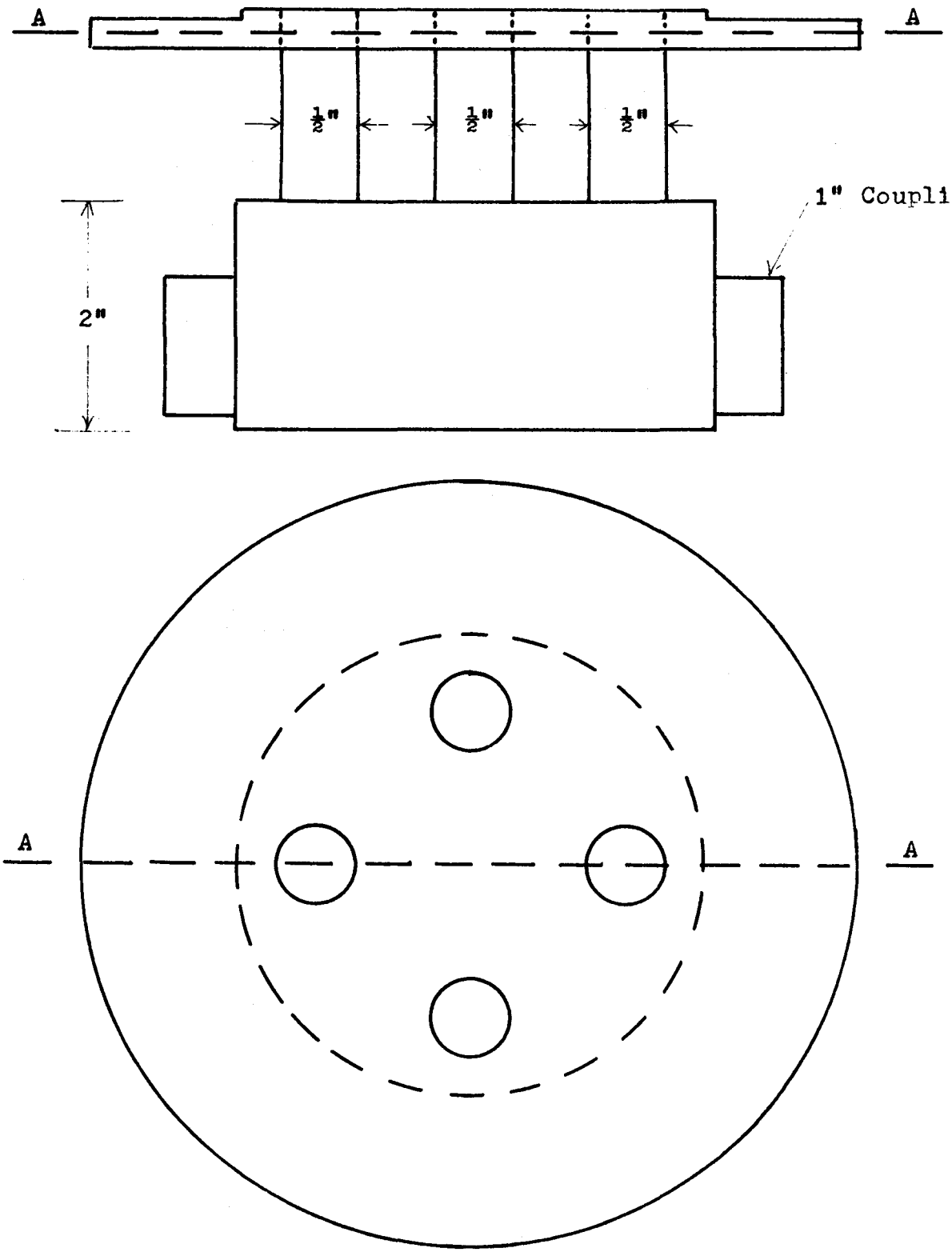

Fig. 3-5

Liquid Discharge System

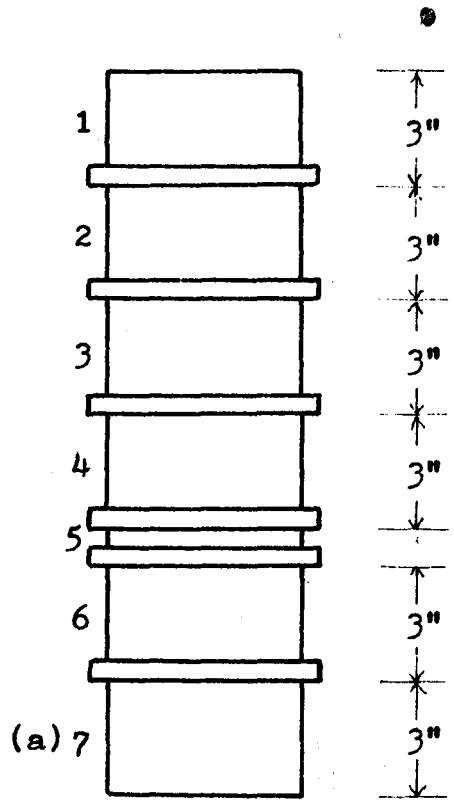

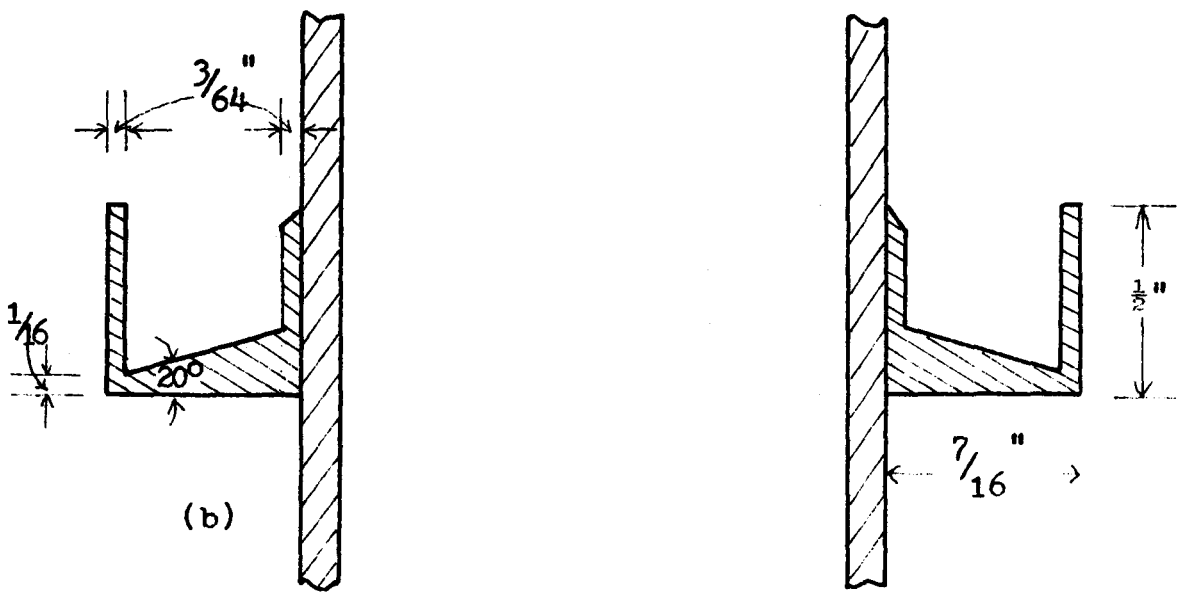

Fig. 3-6

Condensate Collectors

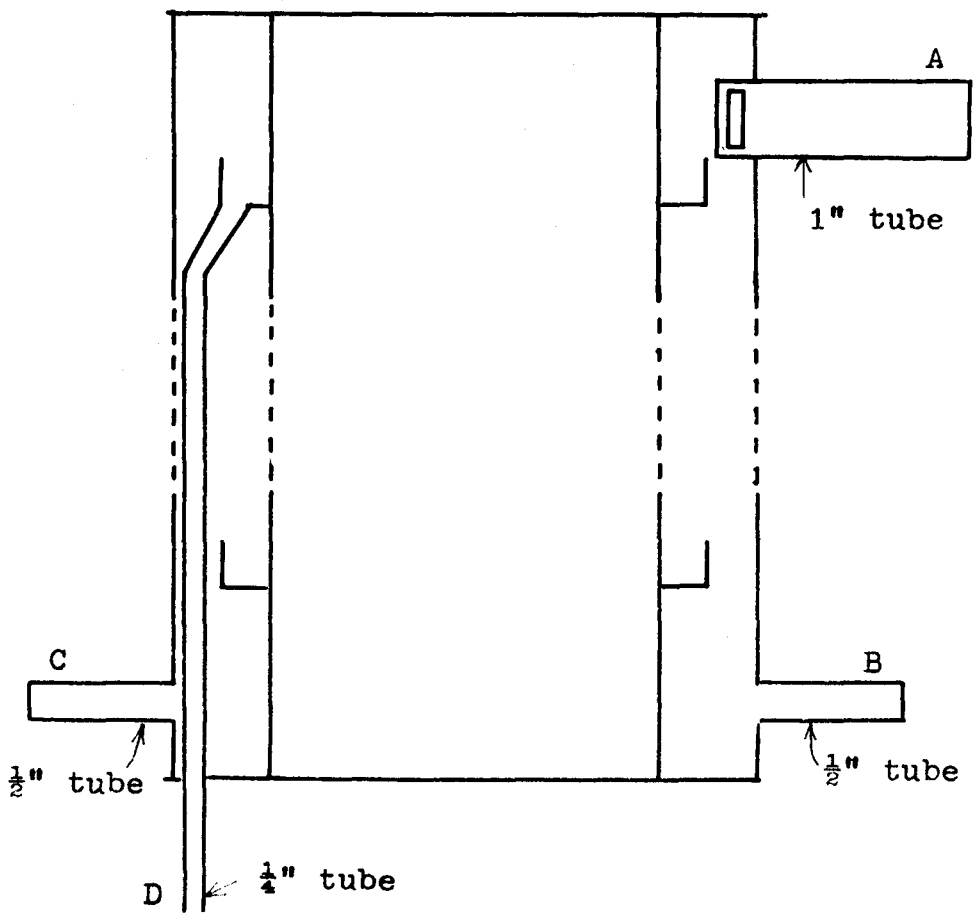

Fig. 3-7

Schematic of Steam Jacket

heat-flux meters were already made to the desired size. The maximum variation in diameter along the tube was about 0.005 in.

Steam was introduced into the jacket via tube A (Fig. 3-7). To prevent direct impinging of steam on the scraped surface, the end of the steam tube was blanked off and steam entered the jacket via two parallel ports in the sides of the tube. Tube B connected the steam jacket with a pressure gauge (0-15 p.s.i.g.) and the pressure controller.

The wipers, 1/8 in. by 1 1/4 in. by 16 in., were made of phenolic laminate, which would prevent wear and conduction of heat along the agitator. Two of them were attached, diametrically opposed, on the blade-supporting part of the shaft, which was made of stainless steel sheet and rod. The scrapers were loosely held on the support with four screws through as many elongated slots. The slots and the loose mounting allowed the scrapers to move inwards or outwards in a radial direction. However, the scrapers were not too loose or else they would tilt. Each scraper was forced onto the transfer surface by two compression springs made of phosphorous bronze. Fig. 3-8.a indicates the wiper design, whereas Fig. 3-8.b and 3-8.c give pertinent information about the shaft. Fig. 3-9 shows a cross-section of the shaft with the wipers mounted.

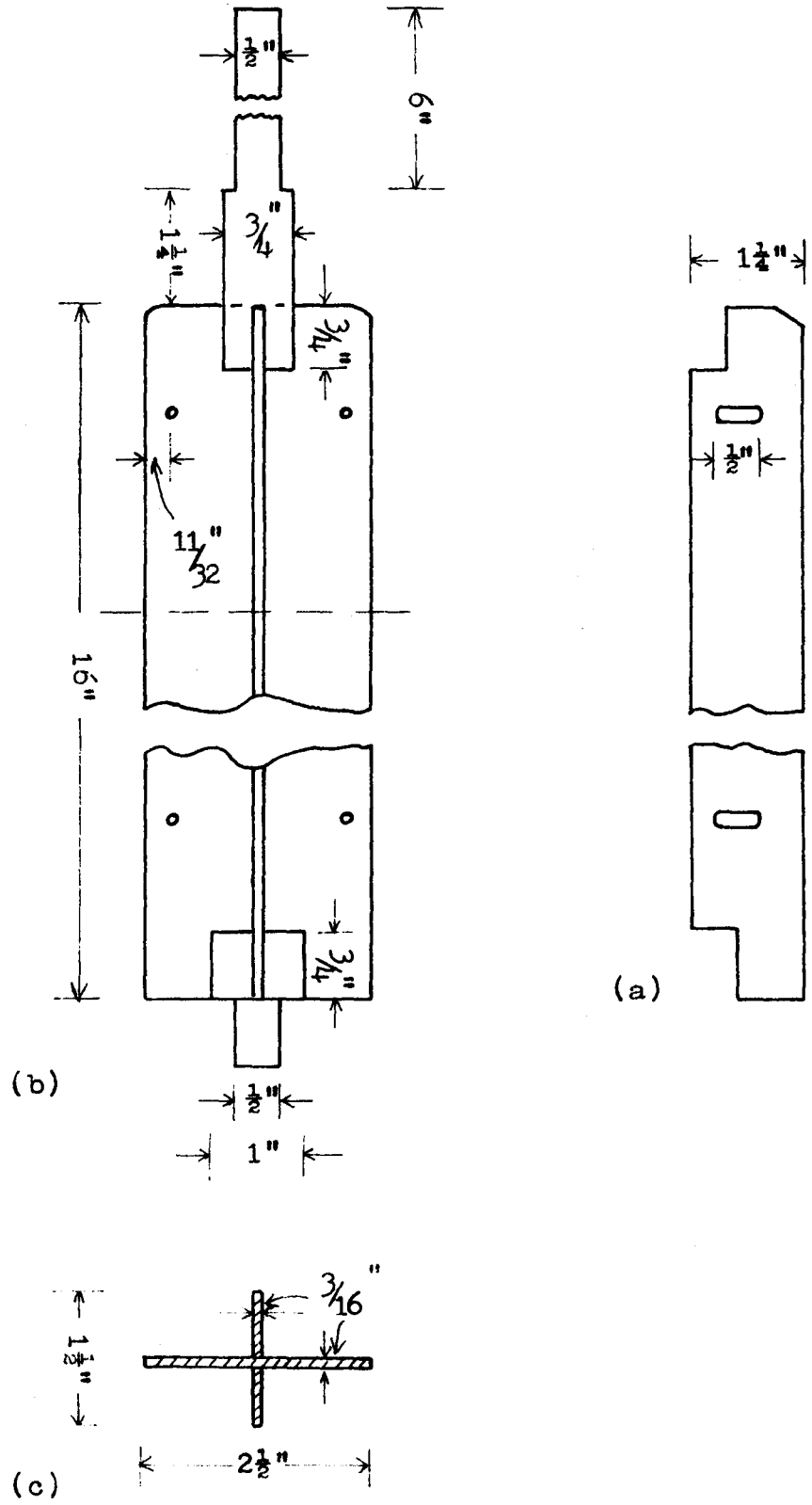

Fig. 3-8

Shaft and Scraper

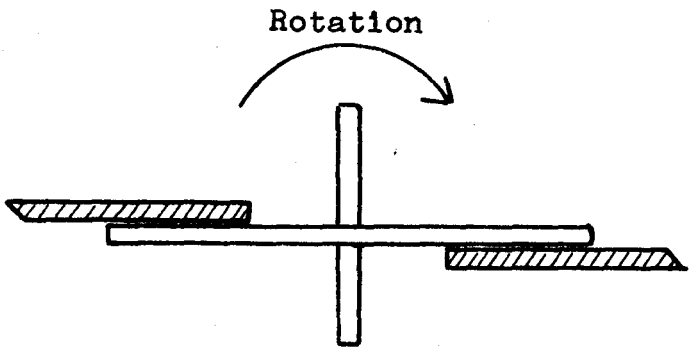

Fig. 3-9
Scrapers

Eight copper-constantan thermocouples installed on the paddle were used to measure the process liquid local temperature. They were stuck on one of the scrapers by means of epoxy resin and located in four pairs at such positions that they would be about 1/8 in. below the four heat-flux meters. The resin was at least 1/4 in. away from the blade-tip, and the thermocouple junctions were within 0.010 in. from the edge of the wiper. The thermocouple wires were taken out of the exchanger through slots at the upper part of the shaft and soldered to slip rings (Fig. 3-10.a), made of copper and constantan thermocouple wire. The slip rings were mounted on a drum, Fig. 3-10.b, which was made of phenolic-bonded paper and held on the shaft by a screw. They were keyed into a slot machined in the drum. Washers made of phenolic laminate were placed in between the rings, insulating them from one another. The rings slipped past pick-up arms made of thermo-

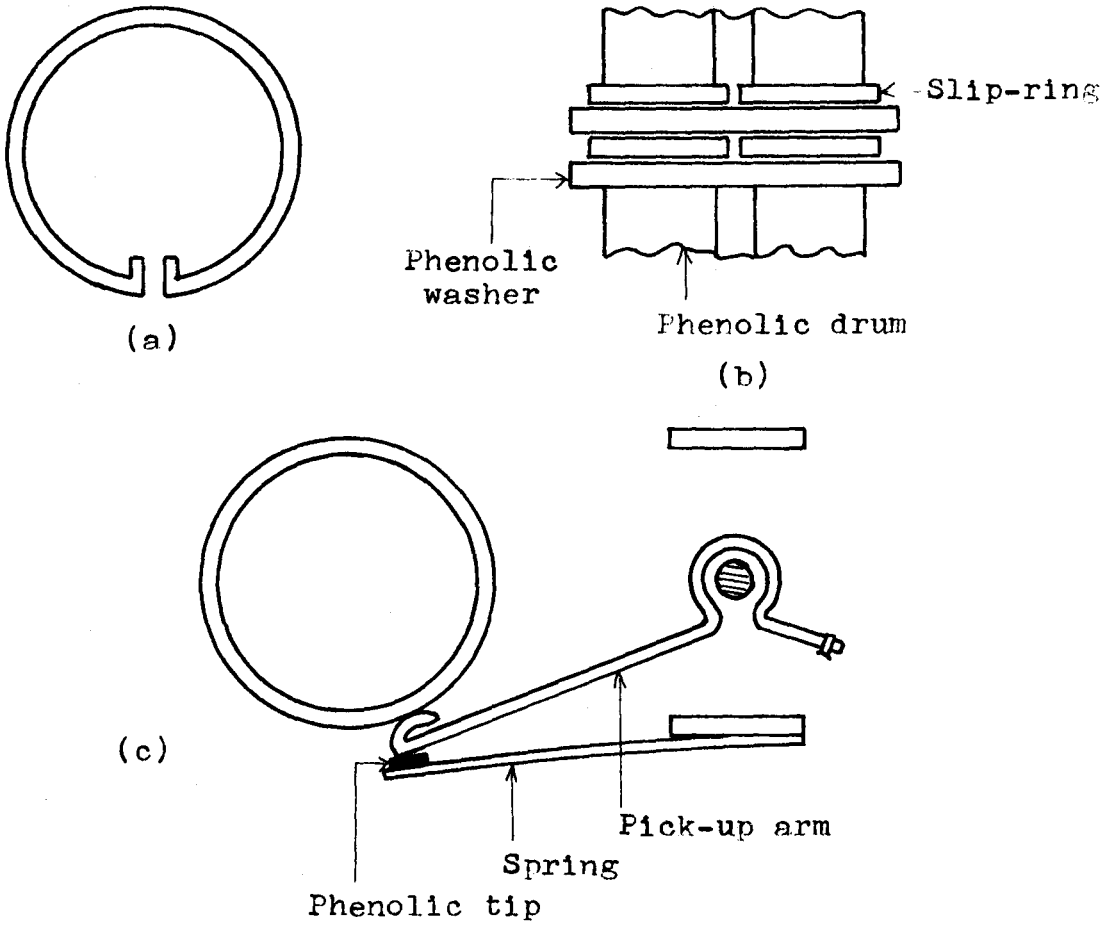

Fig. 3-10
Emf Pick-Up System

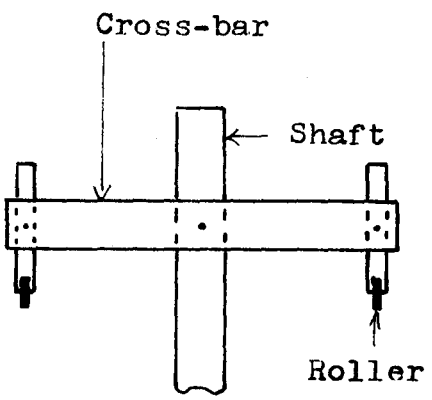

Fig. 3-11
Rollers

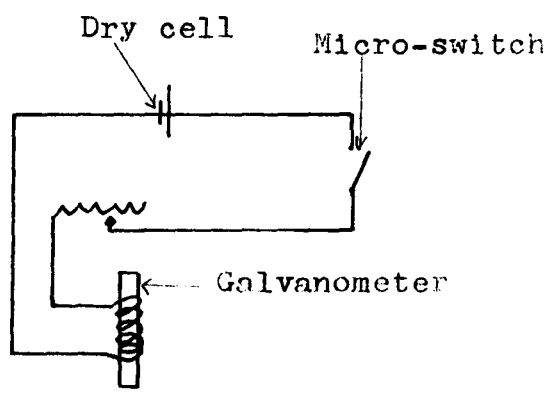

Fig. 3-12
Micro-Switch Circuit

couple wire (copper to copper, constantan to constantan). The pick-up arms were forced against the rings by springs made of phosphorous bronze. Fig. 3-10.c shows the arrangement.

A crossbar was attached to the shaft just above the slip-ring assembly (See Fig. 3-11). The crossbar was fitted with two rollers, which were in line with the blade tips. The rollers actuated a microswitch which was bolted on a bracket. The plunger of the microswitch was in a known position relative to the vertical line passing through the heat-flux meter centres. When the micro-switch was actuated an almost instantaneous current (See Fig. 3-12) passed through the coil of a galvanometer in the Visicorder and a spike was recorded. This arrangement furnished an indication of the position of the blade with respect to a heat-flux meter; it also provided a means of recording the revolutions of the shaft per unit time.

3.1.3 Model Heat Exchanger

In order to observe the fluid mechanical behaviour in a scraped-surface heat exchanger, a model of the exchanger was made of clear plastic (Perspex). Its length was 18 in. Inside and outside diameters were 3 in. and $3\frac{1}{2}$ in. respectively. Feed and distribution system as well as the scrapers were essentially the same as those in the metal one. The vapour offtake was eliminated.

The model was made with the aim of obtaining qualitative information of the liquid flow patterns in the exchanger by direct observation or with high-speed movie pictures.

3.1.4 Condensate Collection System

The copper tubes from the condensate collection rings were connected as shown in Fig. 3-14. Numbers correspond to those of the rings as given in Fig. 3-6.a. To elaborate, a copper tube was connected by polyethylene tubing to a three-way valve which opened either to the condensate tank (T) or to the condensate manifold (M). Trough No 2 was directly connected to a condensate tank whereas troughs No 5 and No 7 discharged only into the manifold.

Fig. 3-15 indicates the condensate collection tank. The letters B, C, and D correspond to those in Fig. 3-7. The tank was made of a 6 in.long, 2 in. O.D. copper tube onto which end-plates were brazed. It was fitted with a level indicator made of $\frac{1}{4}$ in. glass tubing. The tank was connected to the steam jacket via piping B. Lines were so installed as to avoid drainage into the tank. Tubing D connected the tank with the trough. Piping C connected the steam jacket with the coil made of 1/8 in. copper tubing and soldered onto the tank externally. This arrangement brought about (a) equalization of pressures in the jacket and the tank, which allowed setting of the condensate level in the translucent tube by manipulating the needle valve (WHITEY) V1, and (b) compensation for the heat losses by means of steam in the coil thus maintaining the tank at the saturation temperature of steam. The outlet of the tank was made of 3/8 in. tygon tubing; a pinch-cock served as valve V2.

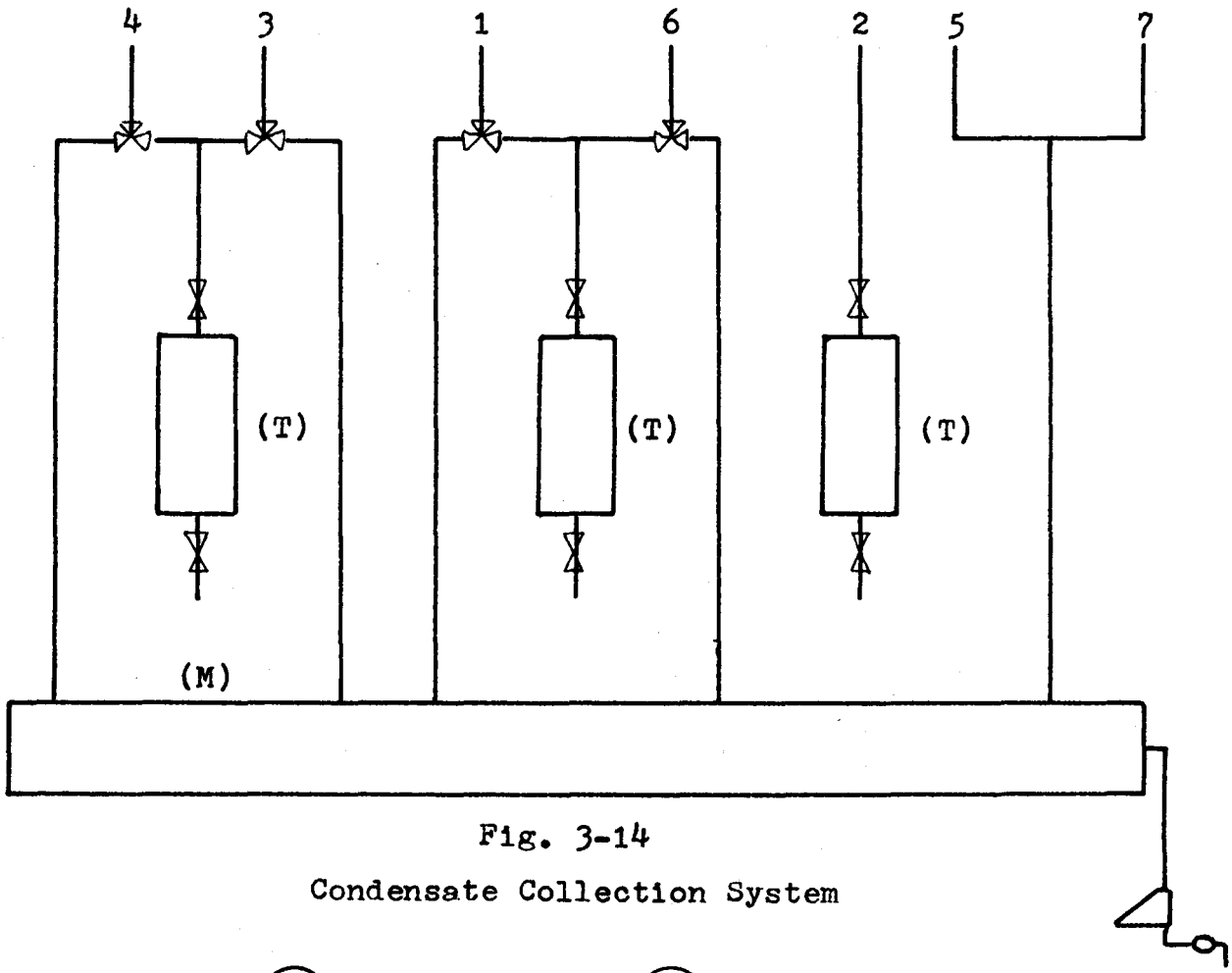

Fig. 3-14

Condensate Collection System

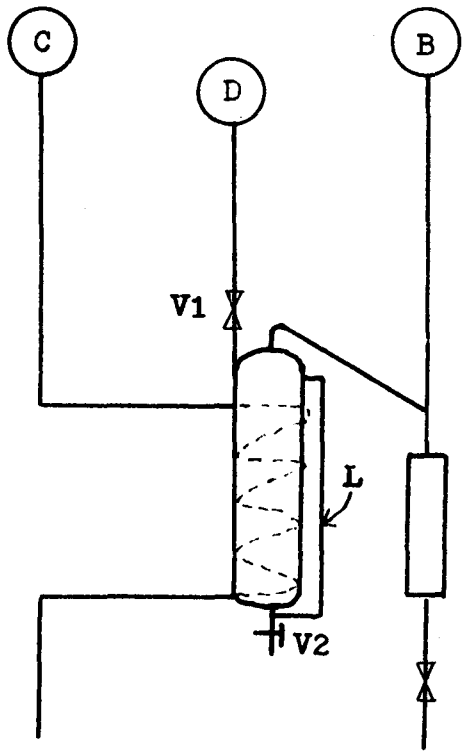

Fig. 3-15

Condensate Tank

3.1.5 Heat-Flux Meters

The heat-flux meters used in this investigation were an integral part of the heat exchanger shell. There were four of them located as shown in Fig. 3-16. The finished configuration and dimensions of a heat-flux meter are shown in Fig. 3-17.a,b,c. Three constantan thermocouple wires were silver-soldered in the heat-flux meter disc. One was located at the centre (See Fig. 3-18) and the other two at the edge of the disc. In particular, thermocouple wires B and C were on a line parallel to the exchanger axis with B lower than C, whereas C and S were on a plane at 90° with the tube axis.

The following steps were taken in the construction of a heat-flux meter. A $\frac{1}{4}$ in. diameter hole was drilled into the heat exchanger wall within, say, 0.015 in. from the inside surface, and the bottom of the recess was machined flat. The disc was taken down to specified thickness and the cylindrical contour established by means of a spark erosion machine, i.e., the inside and outside faces were made parallel. The electrodes used in this spark erosion operation were made of tungsten, and their tip was machined to the same curvature as the inside surface of the tube. The thermocouple wire holes were spark-eroded through the disc using 0.008 in. tungsten electrodes.

The constantan wires used for the heat-flux meters were 29 AWG Ceramo (Thermoelectric Co.) which had been reduced from 0.015 in. to 0.007 in. diameter by electrolytic dissolution.

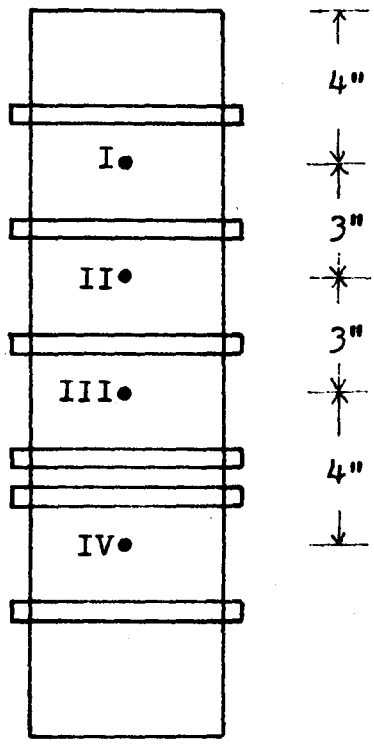

Fig. 3-16

Heat-Flux Meter Locations

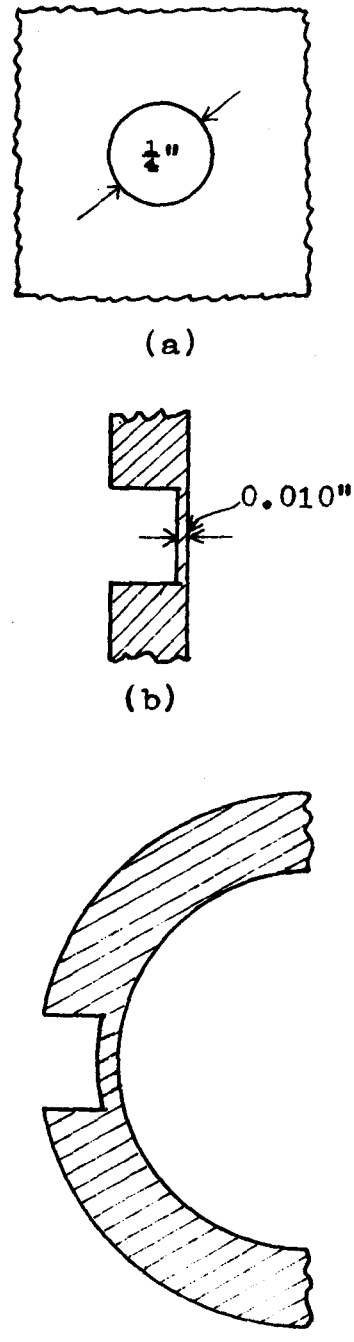

Fig. 3-17

Heat-Flux Meter Design

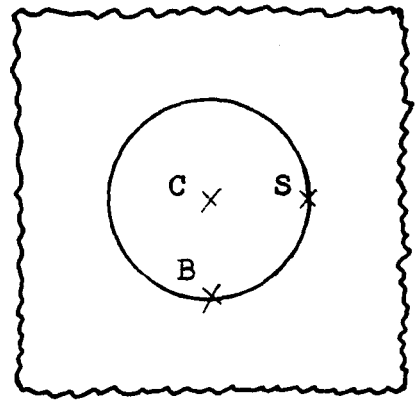

Fig. 3-18
Thermocouple Locations

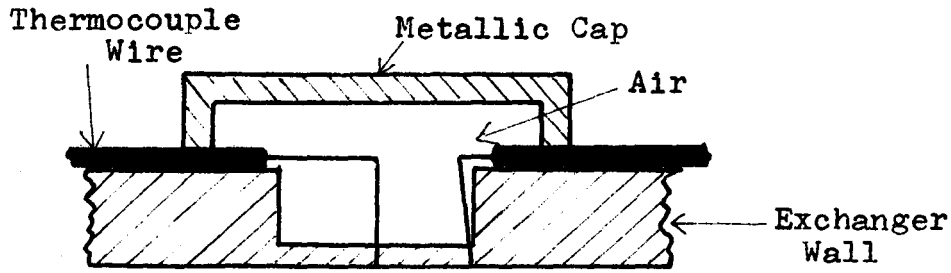

Fig. 3-19
Finished Heat-Flux Meter

The wires were securely installed in the heat-flux meter by silver-soldering in an electrically-heated box containing an oxygen-free nitrogen* atmosphere. Solder and flux were prepared around the wire junctions prior to heating. After the silver-soldering was completed, copper caps were soft-soldered on the tube wall to seal off the heat flux meter cavities as shown in Fig. 3-19 and alleviate some of the problems discussed in Appendix V.

3.1.6 Instruments and Circuitry

A pneumatic pressure controller coupled with a control valve was used to regulate the steam pressure in the jacket.

Inlet and outlet temperatures of the process liquid and steam temperature in the jacket were recorded throughout a run by means of a 12-point recording potentiometer (HONEYWELL). When steady state conditions were achieved the actual readings were taken with a potentiometer (RUBICON model No 2745). Wall temperatures were measured with the potentiometer by means of the edge thermocouples of the heat-flux meters. The circuit for these measurements is shown in Fig. 3-20.

At steady state, the differential emfs from the heat-flux meters were continuously recorded over a short time interval using a recording oscillograph (HONEYWELL, 906c Visicorder). A typical heat-flux meter circuit is given in

---

*By passing the gas through a tube containing a copper screen maintained at about 700°C.

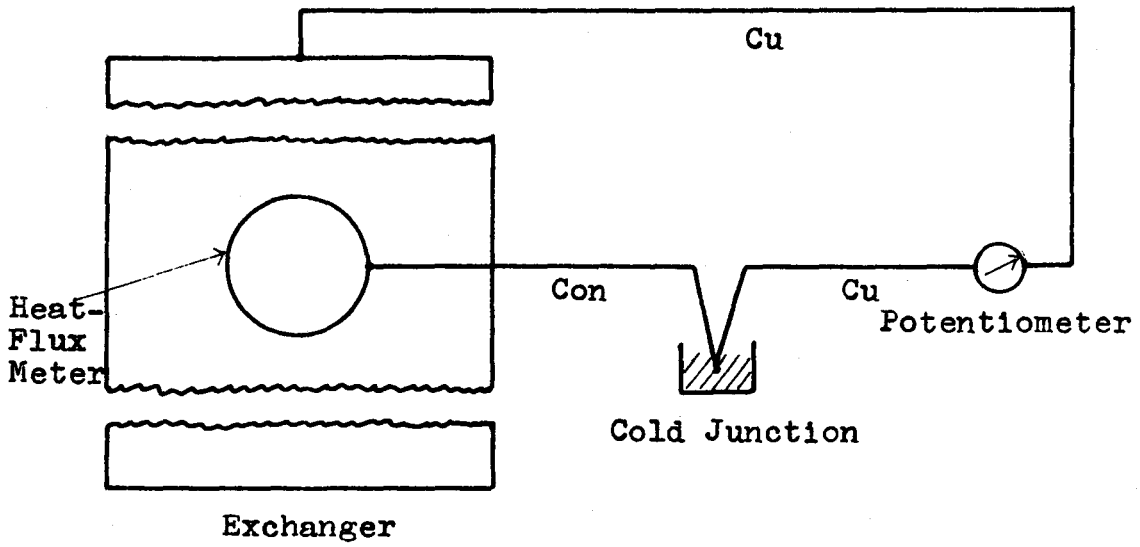

Fig. 3-20

Wall Temperature Circuit

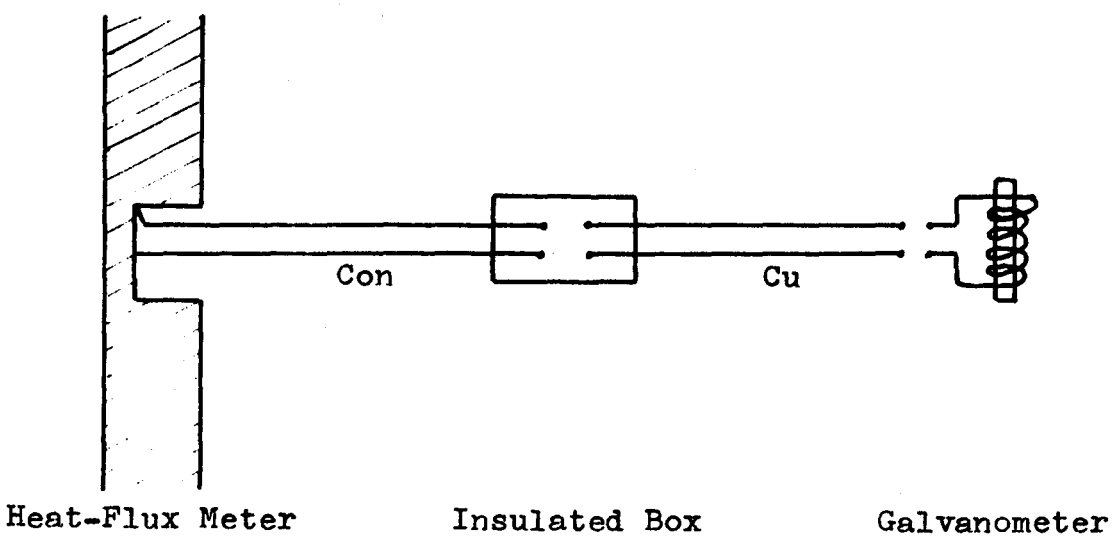

Fig. 3-21

Heat-Flux Meter Circuit

Fig. 3-21 while the procedure for calibrating the Visicorder is described in Appendix I. A Honeywell M40-350 galvanometer was used, and the impedance of the source was kept low for maximum deflection of the galvanometer. The readability of the Visicorder chart was ±0.2 mm (±800 Btu/hr. sq.ft.).

3.1.7 High Speed Photography

Movies of the flow in the model heat exchanger were made by exposing Versapan Negative (Type 2531), black-and-white, 16 mm film with a high-speed camera (HYCAM, Red Lake Laboratories, Inc.). The camera was fitted with 50 mm f/2 (WOLLENSAK) lenses and 1 cm long extension tube. A high speed camera regulator (Red Lake Laboratories, Inc., model F1-115-HC-2) was used to regulate the speed of the camera, which was set at 2000 frames per sec. Illumination was provided by two high intensity (1000 watts) photo-flood lamps.

3.2 EXPERIMENTAL PROCEDURE

Each of the tests followed the same procedure: The supply of cooling water to cooler and condenser was set. The pump was turned on, and process liquid flowed into the exchanger at a fixed flow rate by adjusting the appropriate valve. The agitator motor was switched on, and steam was supplied to the jacket. The multi-point recorder was started recording the inlet, outlet and jacket temperatures. About thirty minutes were allowed for the system to come to a steady state, that is, until all temperatures were steady.

The following measurements were made:

(a) Condensate from rings 1, 2, 3, 4 and 6 (See Fig. 3-6.a) was collected in an appropriate condensate tank (See Fig. 3-14) for a measured time (about six minutes). The condensate was then received into a preweighed amount of ice-water in a beaker and weighed with a balance accurate to 0.1 gms.

(b) Two readings for each of the inlet and outlet temperatures were obtained using a potentiometer.

(c) The four local wall temperatures as given by the side wires of the heat-flux meters were read twice on a potentiometer.

(d) Process liquid was directed to the measuring tank for about four minutes. Exact time and weight of accumulated mass were recorded.

(e) The outputs of the heat-flux meters were recorded on the photographic paper of the Visicorder during the collection of condensate.

3.3 EXPERIMENTS

In all the experimental runs distilled water was used as process liquid.

The main objective of the program was to test the ability of the point heat-flux meter to determine instantaneous local heat transfer coefficients in scraped-surface equipment. For this reason the only variable investigated was the scraper speed. It ranged from 340 to 740 r.p.m.

The flow rate of the process liquid was set at two levels, 500 and 550 lbs/hr.

The steam pressure in the jacket was maintained at 2.5 p.s.i.g. for all the tests.

The cooling water supply to the cooler was such that the inlet temperature of process liquid did not change much from run to run.

The temperature change of the process liquid across the exchanger was substantial. The ratio of outlet to inlet temperatures was close to 2:1.

The model heat exchanger was employed to qualitatively study the flow of process liquid in the exchanger. Two 16 mm films were shot using the high speed movie camera.

4. EXPERIMENTAL DATA

4.1 FLUID FLOW

The model heat exchanger was used to make qualitative observations of the flow in the exchanger. The mass flow rate was set at about 400 lbs/hr, and the rotational speed of the blades at 600 r.p.m. Under these conditions the entire surface was wetted. By means of a stroboscope the blade "was stopped", and the edge of the fillet could be seen in front of the blade-tip. Its configuration was more or less of the form shown in Fig. 4-1.

The liquid could be seen to move down the shell in a spiral trajectory. This characteristic of the flow was distinctly brought out in subsequent tracer tests. A hypodermic needle was installed in the tube wall with its axis almost tangential to the inside tube curvature. By means of a syringe, a tracer (washable royal blue ink) was injected at low velocity in order to avoid external disturbances to the flow. On maintaining a constant supply of tracer a band of tracer-loaded fluid could be seen to spiral down the tube (See Fig. 4-2). It should be noted that this flow characteristic was a macroscopic one. Mixing induced by the blade still took place.

The naked-eye observations were supplemented with pictures taken with the high-speed camera. The camera was so

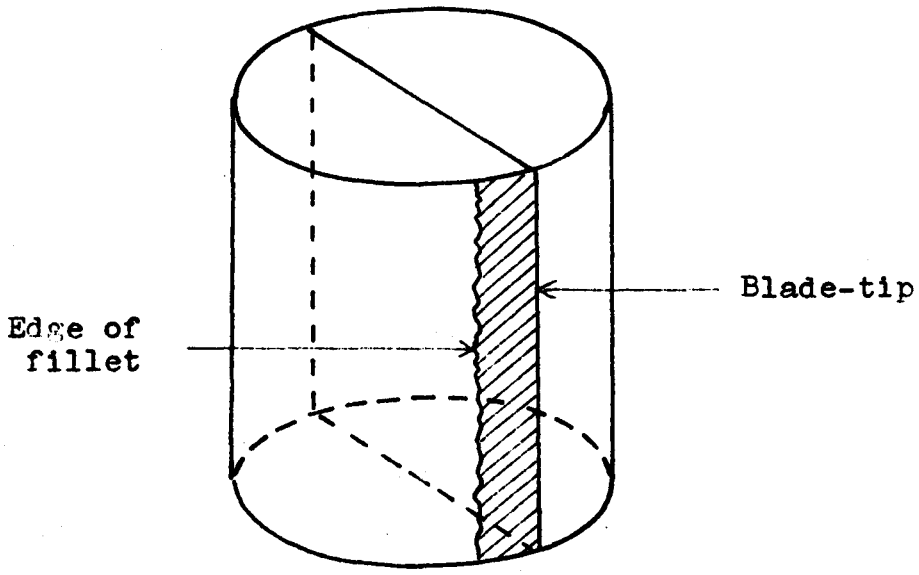

Fig. 4-1
Liquid Fillet

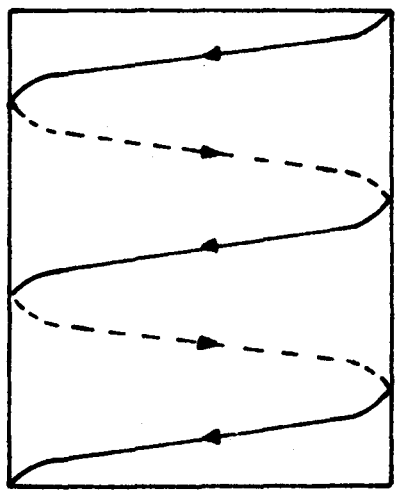

Fig. 4-2
Liquid Flow Path

positioned as to show the point of the tracer injection at the upper-right corner of each frame.

The movie showed that one of the scrapers of the model did not wipe the wall clean locally. This was very conspicuous, especially when the blade had just passed the point of tracer injection where the blade did not show at all. This is shown in Plate 4-1. The lighter band at the left of the plates is due to reflection from the tube cylindrical surface. The darker region at the upper right-hand corner of this Plate is the image of tracer-loaded fluid which covered the inside surface of the tube eclipsing the blade. Plate 4-2 shows the same blade at a later moment and the tracer following the blade for a short distance in an almost horizontal direction which, no doubt, was due to the inertia imparted by the scraper on the fluid. The second blade did scrape the wall. Part of the fillet in front of this blade is shown at the lower right-hand corner of Plate 4-3, while in Plate 4-4 the fillet blanks the entire field of view. In plate 4-5 the blade has just entered the scene. Although the tracer used did not produce a dark enough band to be detectable with the black-and-white film employed, the movie did show the spiral fluid motion. This point was also demonstrated near the tracer injection point where the tracer solution was dense. One could see the boundary of the dark region moving in the same direction (See Plate 4-6).

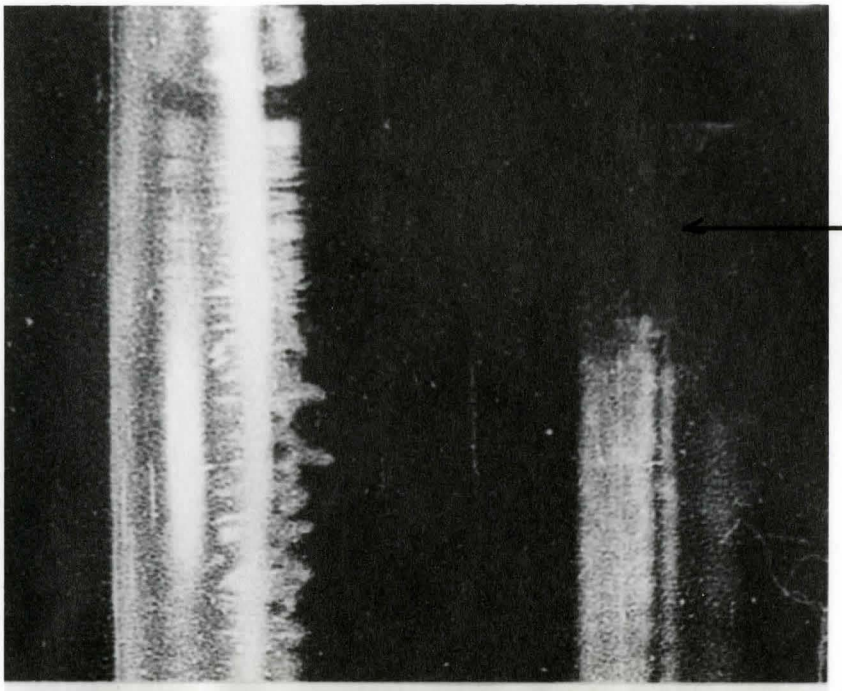

Plate 4-1. Non-Scraping Blade

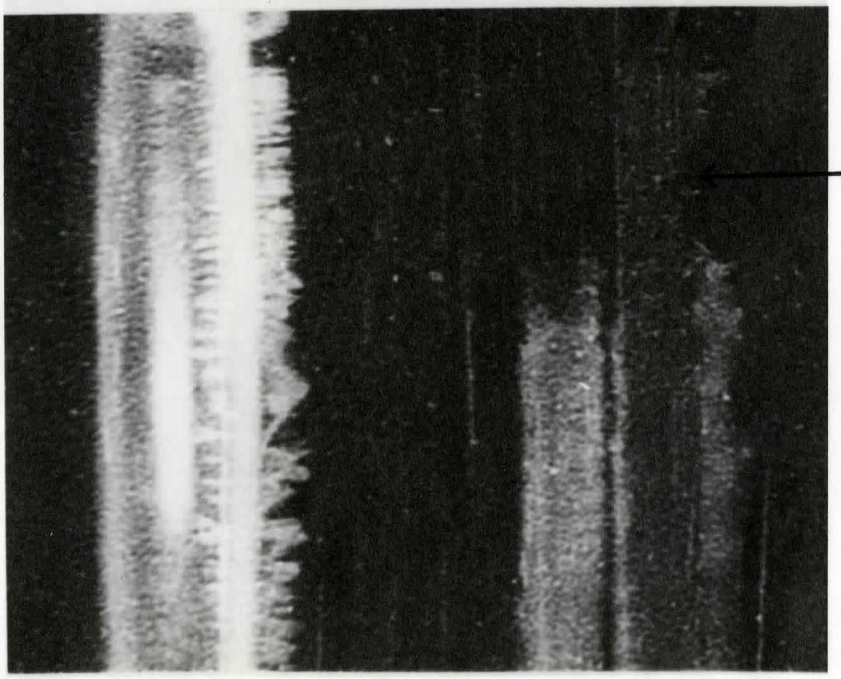

Plate 4-2. Tracer Following Blade

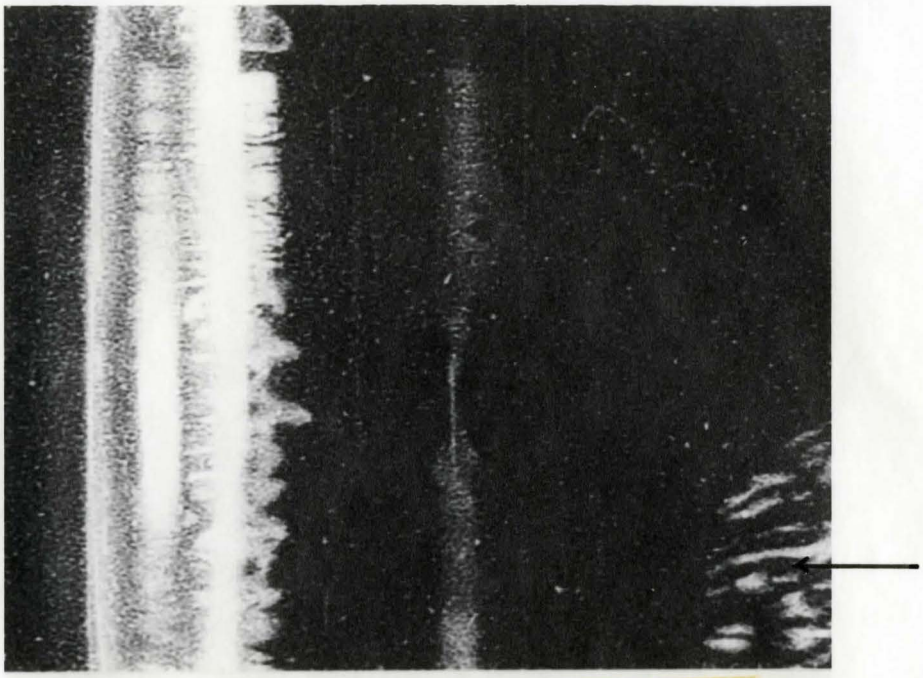

Plate 4-3. Liquid Fillet

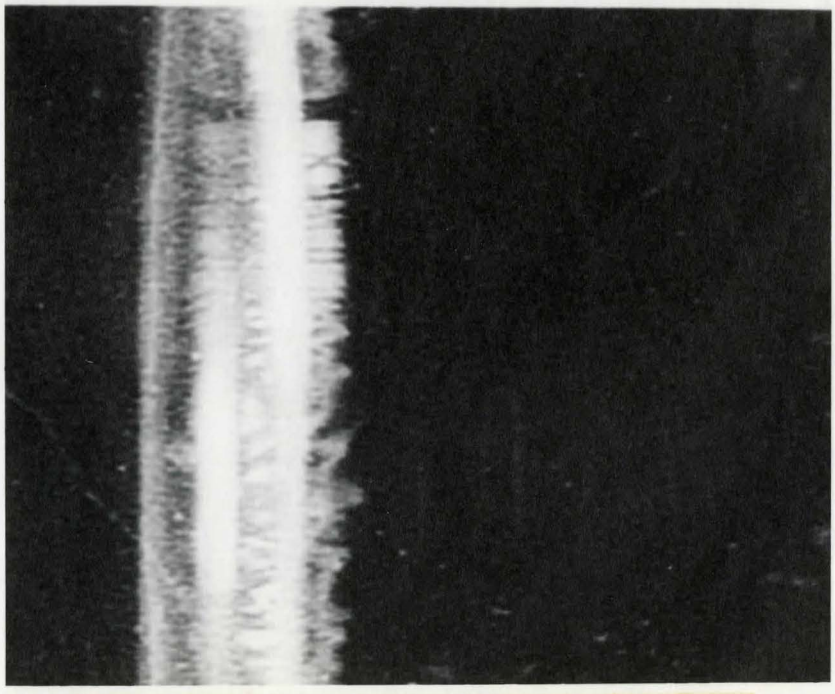

Plate 4-4. Liquid Fillet

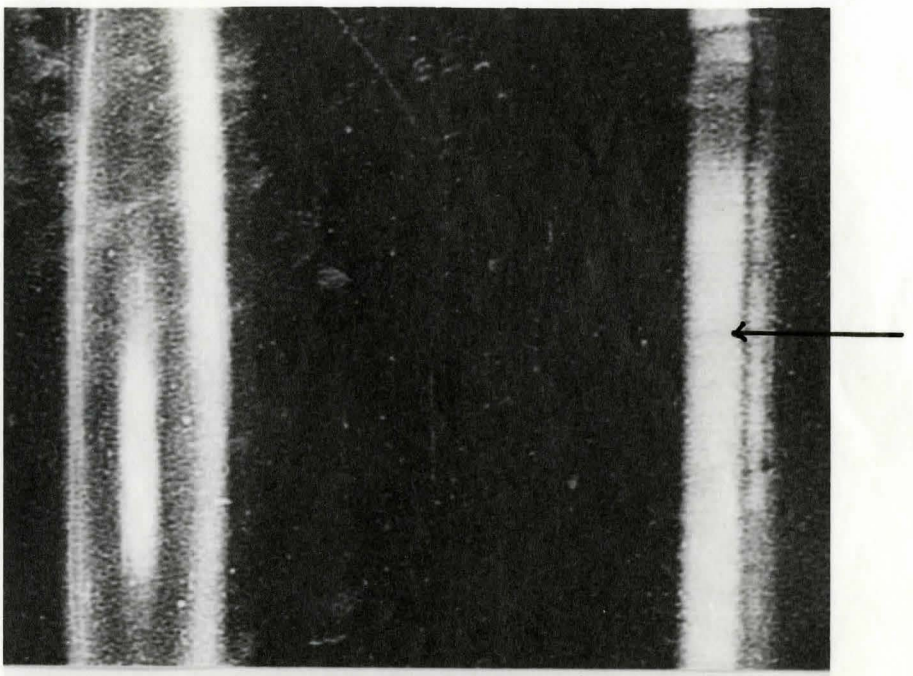

Plate 4-5. Scraping Blade

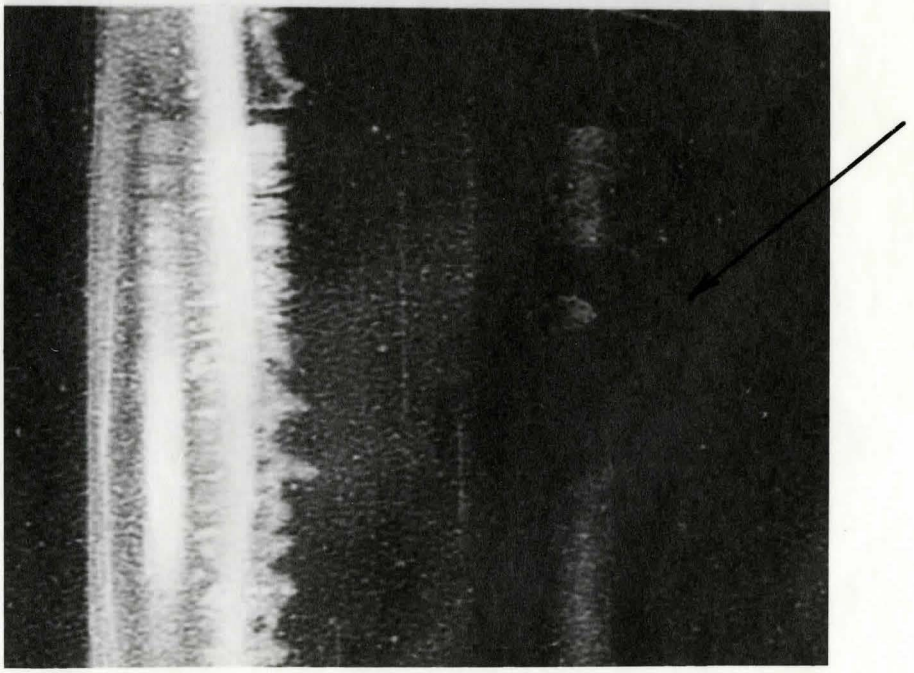

Plate 4-6. Tracer on Spiral Path

Although the model was made of plastic (a material of different wetting characteristics from those of copper), it is believed that similar patterns would be exhibited by the fluid in the experimental apparatus.

Throughout the range of rotational speeds and flow rates investigated in this experimental work, the heat exchanger shell was assumed fully wetted. This assumption was not entirely arbitrary. It was justified by the regularity shown by the heat-flux meter output above a minimum rotational speed. Below this speed the trace was erratic, which could only be due to the assymetry and irregularity of the flow.

4.2 WALL TEMPERATURE PROFILE

The temperature profile of the heat exchanger shell was obtained by measuring four point temperatures by means of the thermocouples at the edges of the heat-flux meters. These local temperatures showed small (maximum amplitude $0.2^{\circ}F$) periodic fluctuations. The period of these fluctuations was very large and had no relation whatsoever to the frequency of the revolving scrapers. Therefore, these temperatures were essentially constant and were taken as such.

In the experiments carried out the four wall temperatures fell in the band shown in Fig. 4-3. The temperature at 7 in. from the top was always about $10^{\circ}F$ lower than the others. If the thermocouple read the true wall temperature at this point, the low temperature would imply that a heat sink existed

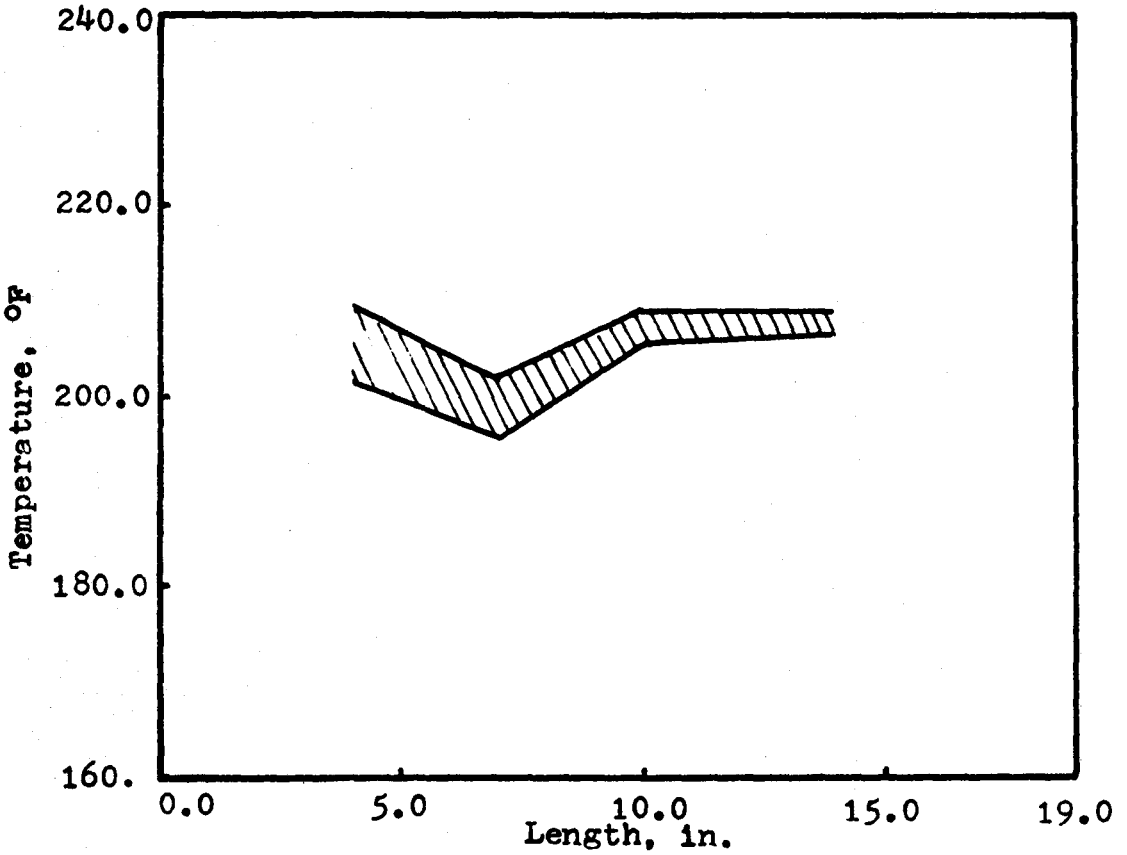

Fig. 4-3. Wall Temperatures

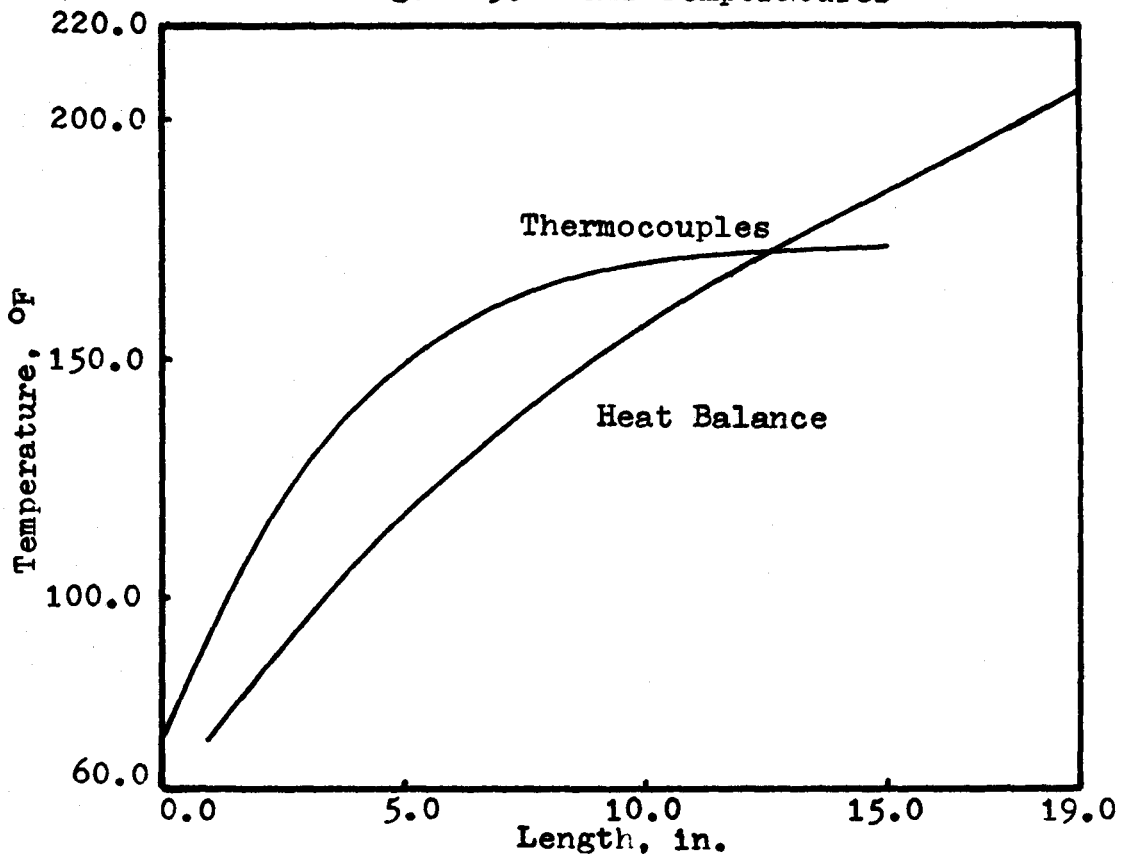

Fig. 4-4. Liquid Temperature

in that neighbourhood. A heat sink, however, was rather unlikely and the assumption was made that the thermocouple was in error. The temperature at this point was obtained by a linear interpolation between those at 4 in. and 10 in. from the top. It should be pointed out that all the temperatures were the same when there was no heat load, i.e., liquid flow in the exchanger but with steam in the jacket. The temperature at 4 in. showed a trend of decreasing values with increasing rotational speed while the third and fourth points showed small random variation.

4.3 LIQUID TEMPERATURE MEASUREMENTS

A series of tests was carried out in which the thermocouples on the paddle were used to measure the local liquid temperature. Since the temperatures were expected to fluctuate continuously the visicorder was chosen to record the thermocouple emfs. The recorded traces were averaged, and average temperatures were obtained from the calibration curve. A typical temperature profile as obtained from the thermocouples is shown in Fig. 4-4. The temperature of the liquid tended to jump to high values just over a short part of the exchanger and change little thereafter. Such a behaviour was not expected for the bulk temperature of the liquid. It could not be justified. A liquid bulk temperature profile estimated from the condensate collected in each ring is also shown in Fig. 4-4. The "high" temperatures recorded by the

thermocouple may be explained as follows: the temperature sensors were located near the blade-tip, and therefore measured the temperature of liquid in the fillet. Although the flow in the fillet was likely to be turbulent some regularity is expected to prevail in the flow. This is shown in Fig. 4-5. If the situation depicted in Fig. 4-5 is close to reality it could be that the thermocouples came in contact with the "hot" fluid just scraped off the wall most of the time, thus giving a false high reading. It is then obvious that the thermocouples could not be used even for obtaining crude approximations of the local liquid bulk temperatures. For this reason they were not used in later work.

4.4 HEAT FLUX AND LIQUID TEMPERATURE PROFILES

The heat-flux profile over the exchanger length as well as that of the liquid bulk temperature could easily be derived from the directly measurable quantities. The calculation of these profiles required certain assumptions which were expected to be realistic. Appendix IV contains justifications for the following assumptions as well as a calculation procedure.

(a) Integral heat transfer rate was symmetric with respect to exchanger axis.

(b) The average heat flux over a ring-to-ring region occurred at the mid-point of the latter.

(c) No heat conduction along the exchanger wall or the scrapers took place.

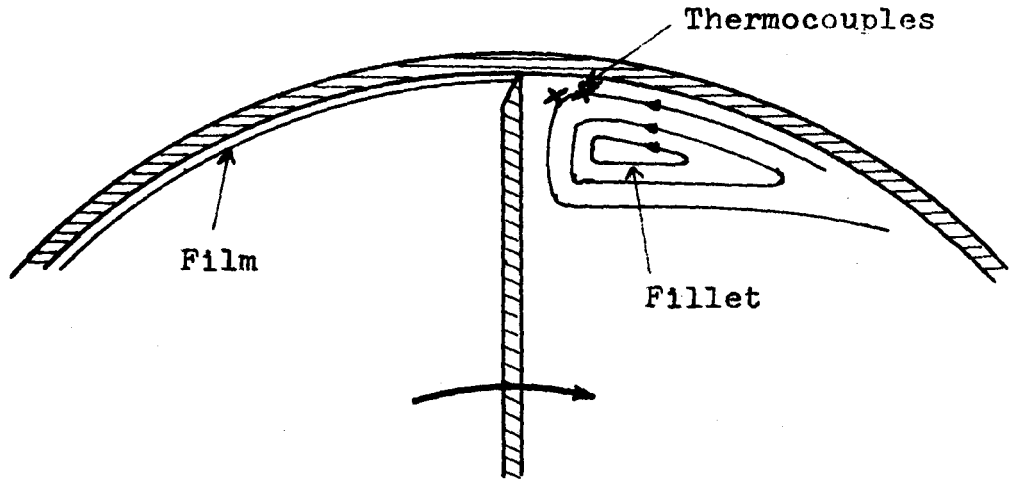

Fig. 4-5

Paddle Thermocouples

(d) The liquid passed through the exchanger in plug flow.

(e) The steam was saturated. Condensate left the exchanger at saturation temperature. No heat was lost.*

The above assumptions allowed a direct calculation of the average heat input rate over a ring-to-ring region from the rate of condensation and the latent heat of vaporization. The average heat flux was calculated from the heat input rate and the geometrical dimensions of the exchanger. The liquid-bulk temperature increase over a ring-to-ring region was obtained from the corresponding heat input rate and the mass flow rate.

The heat flux distributions and the liquid bulk temperature profiles over the exchanger length are given in Fig. 4-6 to 4-19 for 550 lbs/hr mass flow rate and in Fig. 4-21 to 4-25 for the 500 lbs/hr one. The order in both sets is that of increasing rotational speed. The curve drawn in these plots for bulk temperature variation corresponds to quadratic least-squares fit through all the liquid temperature points but the one for the inlet temperature. The latter was not taken into account because the liquid in the exchanger did not cover the entire area of the first three-inch region thus introducing an uncertainty as to the location of this point with respect to the exchanger length. It will be noted

---

*Heat loss was determined to contribute less than 0.5% to the condensate collected by direct test.

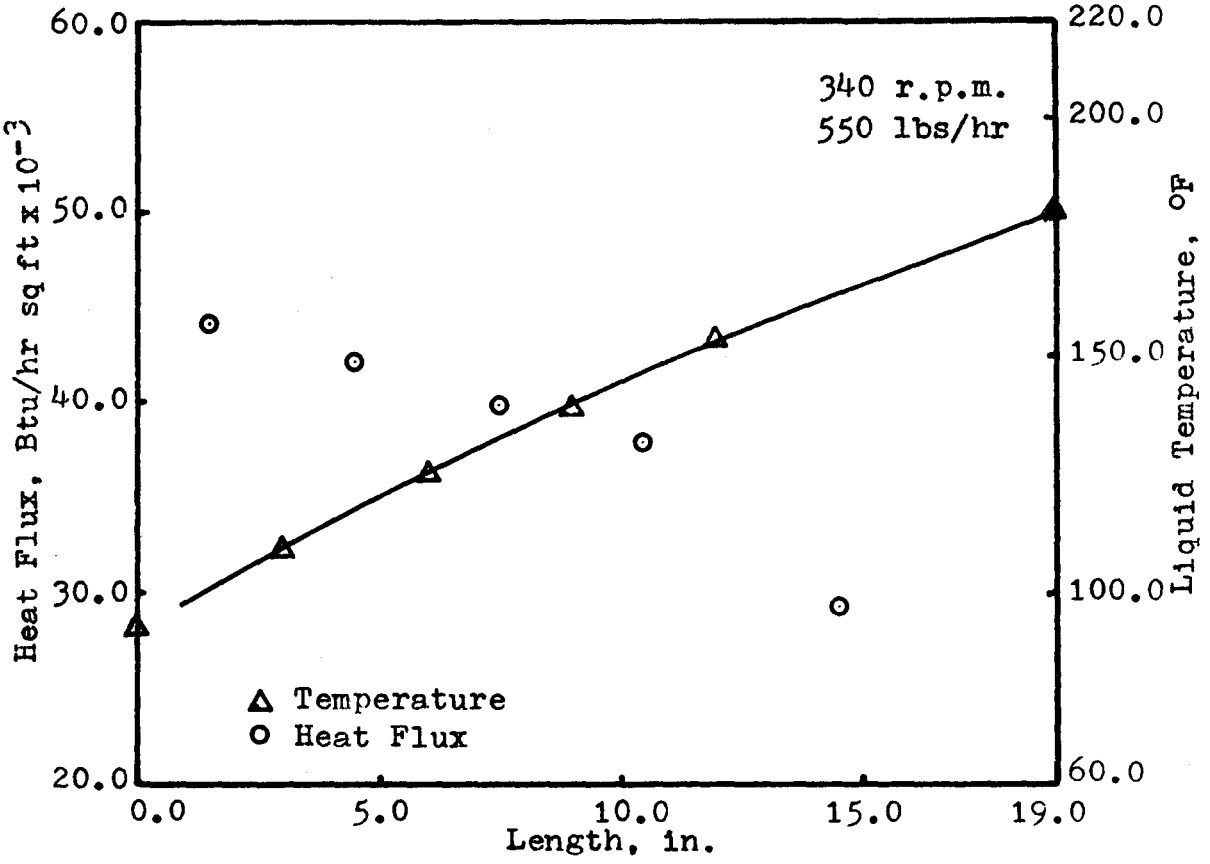

Fig. 4-6. Average Heat Flux and Liquid Temperature

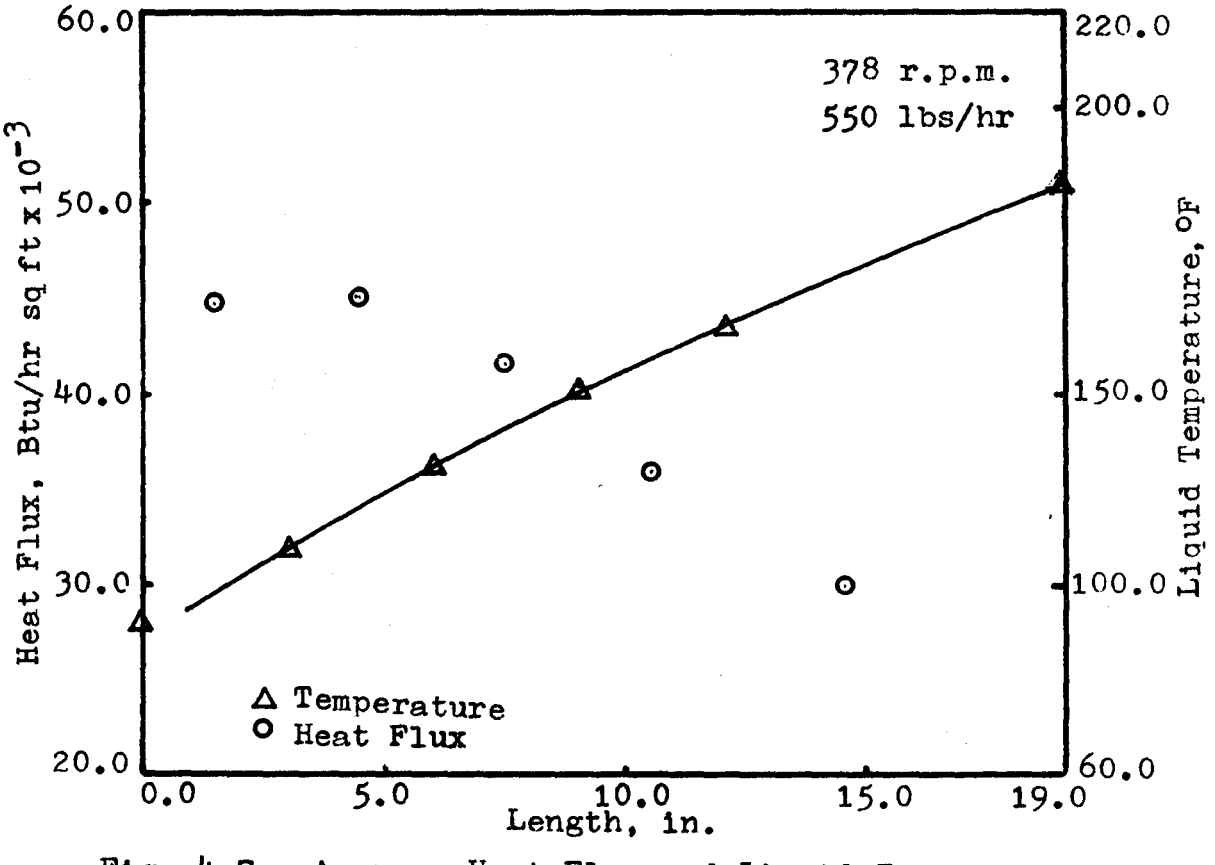

Fig. 4-7. Average Heat Flux and Liquid Temperature

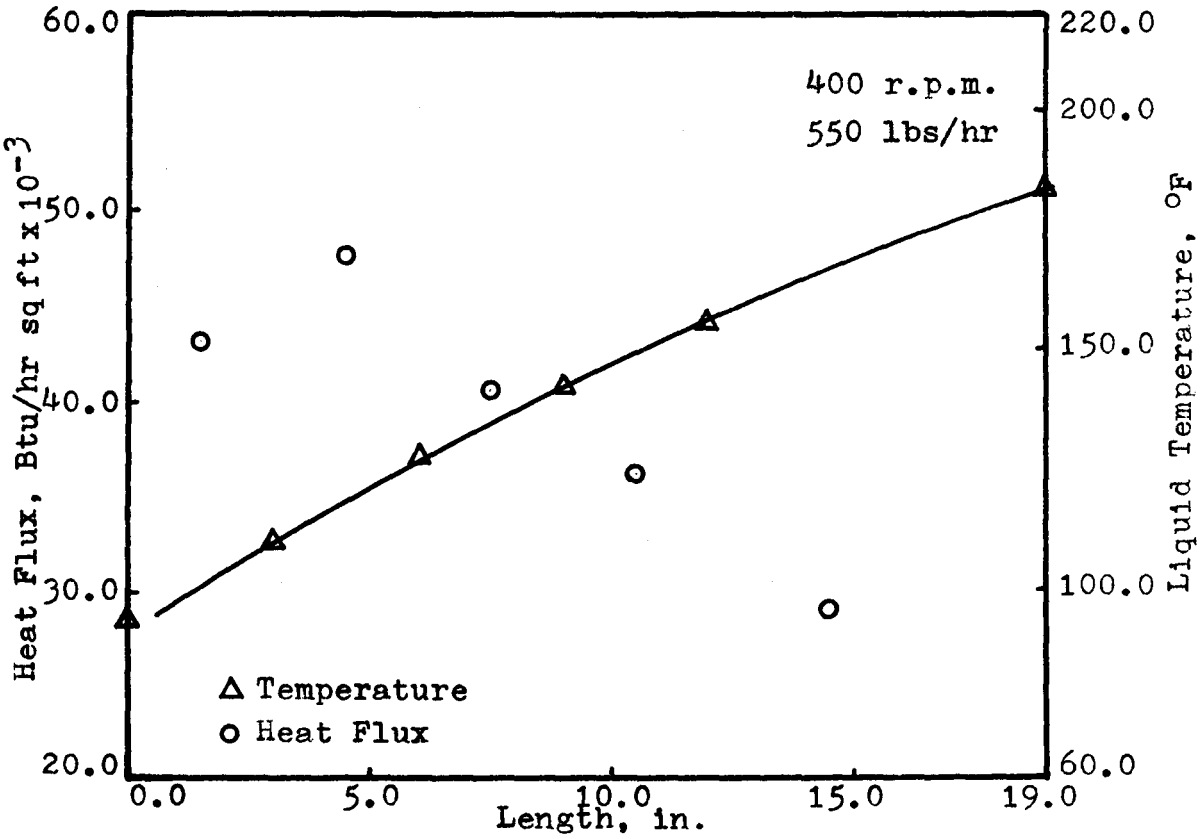

Fig. 4-8. Average Heat Flux and Liquid Temperature

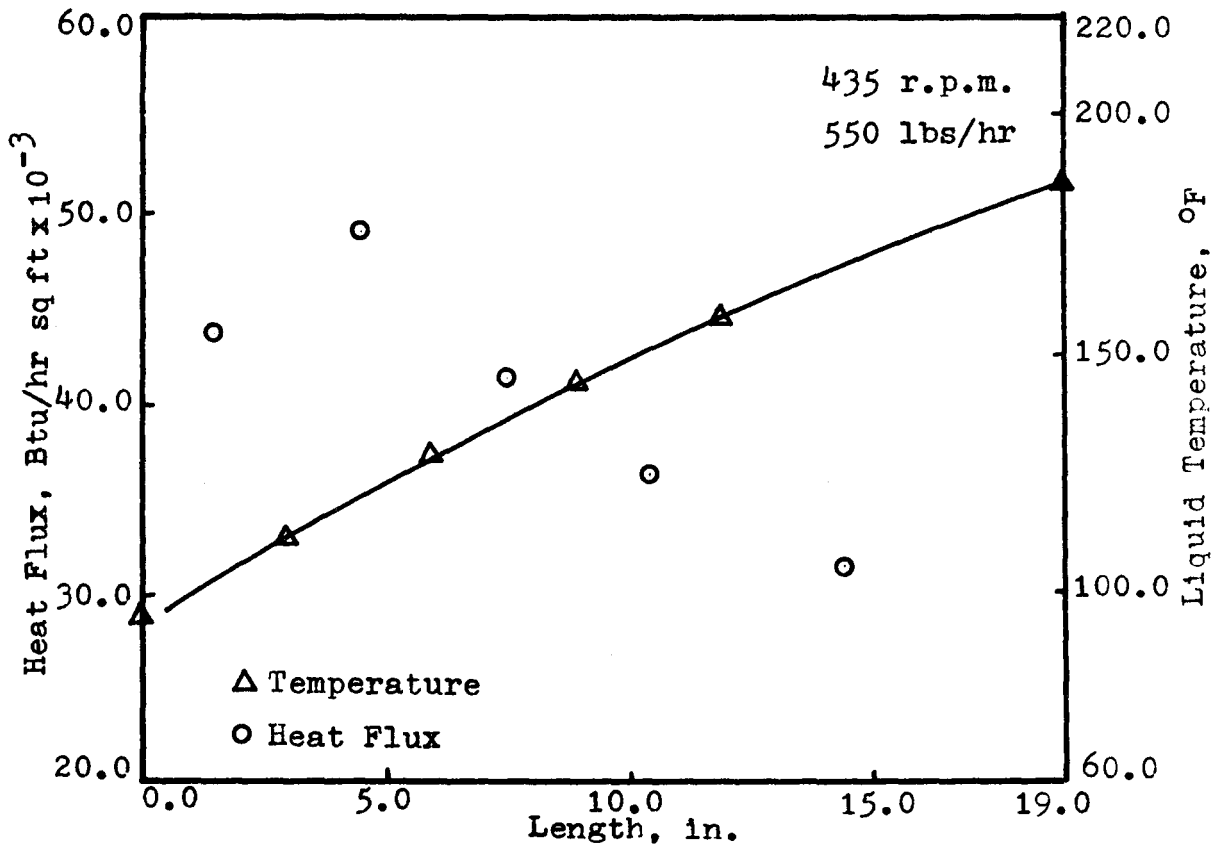

Fig. 4-9. Average Heat Flux and Liquid Temperature

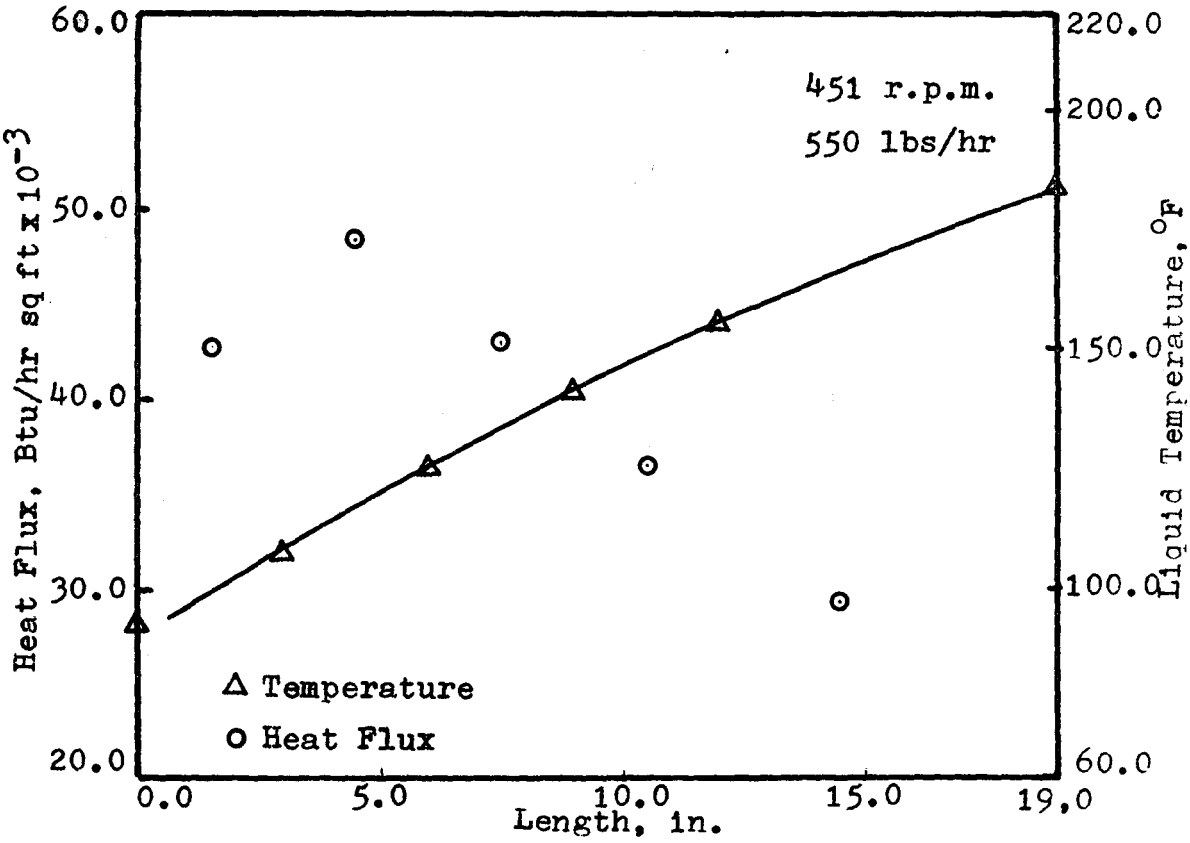

Fig. 4-10. Average Heat Flux and Liquid Temperature

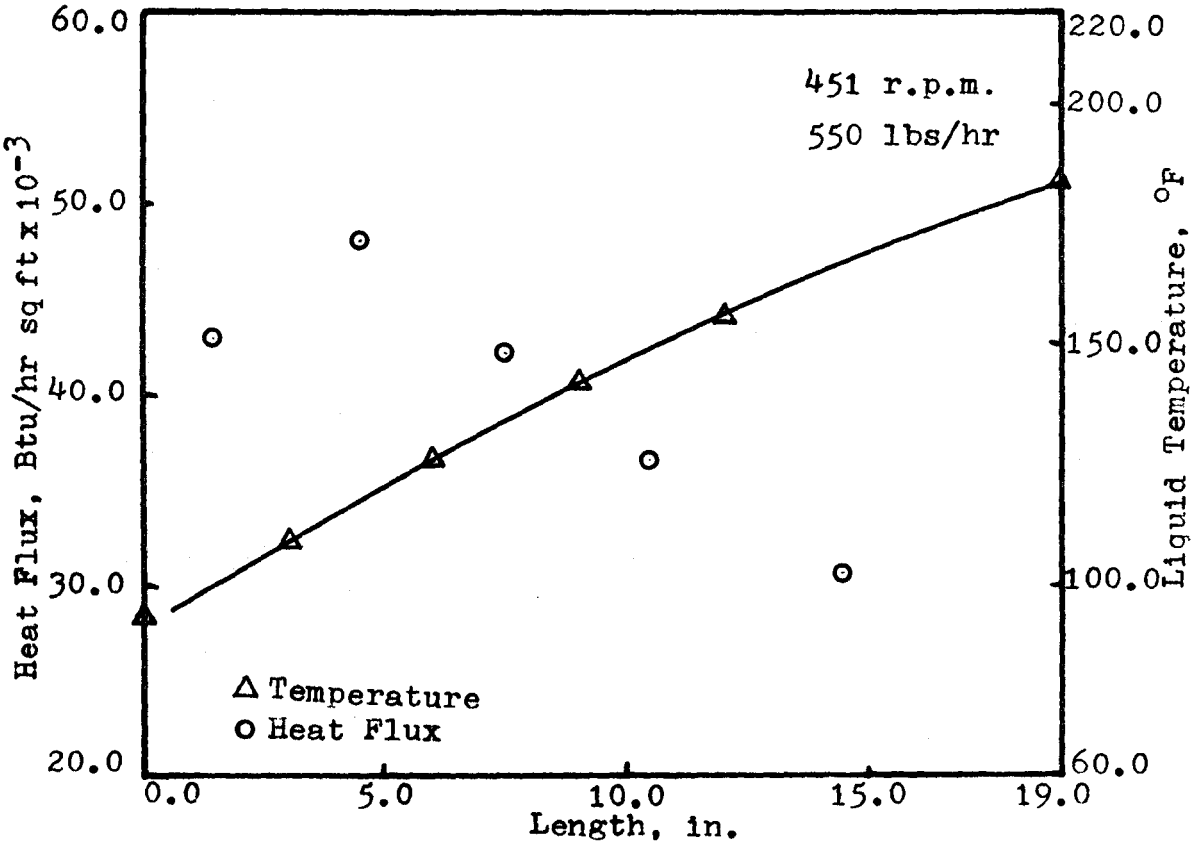

Fig. 4-11. Average Heat Flux and Liquid Temperature

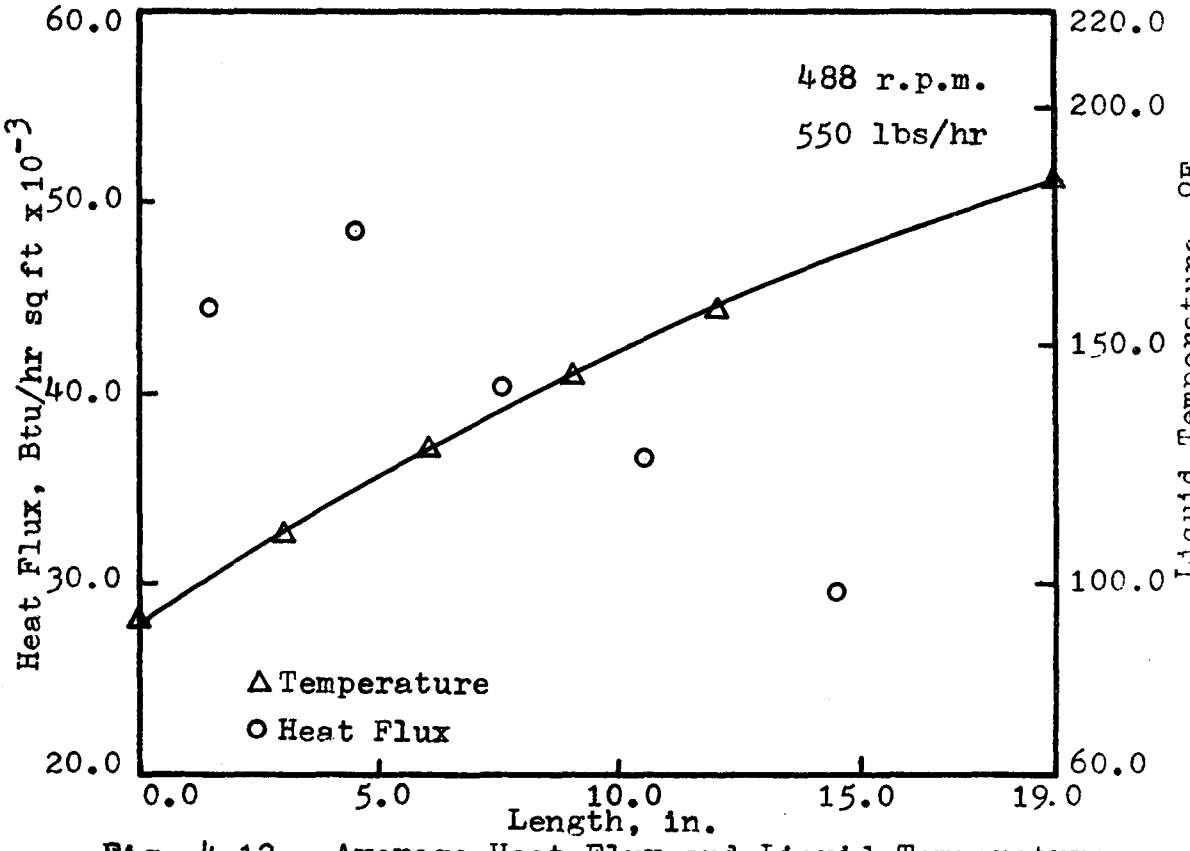

Fig. 4-12. Average Heat Flux and Liquid Temperature

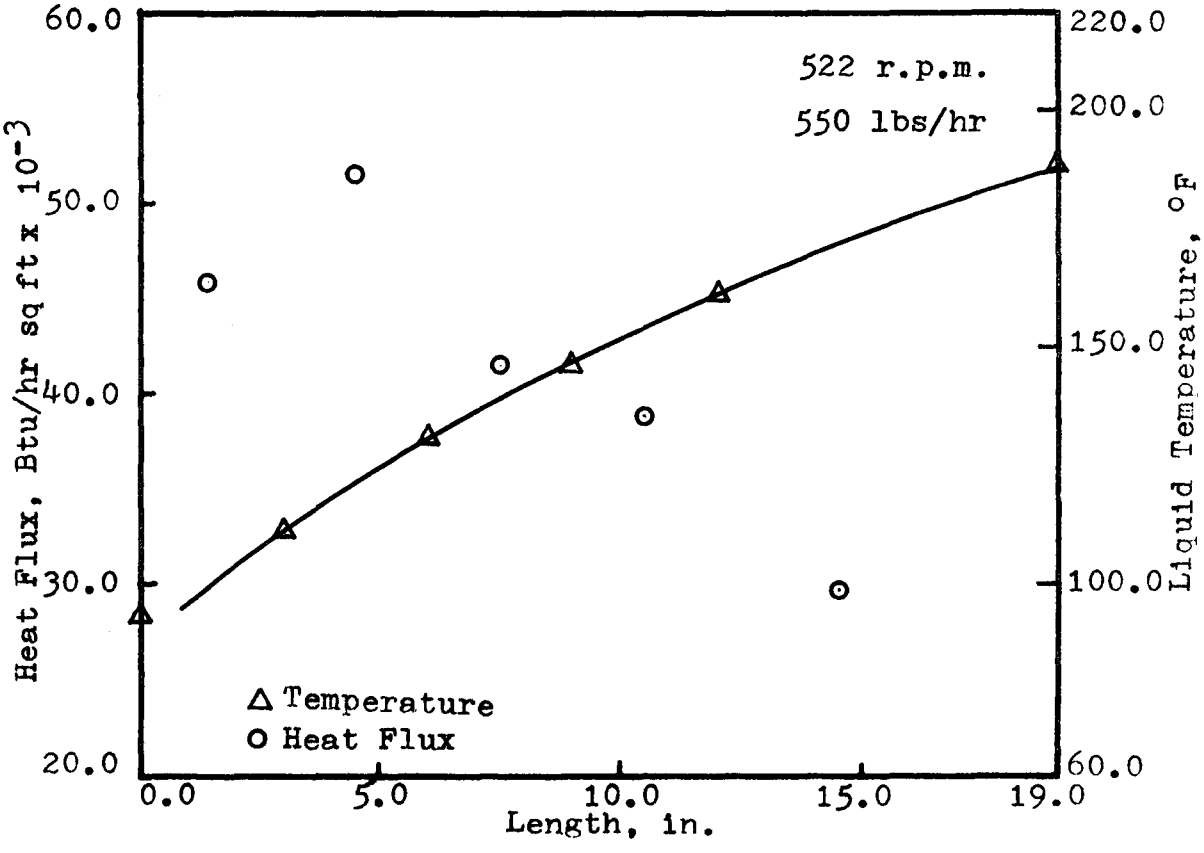

Fig. 4-13. Average Heat Flux and Liquid Temperature

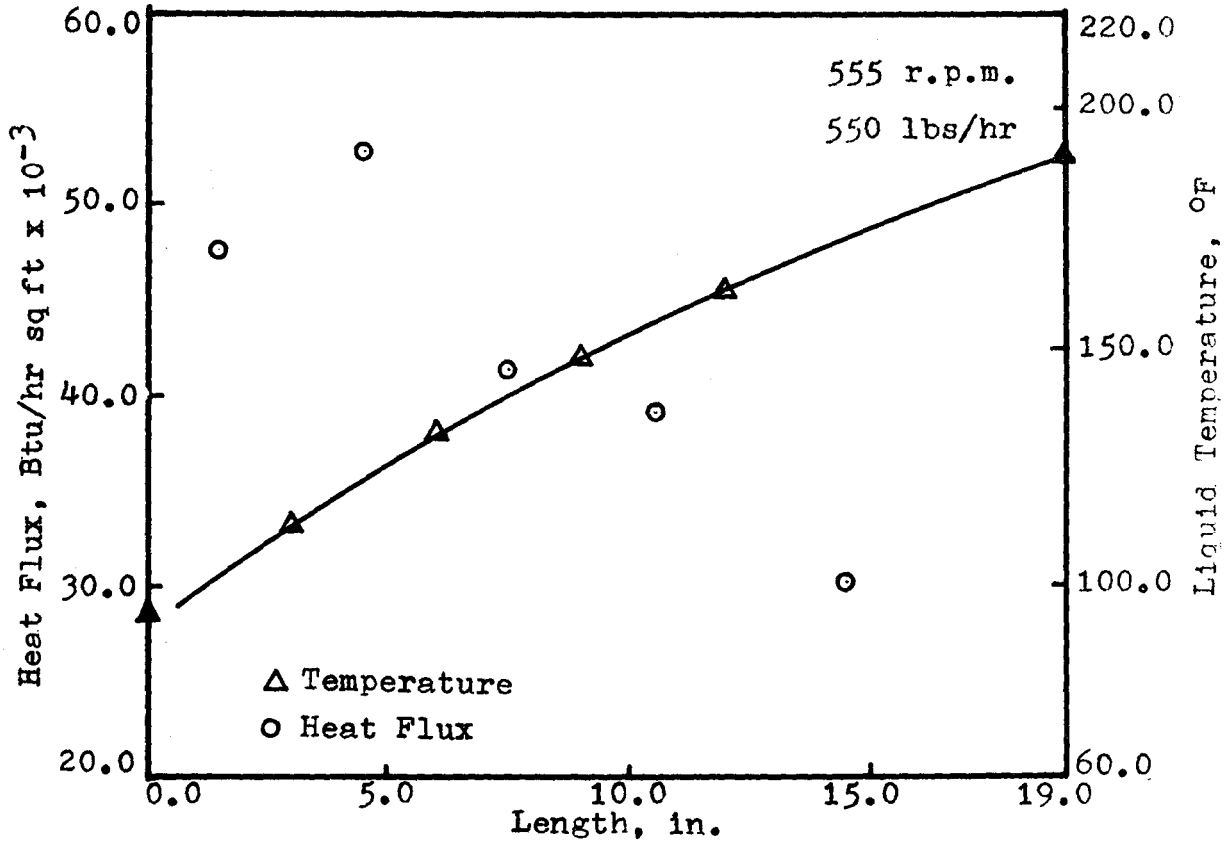

Fig. 4-14. Average Heat Flux and Liquid Temperature

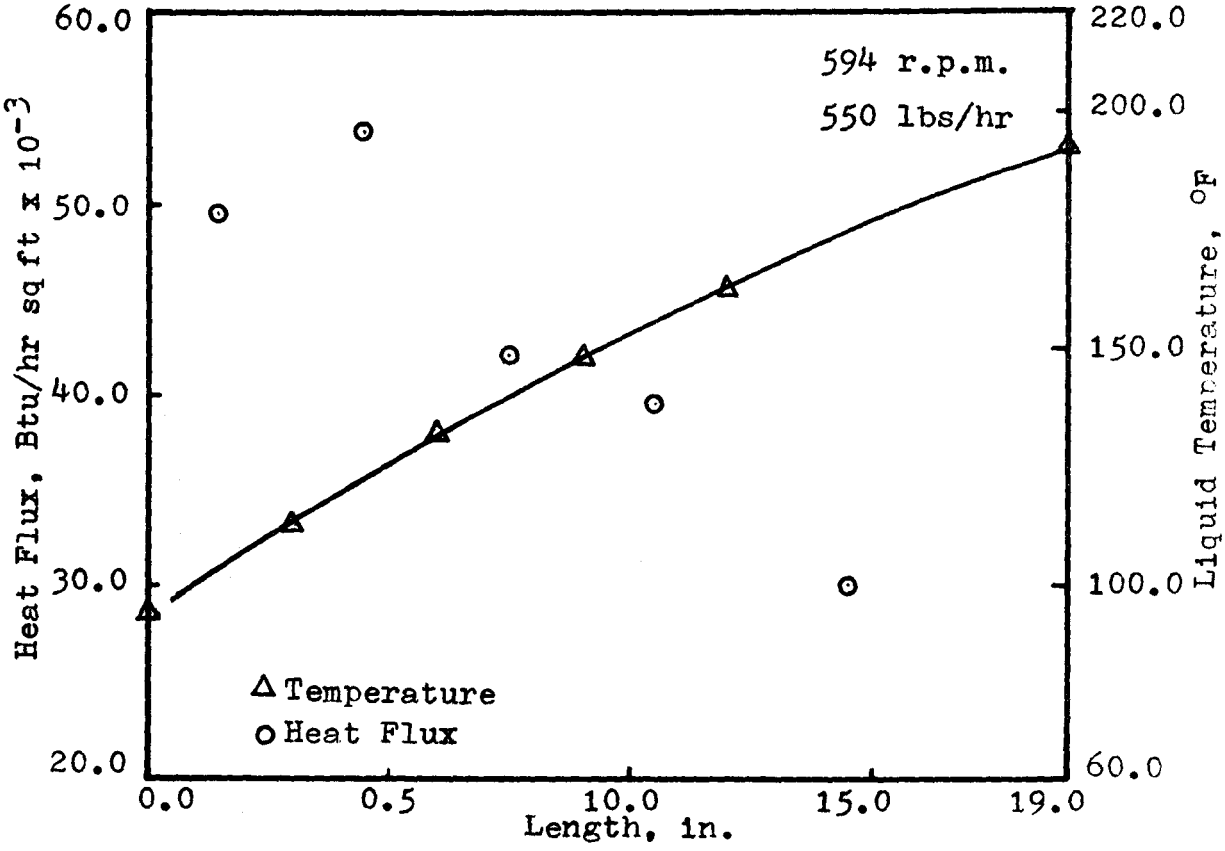

Fig. 4-15. Average Heat Flux and Liquid Temperature

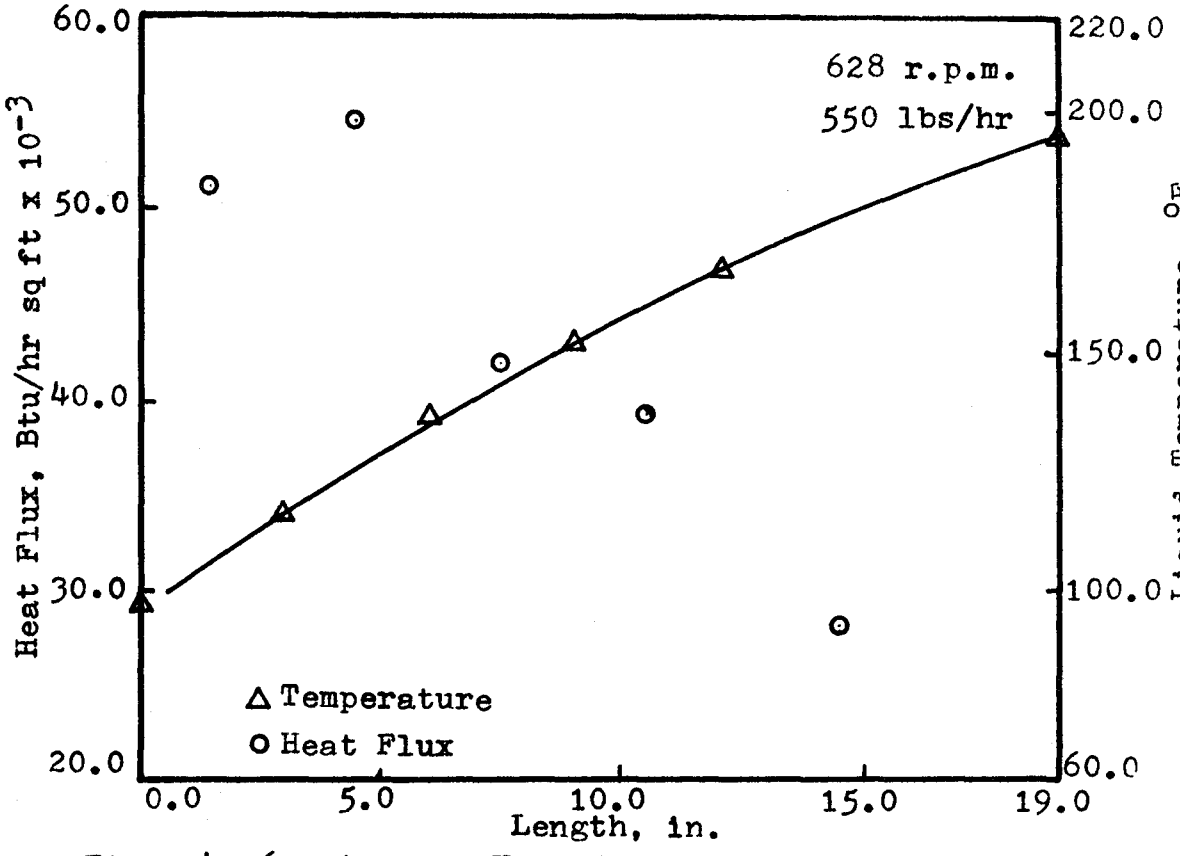

Fig. 4-16. Average Heat Flux and Liquid Temperature

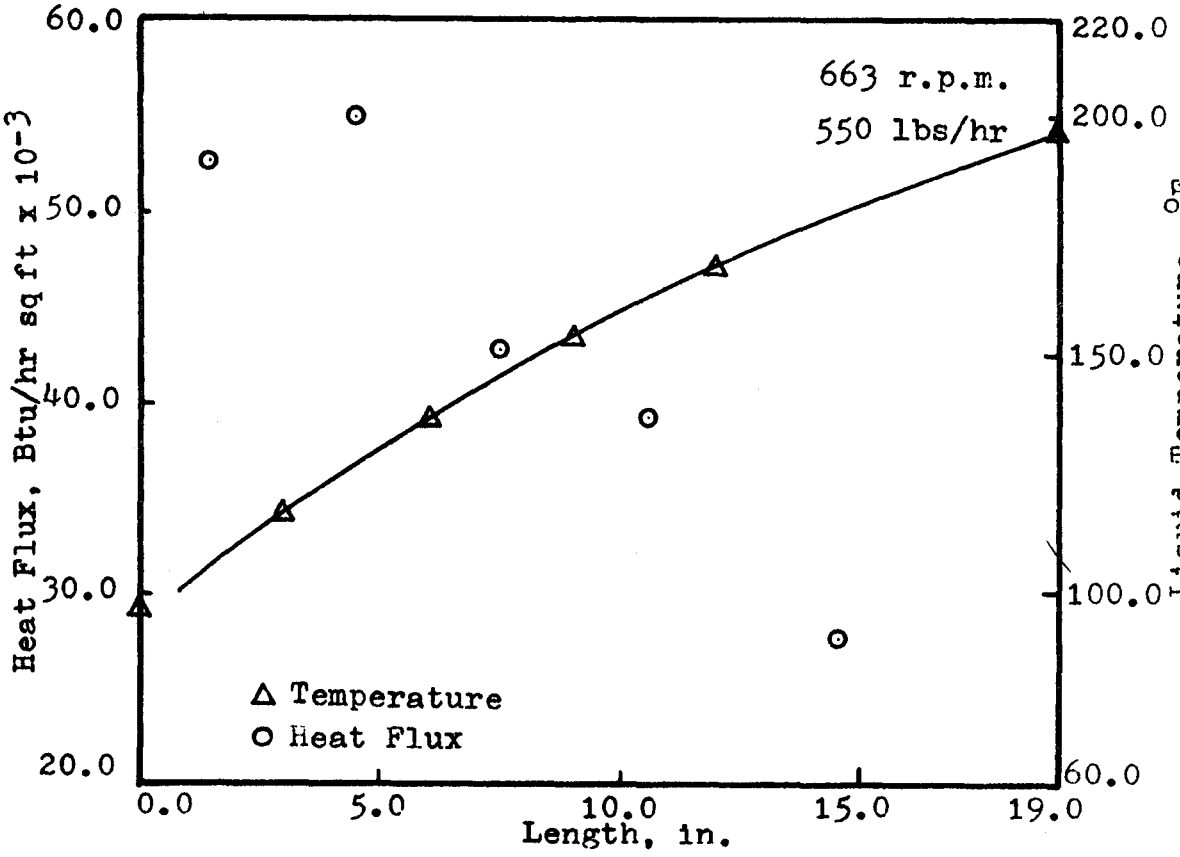

Fig. 4-17. Average Heat Flux and Liquid Temperature

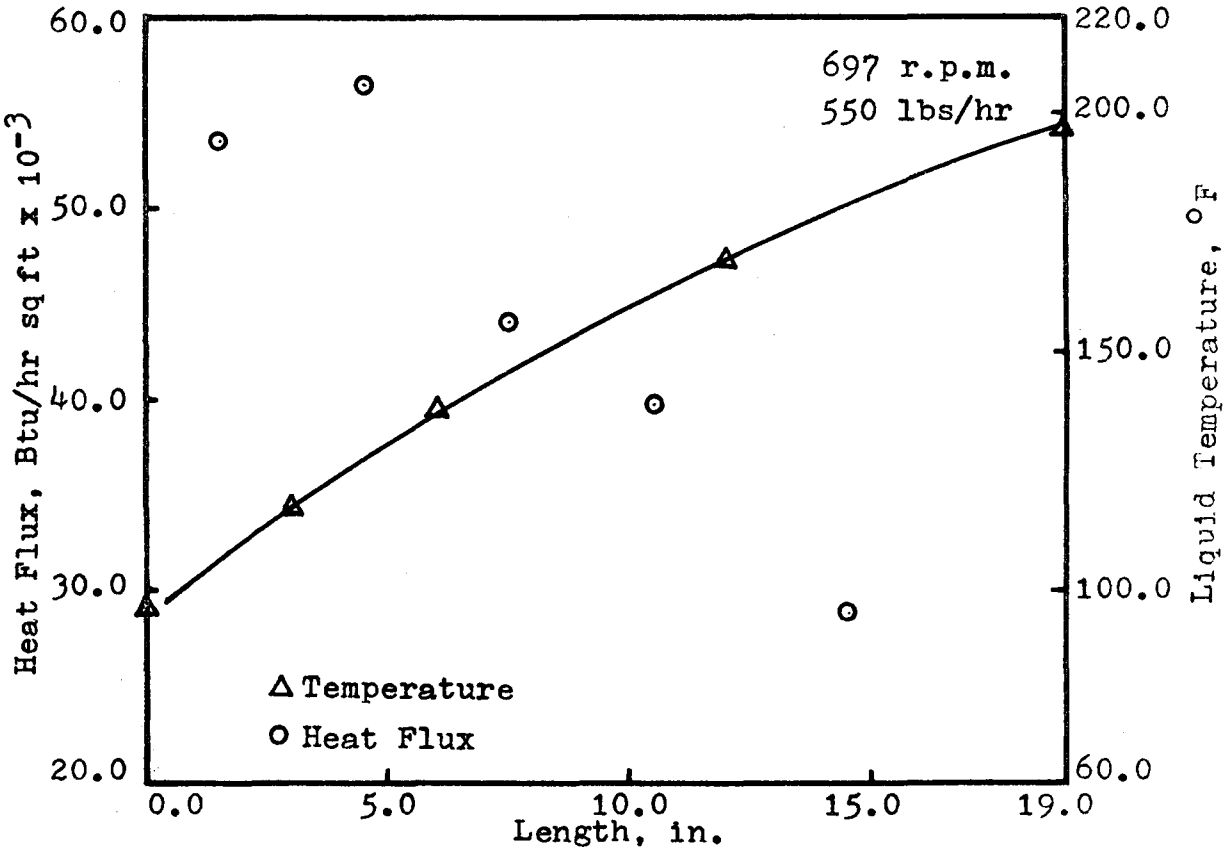

Fig. 4-18. Average Heat Flux and Liquid Temperature

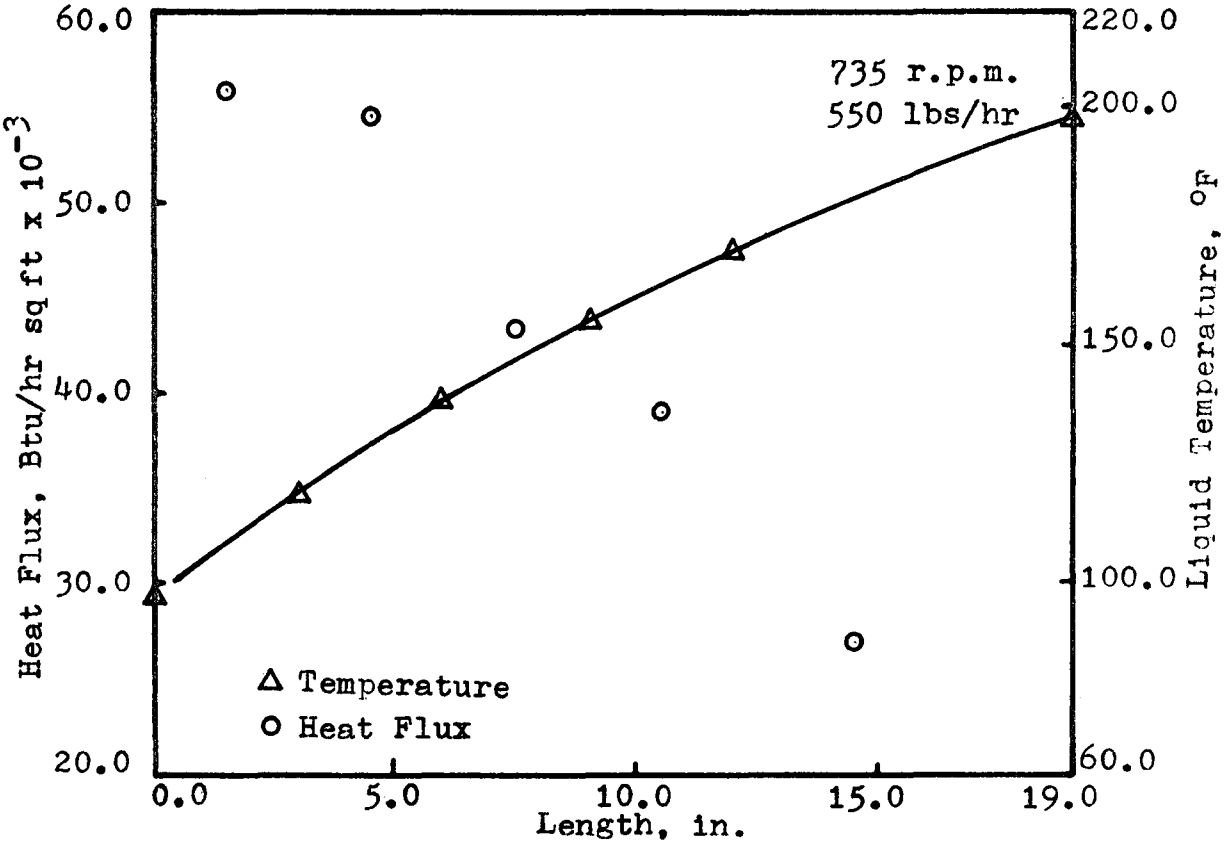

Fig. 4-19. Average Heat Flux and Liquid Temperature

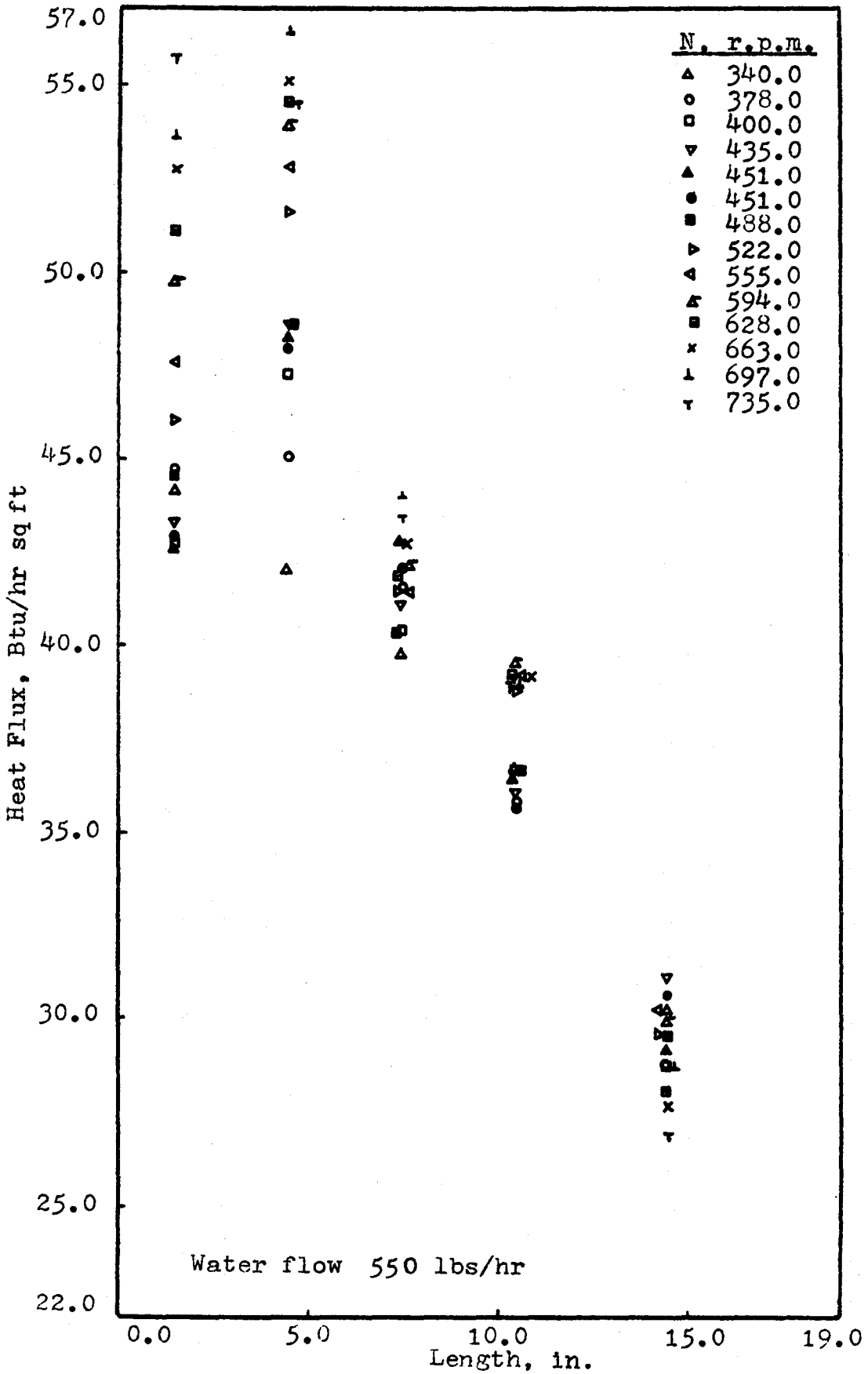

Fig. 4-20. Effect of Rotational Speed on Heat Flux

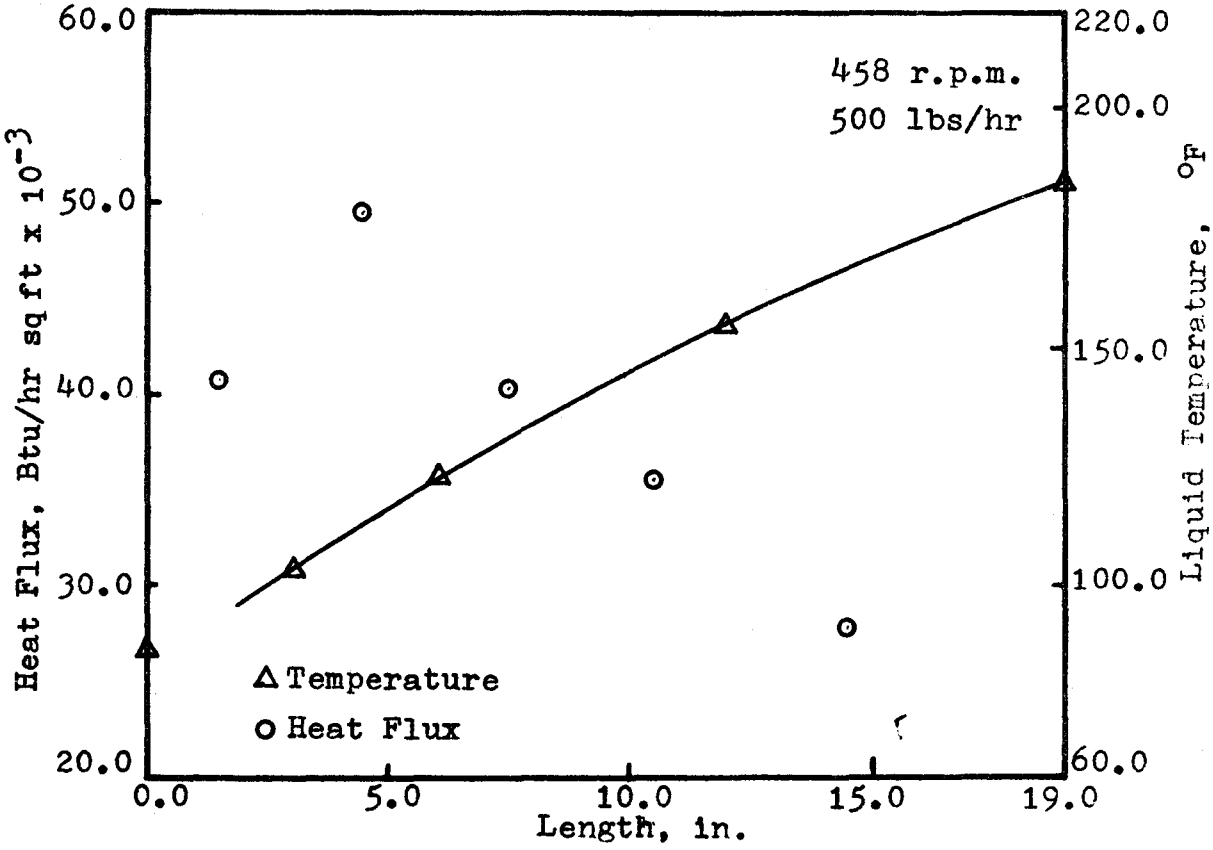

Fig. 4-21. Average Heat Flux and Liquid Temperature

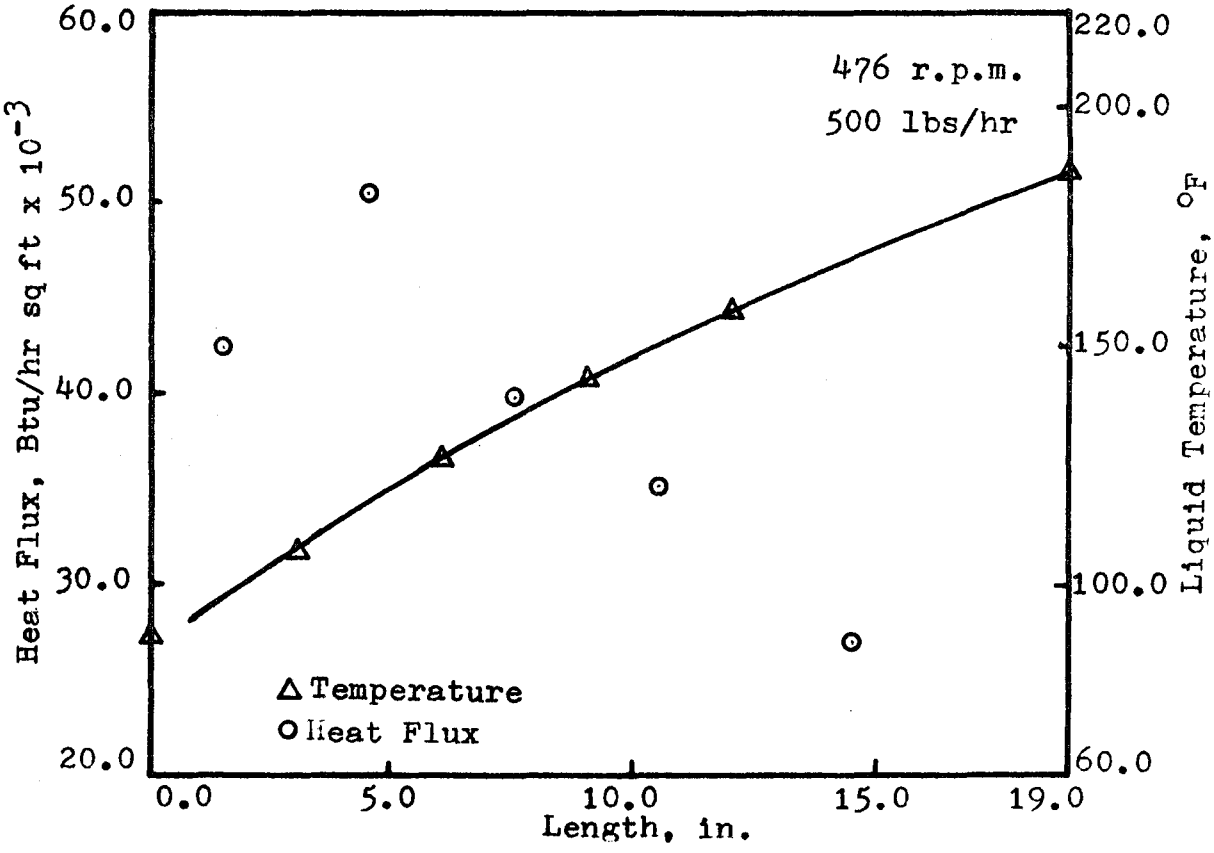

Fig. 4-22. Average Heat Flux and Liquid Temperature

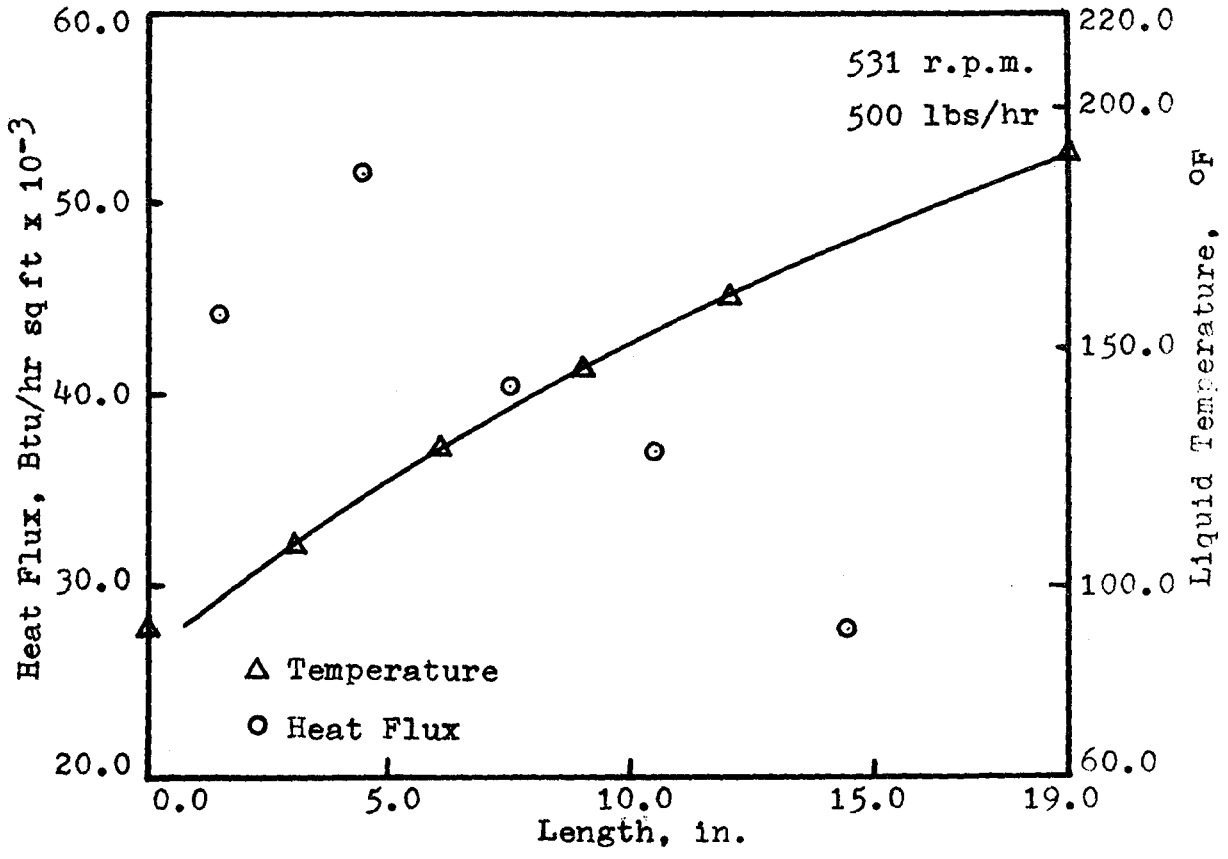

Fig. 4-23. Average Heat Flux and Liquid Temperature

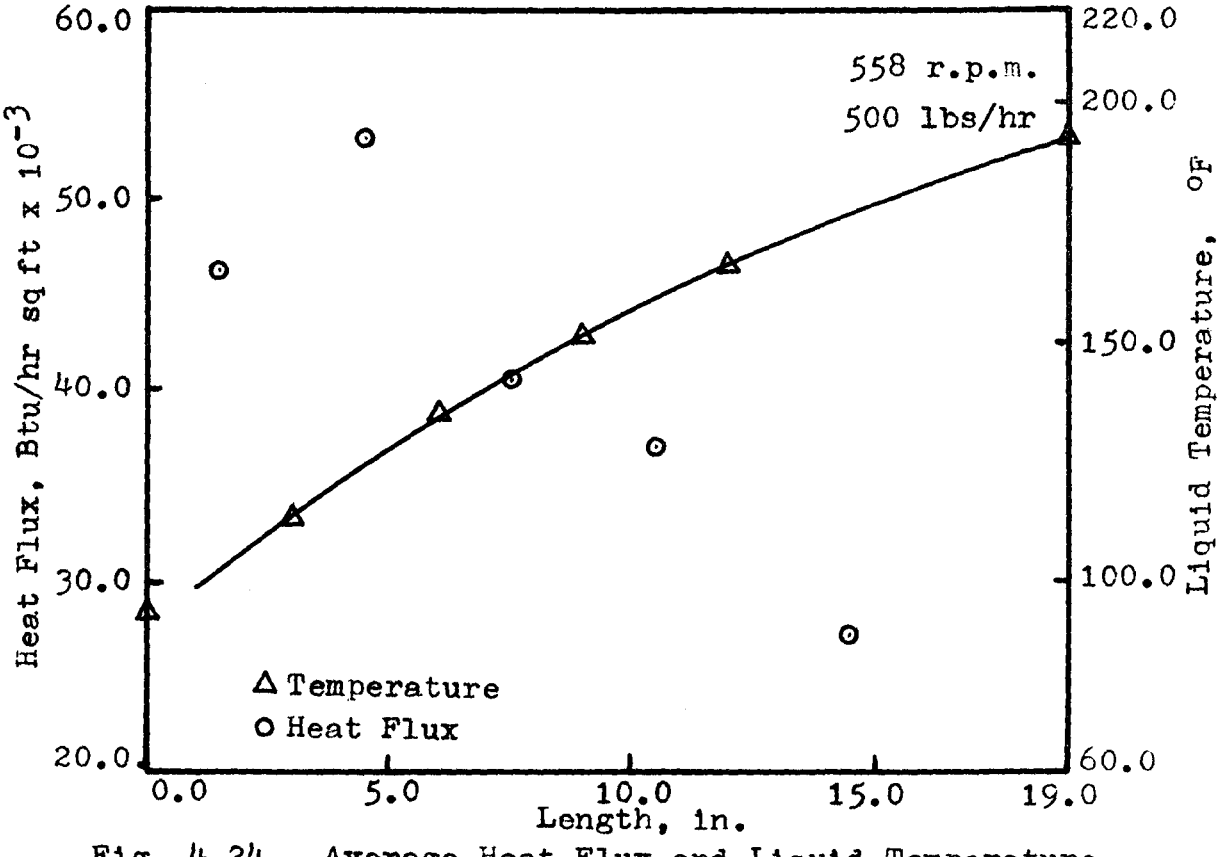

Fig. 4-24. Average Heat Flux and Liquid Temperature

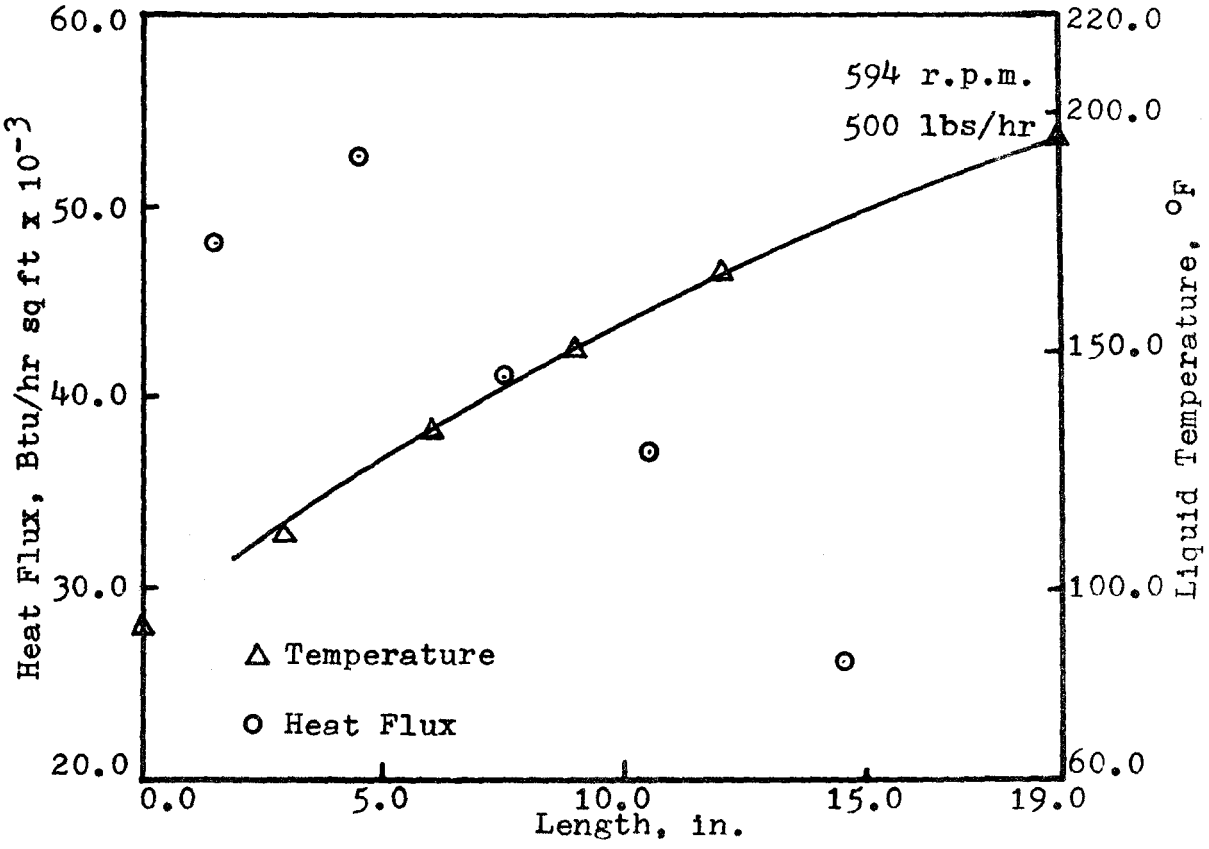

Fig. 4-25. Average Heat Flux and Liquid Temperature

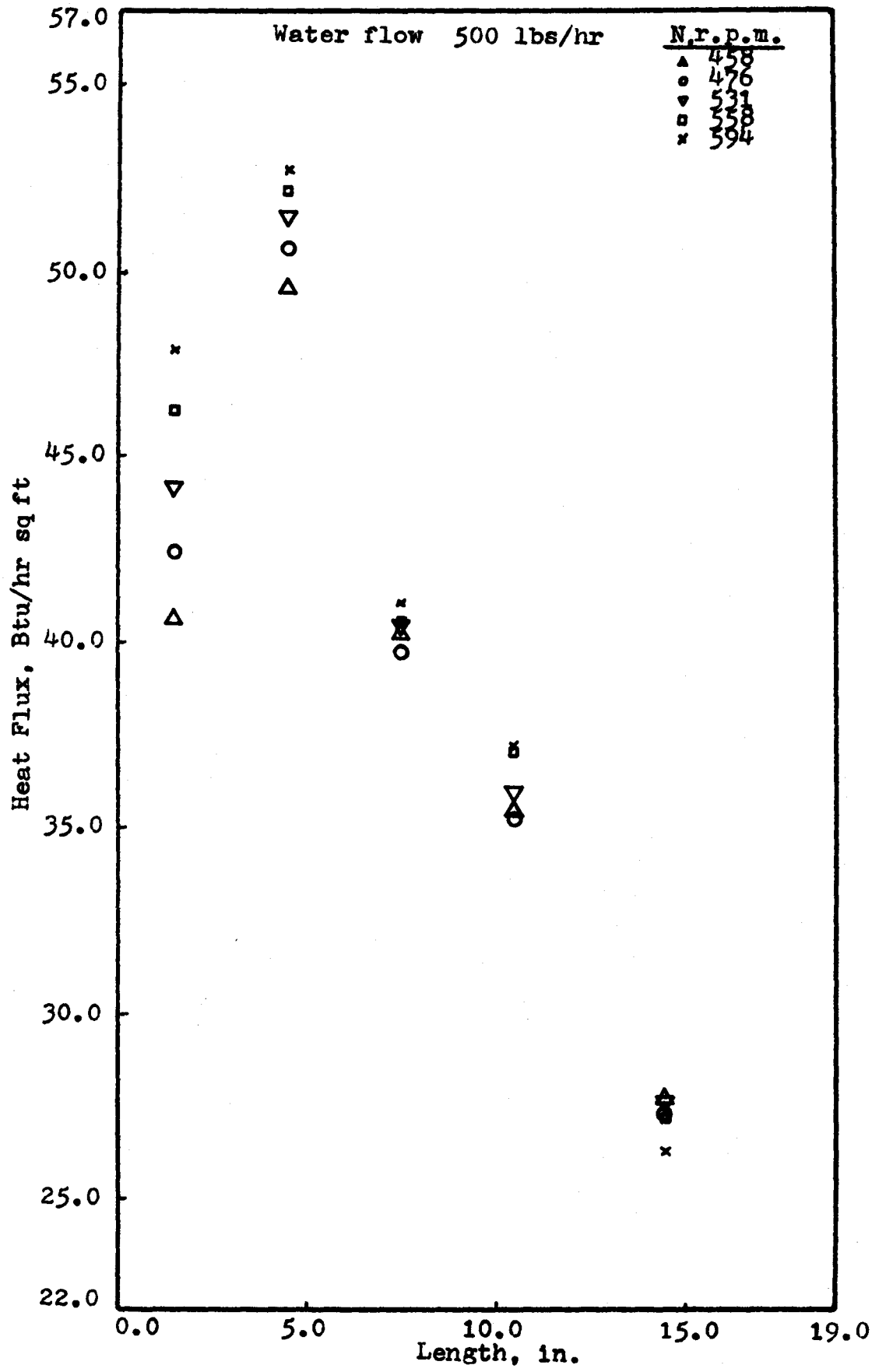

Fig. 4-26. Effect of Rotational Speed on Heat Flux

from these graphs that the heat flux over the first region is, generally, lower than the one over the second section thus giving rise to a maximum in the heat flux distribution curve. This is by no means true. It is due to the fact that the heat transfer rate over the first section has been divided by the entire area of the section which is larger than the actual transfer area. Fig. 4-20 and 4-26 show the variation in heat flux distribution with rotational speed for the two levels of the mass flow rate.

4.5 TIME-AVERAGE LOCAL HEAT TRANSFER COEFFICIENTS

The time-average heat-flux distributions given in Sec. 4.4 were used to calculate time-average local heat transfer coefficients. Four such coefficients could be calculated for each run corresponding to the mid-points of regions 2, 3, 4 and 6 of the heat exchanger shell (See Fig. 3-6.a). These coefficients were obtained using the definition of the heat transfer coefficient

$$\overline{(q/A)} = \bar{h}\,\Delta T \qquad (4\text{-}1)$$

where ΔT is the difference between local wall temperature obtained from actual measurements as discussed in Sec. 4.2 and the local liquid bulk temperature as calculated by the heat balance. The distances from the top of the exchanger at which time-average point coefficients were calculated are 4.5, 7.5, 10.5 and 14.5 in.

The derived time-average local heat transfer coefficients are plotted against rotational speed in Fig. 4-27.

4.6 LOCAL NUSSELT AND ROTARY REYNOLDS NUMBERS

Local Nusselt and rotary Reynolds Numbers were obtained from the derived local heat transfer coefficients and the experimental data. Both moduli were calculated for a characteristic length equal to the diameter of the scrapers which is the same as that of the exchanger. The physical properties of the process liquid were taken at the local liquid bulk temperature. Four local values of each modulus were calculated for each run. The locations correspond to those of the local heat transfer coefficients (See Sec. 4.5). The temperature of the process liquid at each of these locations did not change much (maximum variation 12°F) from one test to another, thus the local Prandtl Number was essentially constant (maximum variation 10%) for all the experimental runs. Since, in addition, the geometrical characteristics of the exchanger were constant, the local Nusselt Number could be plotted against local rotary Reynolds Number, as is shown in Fig. 4-28. The local Nu is plotted against local Re_r for all four locations in Fig. 4-29, but it should be pointed out that in this plot the local Pr varies as much as 50%.

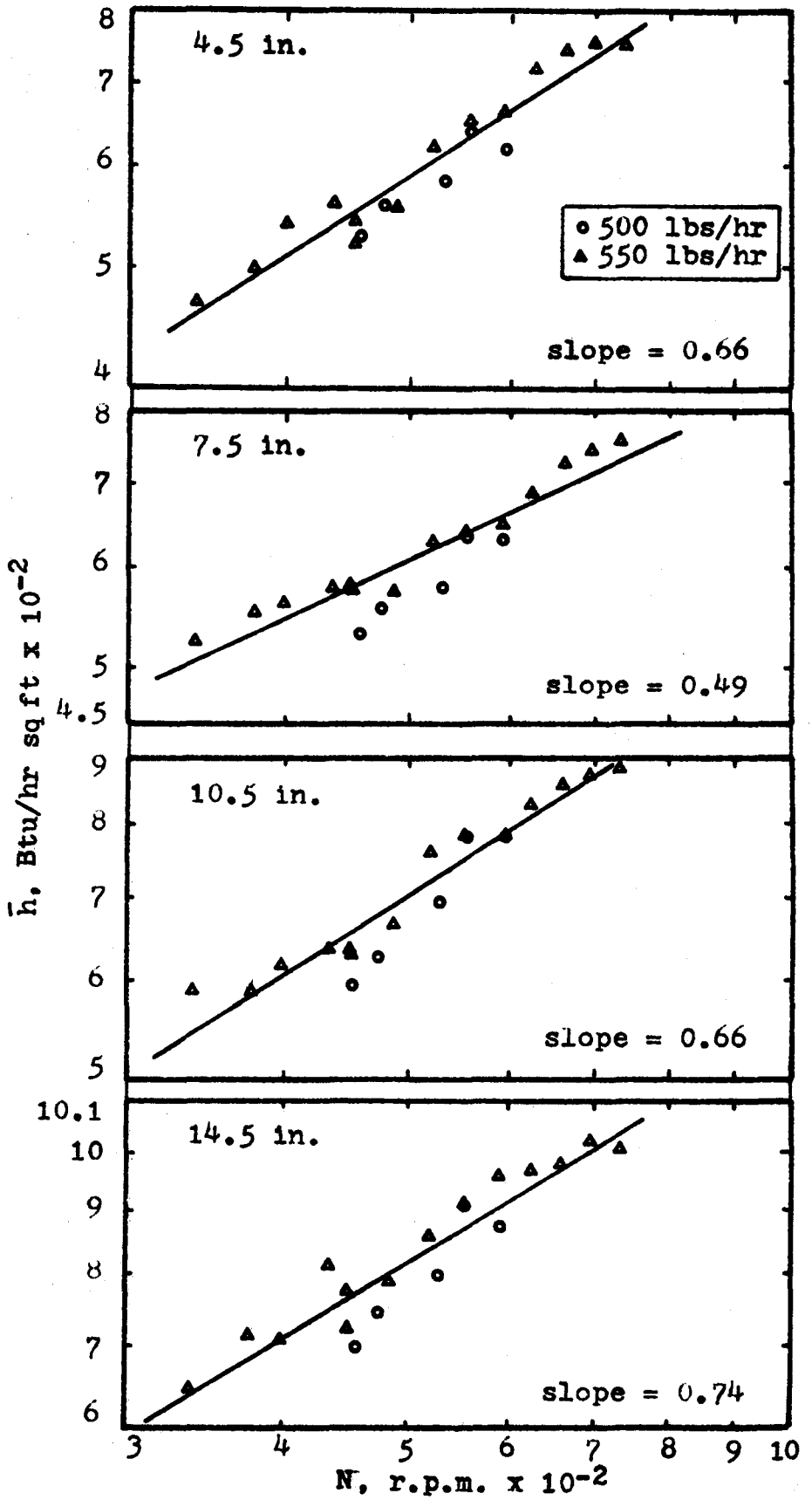

Fig. 4-27. Average Local Coefficients

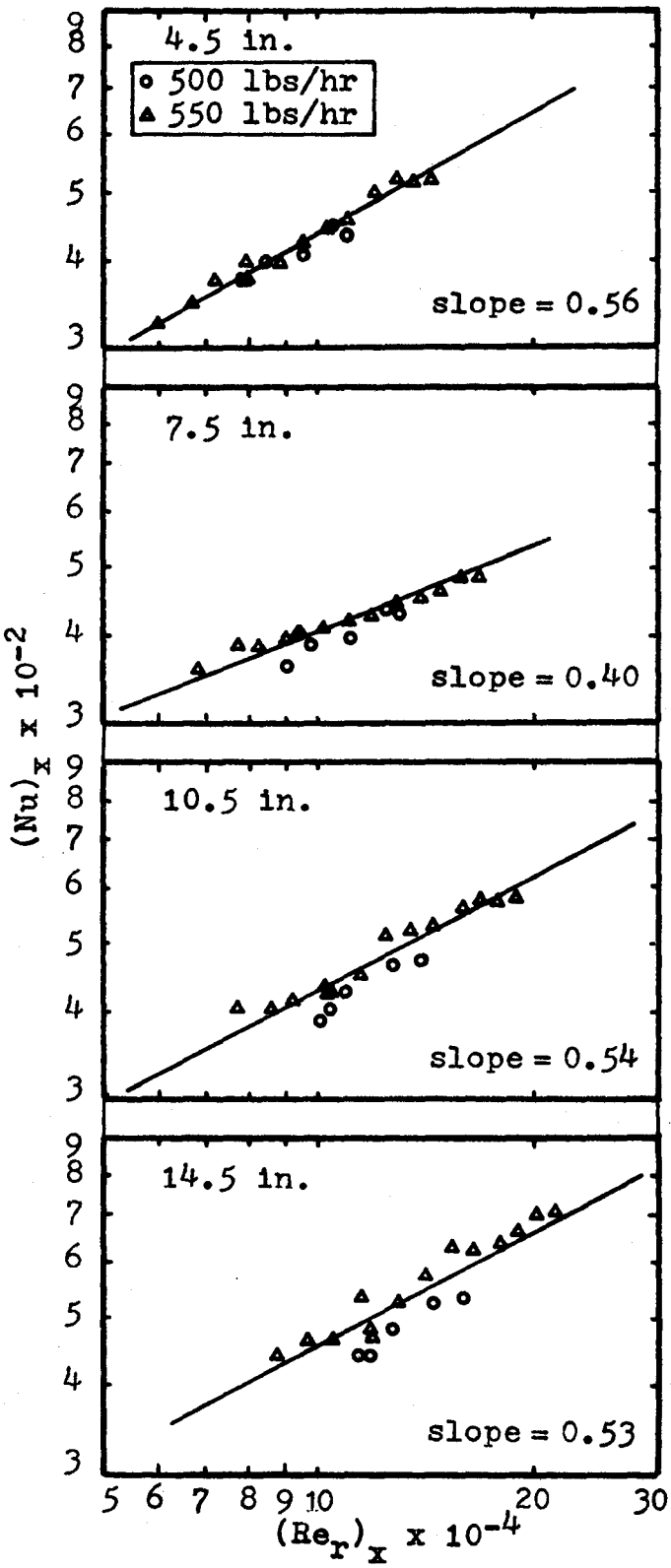

Fig. 4-28. Local Nusselt Number

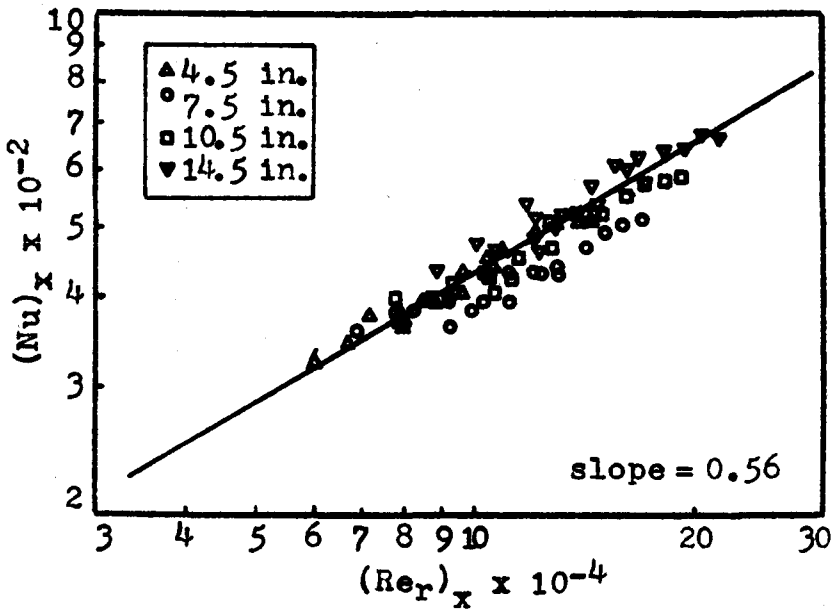

Fig. 4-29

Local Nusselt Number

5. ANALYSIS OF DATA

5.1 HEAT-FLUX METER EMF

Heat-flux meter I always gave a differential emf which was much larger than expected. It was noticed that the disc of this meter had two small holes in it, probably arising during the spark-erosion operation during their construction. These holes may well have been the cause of the great temperature differences developed. Meters II and III did not generate any emf except at such times that a blade was in their neighbourhood. This unexpected behaviour must have been due to some malfunction of the thermocouples. Heat-flux meter IV was the only one to respond to applied heat fluxes. An idealized trace of this meter is shown in Fig. 5-1. The spikes of the micro-switch signal correspond to the times at which the blade-tip was over the heat-flux meter.

In the ideal situation the signal would be a periodic function of time with period the time for a half revolution of the scrapers as shown in Fig. 5-1. In our experiments, however, there was a small difference between the signals obtained for each half revolution. In Fig. 5-2 a typical trace is shown; this output curve is exaggerated so as to emphasize the difference between the two half cycles.

There seems to be little doubt that this difference is associated with the action of the blade, since the heat-

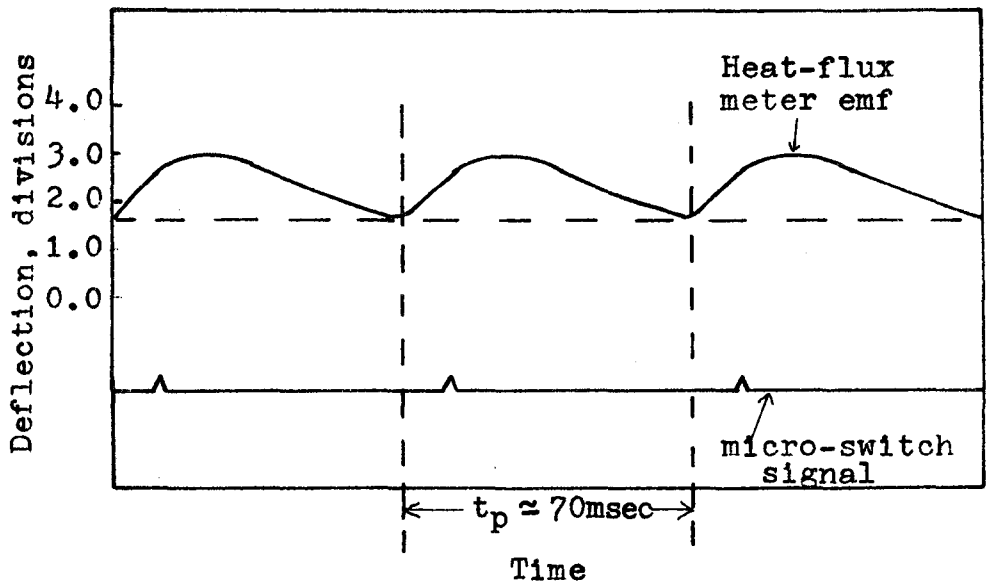

Fig. 5-1

Ideal Heat-Flux Meter Trace

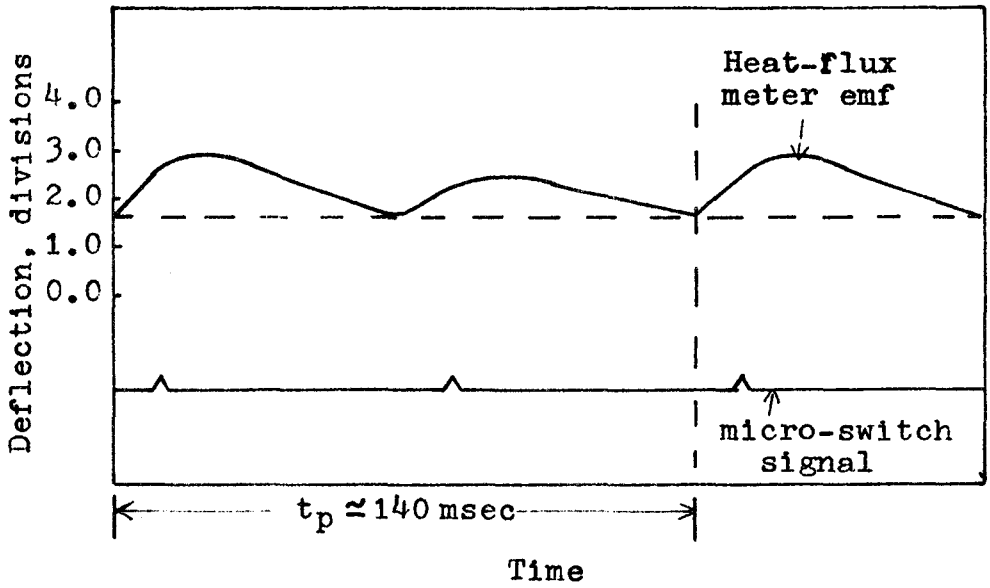

Fig. 5-2

Exaggerated Experimental Trace

flux meter is identical in each case. Different hydrodynamic and thermal conditions have been generated by each of these two blades.

Heat-flux meter IV was the only one to be analysed. Its emf versus time plots were obtained from the Visicorder charts by means of the calibration curve. The temperature and temperature differences were easily obtained from standard tables (See Appendix III). A typical temperature difference plot is given in Fig. 5-3.

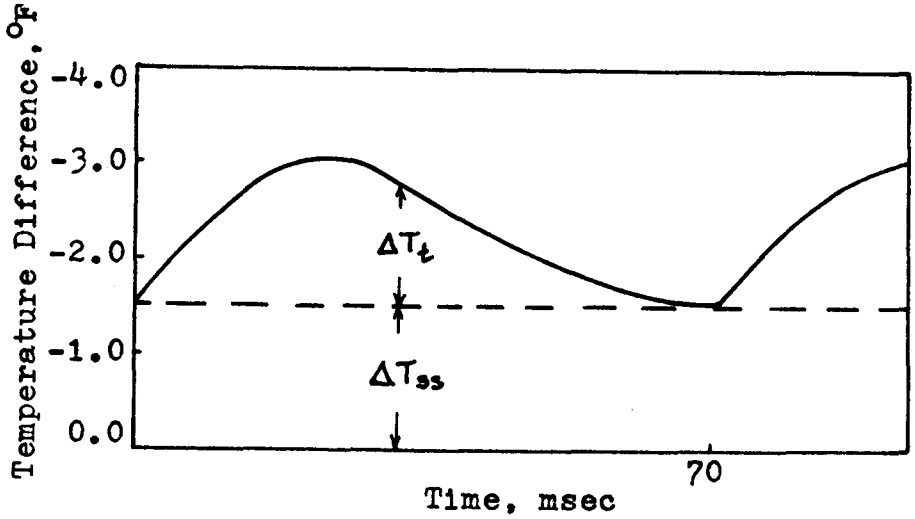

Fig. 5-3. Instantaneous Temperature Difference

The differential temperature for the heat-flux meter under zero heat flux was measured at room temperature and at about 220°F. At both these temperatures the emf was zero. Therefore, the emf developed in any one test was considered to arise solely from the applied heat flux.

5.2 HEAT FLUX MODEL

The temperature difference profile of the heat-flux

meter, shown in Fig. 5-3, was assumed periodic with period the time for half revolution in order to make mathematical analysis simpler. This graph suggested that the temperature difference could be considered as composed of an unsteady state part, ΔT_t, superposed on a steady state one, ΔT_{ss}. On this basis the heat flux could be viewed as consisting of a steady state term which gave rise to ΔT_{ss}, and a time-dependent one which caused ΔT_t to develop. The time-dependent part of the heat flux would be expected to have a graph similar to that of ΔT_t, namely, it would be zero at the beginning of the cycle, increase for some time-interval, and fall off to zero at the end of the cycle. A function that would exhibit such a behaviour was found to be of the form

$$P\theta^* \exp(-\gamma\theta^*)$$

where P and γ are constants. A heat flux model which would give rise to the temperature difference profile of the heat-flux meter could have the form

$$F(\theta^*) = Q + P\theta^* \exp(-\gamma\theta^*) \qquad (5\text{-}1)$$

where Q, P and γ are parameters which would have to be estimated. Repetition of this model would give the cyclic variation of the heat-flux-meter temperature difference with time.

5.3 THEORETICAL TEMPERATURE DIFFERENCE

The theoretical time-dependent temperature profile in the heat-flux meter disc was obtained from the heat conduction equation with the following assumptions:

(a) the heat-flux meter disc exhibits axial symmetry

(b) the temperature at the edge of the disc is constant

(c) the heat flux over the disc is uniform

(d) no heat is lost from the underside of the disc

(e) the curvature of the disc is so small that the disc can be considered flat

(f) the passage of the blade over the meter does not disturb its summetry.

Based on these assumptions and a general heat flux of the form

$$F(\overset{*}{\theta}) = Q + G(\overset{*}{\theta}) \qquad (5\text{-}2)$$

where Q is a constant, the system to be solved was (See also Fig. 5-4):

$$\frac{\partial \overset{*}{T}}{\partial \overset{*}{\theta}} = \alpha \left(\frac{\partial^2 \overset{*}{T}}{\partial \overset{*2}{r}} + \frac{1}{\overset{*}{r}} \frac{\partial \overset{*}{T}}{\partial \overset{*}{r}} + \frac{\partial^2 \overset{*}{T}}{\partial \overset{*2}{z}} \right) \qquad (5\text{-}3.a)$$

$$\overset{*}{\theta} = 0 \qquad \forall\ \overset{*}{r},\overset{*}{z} \qquad \overset{*}{T} = \overset{*}{T}_o(\overset{*}{r},\overset{*}{z}) \qquad (5\text{-}3.b)$$

$$\overset{*}{r} = 0 \qquad \forall\ \overset{*}{\theta},\overset{*}{z} \qquad \frac{\partial \overset{*}{T}}{\partial \overset{*}{r}} = 0 \qquad (5\text{-}3.c)$$

$$\overset{*}{r} = R_o \qquad \forall\ \overset{*}{\theta},\overset{*}{z} \qquad \overset{*}{T} = \overset{*}{T}_w \qquad (5\text{-}3.d)$$

$$\overset{*}{z} = 0 \qquad \forall\ \overset{*}{\theta},\overset{*}{r} \qquad \frac{\partial \overset{*}{T}}{\partial \overset{*}{z}} = 0 \qquad (5\text{-}3.e)$$

$$\overset{*}{z} = t \qquad \forall\ \overset{*}{\theta},\overset{*}{r} \qquad \frac{\partial \overset{*}{T}}{\partial \overset{*}{z}} = -\frac{Q}{k} - \frac{G(\overset{*}{\theta})}{k} \qquad (5\text{-}3.f)$$

The following transformations were made

$$T = \overset{*}{T} - \overset{*}{T}_w, \qquad T_o(r,z) = \overset{*}{T}_o(r,z) - \overset{*}{T}_w,$$

$$\theta = \frac{\alpha\, \overset{*}{\theta}}{R_o^2}, \qquad r = \frac{\overset{*}{r}}{R_o}, \qquad z = \frac{\overset{*}{z}}{t},$$

which resulted in the equations (5-4)

$$\frac{\partial T}{\partial \theta} = \frac{\partial^2 T}{\partial r^2} + \frac{1}{r}\frac{\partial T}{\partial r} + \left(\frac{R_o}{t}\right)^2 \frac{\partial^2 T}{\partial z^2} \qquad (5\text{-}4.a)$$

$$\theta = 0 \qquad \forall\ r,z \qquad T = T_o(r,z) \qquad (5\text{-}4.b)$$

$$r = 0 \qquad \forall\ \theta,z \qquad \frac{\partial T}{\partial r} = 0 \qquad (5\text{-}4.c)$$

$$r = 1 \qquad \forall\ \theta,z \qquad T = 0 \qquad (5\text{-}4.d)$$

$$z = 0 \qquad \forall\ \theta,r \qquad \frac{\partial T}{\partial z} = 0 \qquad (5\text{-}4.e)$$

$$z = 1 \qquad \forall\ \theta,r \qquad \frac{\partial T}{\partial z} = -\frac{tQ}{k} - \frac{tG(\theta)}{k} \qquad (5\text{-}4.f)$$

As it was suggested in section 5-2, the temperature was considered made up of two terms

$$T = T_t + T_{ss} \qquad (5\text{-}5)$$

where $T_t = T(r,z,\theta) - T_w$

and $T_{ss} = T_o(r,z)$

namely the initial condition in equations (5-4) was assumed to be the steady state solution which would satisfy the system of equations (5-6):

$$\frac{\partial^2 T_{ss}}{\partial r^2} + \frac{1}{r}\frac{\partial T_{ss}}{\partial r} + \left(\frac{R_o}{t}\right)^2 \frac{\partial^2 T_{ss}}{\partial z^2} = 0 \qquad (5\text{-}6.a)$$

$$r = 0 \quad \forall\, z \quad \frac{\partial T_{ss}}{\partial r} = 0 \qquad (5\text{-}6.b)$$

$$r = 1 \quad \forall\, z \quad T_{ss} = 0 \qquad (5\text{-}6.c)$$

$$z = 0 \quad \forall\, r \quad \frac{\partial T_{ss}}{\partial z} = 0 \qquad (5\text{-}6.d)$$

$$z = 1 \quad \forall\, r \quad \frac{\partial T_{ss}}{\partial z} = -\frac{t}{k} Q \qquad (5\text{-}6.e)$$

In other words T_{ss} would be the steady state temperature that arose from an applied constant heat flux, Q. By substituting equation (5-5) in equations (5-4) and subtracting equations (5-6), equations (5-7) were obtained which must be satisfied by the transient part, T_t.

$$\frac{\partial T_t}{\partial \theta} = \frac{\partial^2 T_t}{\partial r^2} + \frac{1}{r}\frac{\partial T_t}{\partial r} + \left(\frac{R_o}{t}\right)^2 \frac{\partial^2 T_t}{\partial z^2} \qquad (5\text{-}7.a)$$

$$\theta = 0 \quad \forall\, r,z \quad T_t = 0 \qquad (5\text{-}7.b)$$

$$r = 0 \quad \forall\, \theta,z \quad \frac{\partial T_t}{\partial r} = 0 \qquad (5\text{-}7.c)$$

$$r = 1 \quad \forall\, \theta,z \quad T_t = 0 \qquad (5\text{-}7.d)$$

$$z = 0 \quad \forall\, \theta,r \quad \frac{\partial T_t}{\partial z} = 0 \qquad (5\text{-}7.e)$$

$$z = 1 \quad \forall\, \theta,r \quad \frac{\partial T_t}{\partial z} = -\frac{t}{k} G(\theta) \qquad (5\text{-}7.f)$$

The system of equations (5-7) was solved using the Laplace transformation method. The Laplace transform of T_t

was obtained for a general heat flux G(θ), provided that the transform of G(θ) exists. When applied to the problem at hand, the complete solution of system (5-7) was obtained for the particular heat flux

$$G(\theta) = P\,\theta \exp(-\gamma\theta) \tag{5-8}$$

The solution of this system is given in Appendix II. The solution of equations (5-6) was given by Dernedde (D2).

The theoretical temperature profile in the heat-flux meter disc due to an applied heat flux of the form

$$F(\theta) = Q + P\,\theta \exp(-\gamma\theta) \tag{5-9}$$

was found to be:

$$T = -\sum_{m=1}^{\infty} \frac{2QR_o}{\lambda_m^2 k} \frac{J_o(\lambda_m r)}{J_1(\lambda_m)} \frac{\cosh\left(\frac{\lambda_m tz}{R_o}\right)}{\sinh\left(\frac{\lambda_m t}{R_o}\right)}$$

$$-\sum_{m=1}^{\infty} \frac{2PR_o^2 J_o(\lambda_m r)}{kt\lambda_m J_1(\lambda_m)} \left[\frac{\exp(-\lambda_m^2\theta) + \left[(\lambda_m^2 - \gamma) - 1\right]\exp(-\gamma\theta)}{(\lambda_m^2 - \gamma)^2}\right]$$

$$-\sum_{m=1}^{\infty}\sum_{n=1}^{\infty} \frac{4PR_o(-1)^m \cos(m\pi z) J_o(\lambda_m r)}{kt\lambda_m J_1(\lambda_m)}$$

$$\left[\frac{\exp(-\psi_{m,n}^2\theta) + \left[(\psi_{m,n}^2 - \gamma)\theta - 1\right]\exp(-\gamma\theta)}{(\psi_{m,n}^2 - \gamma)^2}\right] \tag{5-10}$$

where $\psi^2_{m,n} = \lambda^2_m + \left(\frac{n\pi R_o}{t}\right)^2$ and λ_m

are the roots of $J_o(\lambda_m) = 0$.

The theoretical temperature difference of the heat-flux meter was obtained from equation (5-10) for $r = 0$ and $z = 1$. It is given in equation (5-11):

$$T = T_C - T_W = T(0, 1, \theta)$$

$$= -\sum_{m=1}^{\infty} \frac{2QR_o}{k\lambda_m^2 J_1(\lambda_m)} \frac{\cosh(\frac{\lambda_m t}{R_o})}{\sinh(\frac{\lambda_m t}{R_o})}$$

$$-\sum_{m=1}^{\infty} \frac{2PR_o^2}{kt\lambda_m J_1(\lambda_m)} \left[\frac{\exp(-\lambda_m^2\theta) + \left[(\lambda_m^2 - \gamma)\theta - 1\right]\exp(-\gamma\theta)}{(\lambda_m^2 - \gamma)^2}\right]$$

$$-\sum_{m=1}^{\infty}\sum_{n=1}^{\infty} \frac{4PR_o^2}{kt\lambda_m J_1(\lambda_m)} \left[\frac{\exp(-\psi^2_{m,n}\theta) + \left[(\psi^2_{m,n} - \gamma)\theta - 1\right]\exp(-\gamma\theta)}{(\psi^2_{m,n} - \gamma)^2}\right] \quad (5\text{-}11)$$

where Q, P and γ are parameters which would have to be estimated to make the predicted temperatures agree with those measured.

5.4 PARAMETER ESTIMATION

The parameters Q, P and γ in equation (5-9) could be chosen so that the predicted time-response of the heat-flux meter would correspond to that observed experimentally. To elaborate, the steady state part of equation (5-11) was used

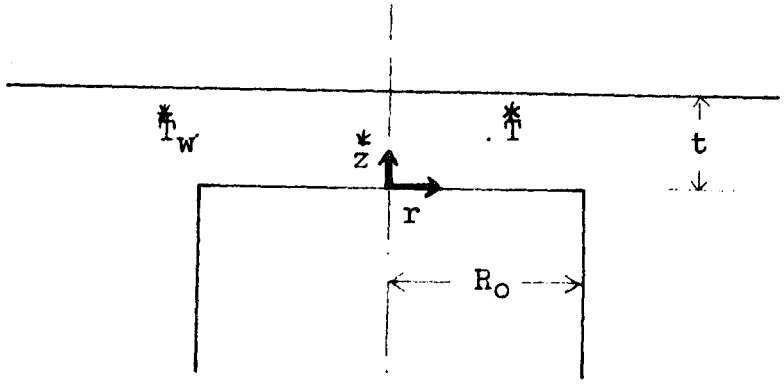

Fig. 5-4

Meter Coordinates

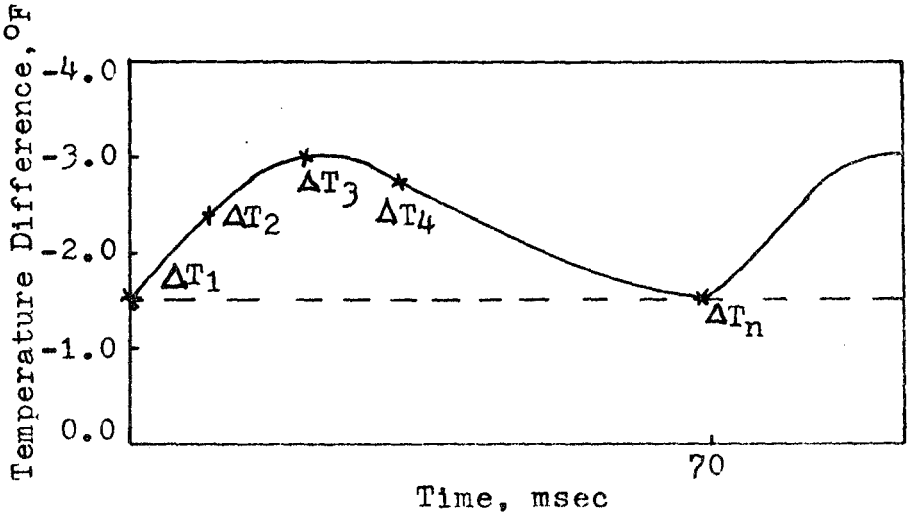

Fig. 5-5

Temperature Difference Points

to find Q through use of the first experimental temperature difference, ΔT_1 (See Fig. 5-5); Reguli-Falsi convergence promotion was used. The other two parameters were estimated using equation (5-11). In this case P and γ were chosen and the temperatures were predicted for the times corresponding to the experimental temperature differences ΔT_2, ΔT_3,... ΔT_n; the sum of the squares of the difference between predicted and observed temperatures,

$$\sum_i \left[\Delta T_i - \Delta T_i(t)\right]^2$$

was evaluated. The best parameters were taken as those where the sum of squares was a minimum. A Rosenbrock search routine (H4) was used as an aid in finding the minimum. The algorithm of the computer program is given in Appendix III.

5.5 CORRECTION OF THE EXPERIMENTAL TEMPERATURE DIFFERENCE

The theoretical, time-averaged, heat flux could be obtained by averaging the model, equation (5-9) over the time for half revolution ($\theta_c = \frac{\alpha \dot{\theta}_c}{R_o^2}$), namely:

$$\bar{F} = \frac{\int_o^{\theta_c} F(\theta)d\theta}{\theta_c} = \frac{\int_o^{\theta_c} \left[Q + P\theta \exp(-\gamma\theta)\right]d\theta}{\theta_c} \qquad (5\text{-}12)$$

or

$$\bar{F} = Q + \frac{P}{\gamma^2\theta_c}\left[1 - \exp(-\gamma\theta_c)\right] - \frac{P}{\gamma}\exp(-\gamma\theta_c) \qquad (5\text{-}13)$$

When the parameters Q, P and γ had been estimated with the nominal heat-flux meter thickness (0.010 in.) in

equation (5-11), the resulting time-averaged theoretical heat flux was much lower than the heat flux evaluated from condensation measurements. Equality between the two fluxes could only be achieved by increasing the disc thickness beyond realistic values. The effect of disc thickness on heat flux is shown in Fig. 5-6. This indicated that the discrepancy between the two fluxes must have been due to other causes and attention was focused on the conduction of heat along the centre thermocouple wire. Heat must have been conducted into the disc since the temperature of the part of the wire exposed to steam was higher than that of the disc. Assuming the wire outside the meter enclosure to be at the saturation temperature of steam, an average temperature difference of 15°F would arise between this point and the centre of the disc. Considering the wire to be insulated, an average heat flux of 6000 Btu/hr sq ft would be entering the disc over the cross sectional area of the wire (0.0035 in. radius). Using Dernedde's steady state solution, it was found that this heat flux would develop a temperature difference of 1°F in the meter. This temperature, being positive, would "neutralize" part of the negative temperature difference measured by the meter because of heat flow to the water film. Although the control temperature varies with time, the variation in the 15°F driving force is less than ±10% and since the accuracy of the "insulated-wire" assumption is unknown the increased accuracy in which a continuous correction is applied was not

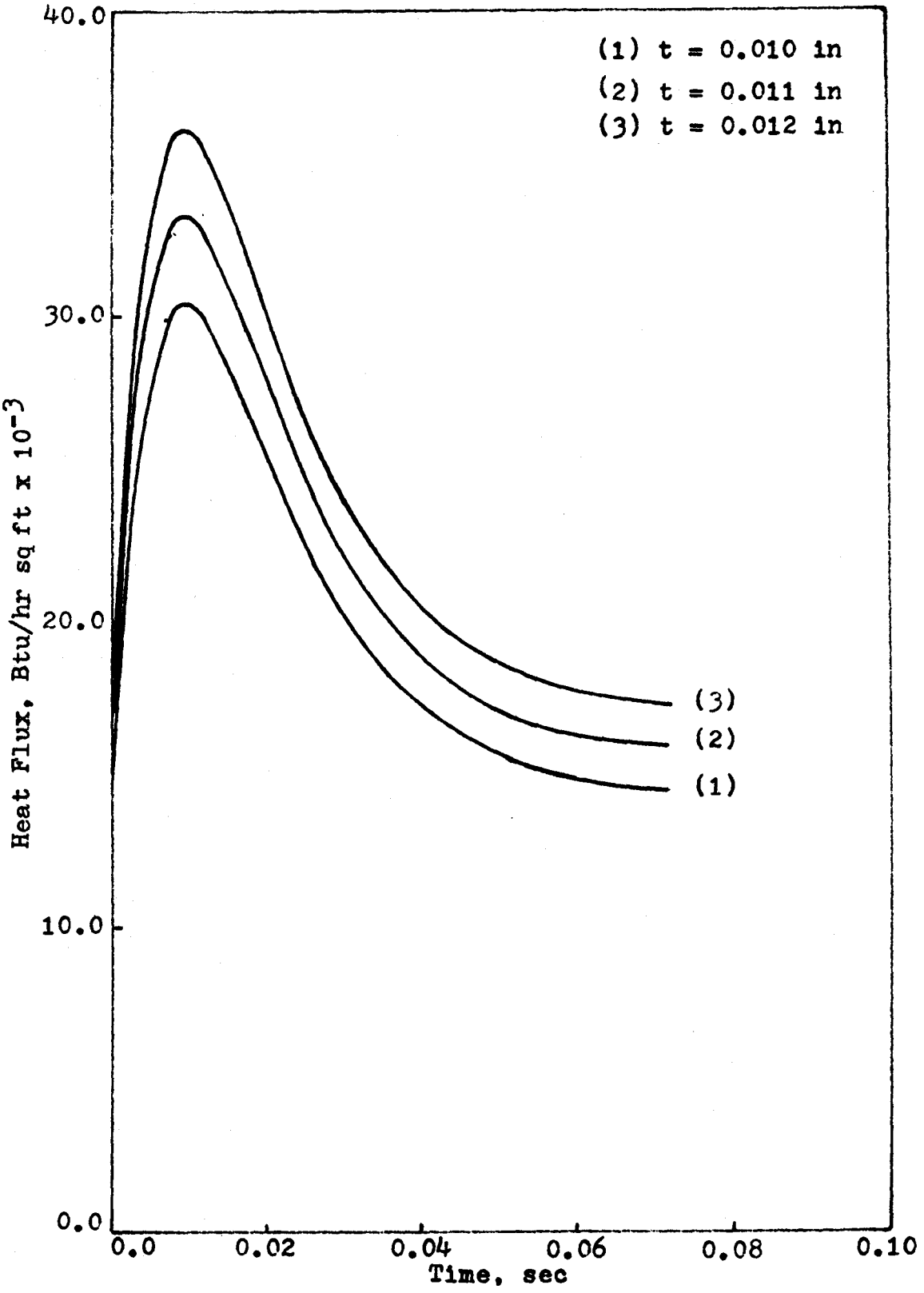

Fig. 5-6

Effect of Disc Thickness

deemed warranted. Based on these arguments a correction term of -1°F was added to the experimental temperature difference profile, and to this corrected profile the theoretical temperature difference was fitted. Without the applied correction the heat-flux meter would have given heat fluxes about 25% lower than those obtained from condensation. The effect of the correction term is to displace the heat-flux curve vertically (See Fig. 5-7).

5.6 INSTANTANEOUS LOCAL HEAT FLUX

The instantaneous local heat flux at the location of the fourth heat-flux meter was obtained from the heat flux model after the parameters Q, P and χ had been estimated. As it was mentioned in Sec. 5.1 there was some difference in the two half-cycles of the periodic differential emf of the meter. A typical sample of this pehnomenon is given in Fig. 5-8, and the corresponding difference in the heat-flux profiles is shown in Fig. 5-9. The difference between the average heat fluxes resulting from different half-cycles was less than 3000 Btu/hr sq ft. In Fig. 5-10 to 5-19 heat fluxes, corresponding to the half-cycles that resulted in highest maximum heat flux, are plotted against real and dimensionless time. The order is that of increasing rotational speed.

The times at which the maximum heat fluxes occurred approximately corresponded to the times at which the blade-tip was over the heat-flux meter.

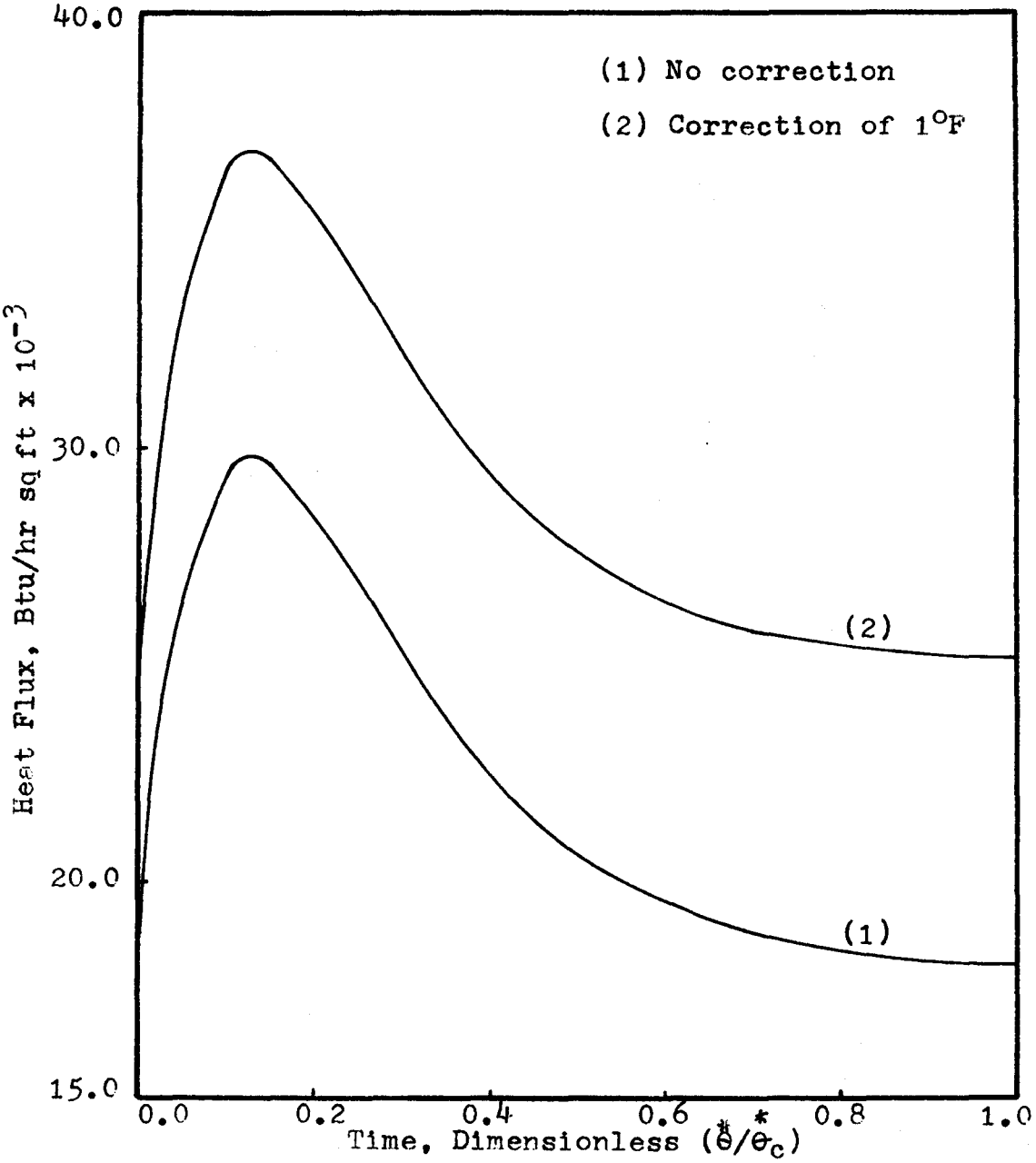

Fig. 5-7

Effect of Conduction Correction

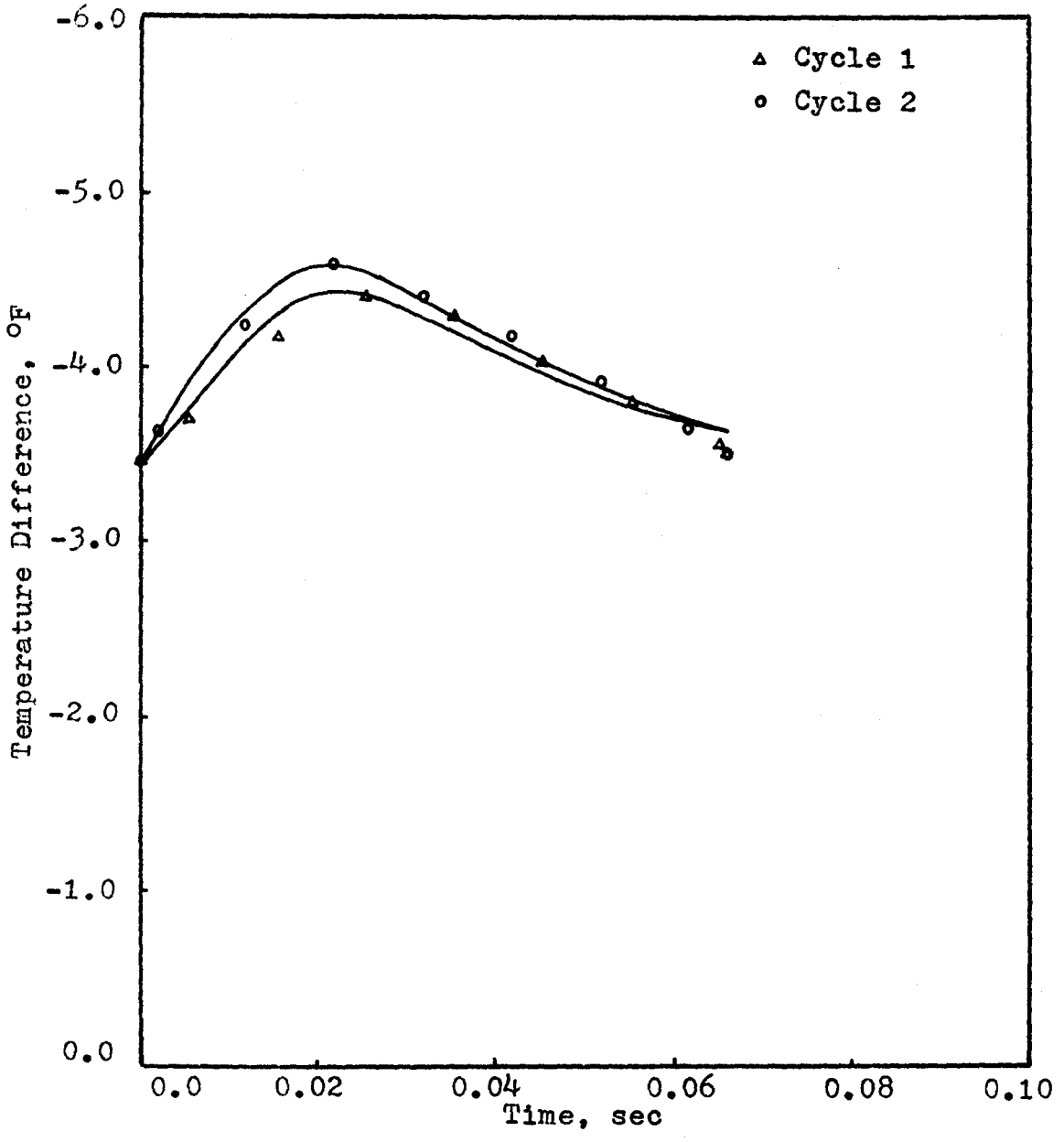

Fig. 5-8

Cycle Difference in Temperature

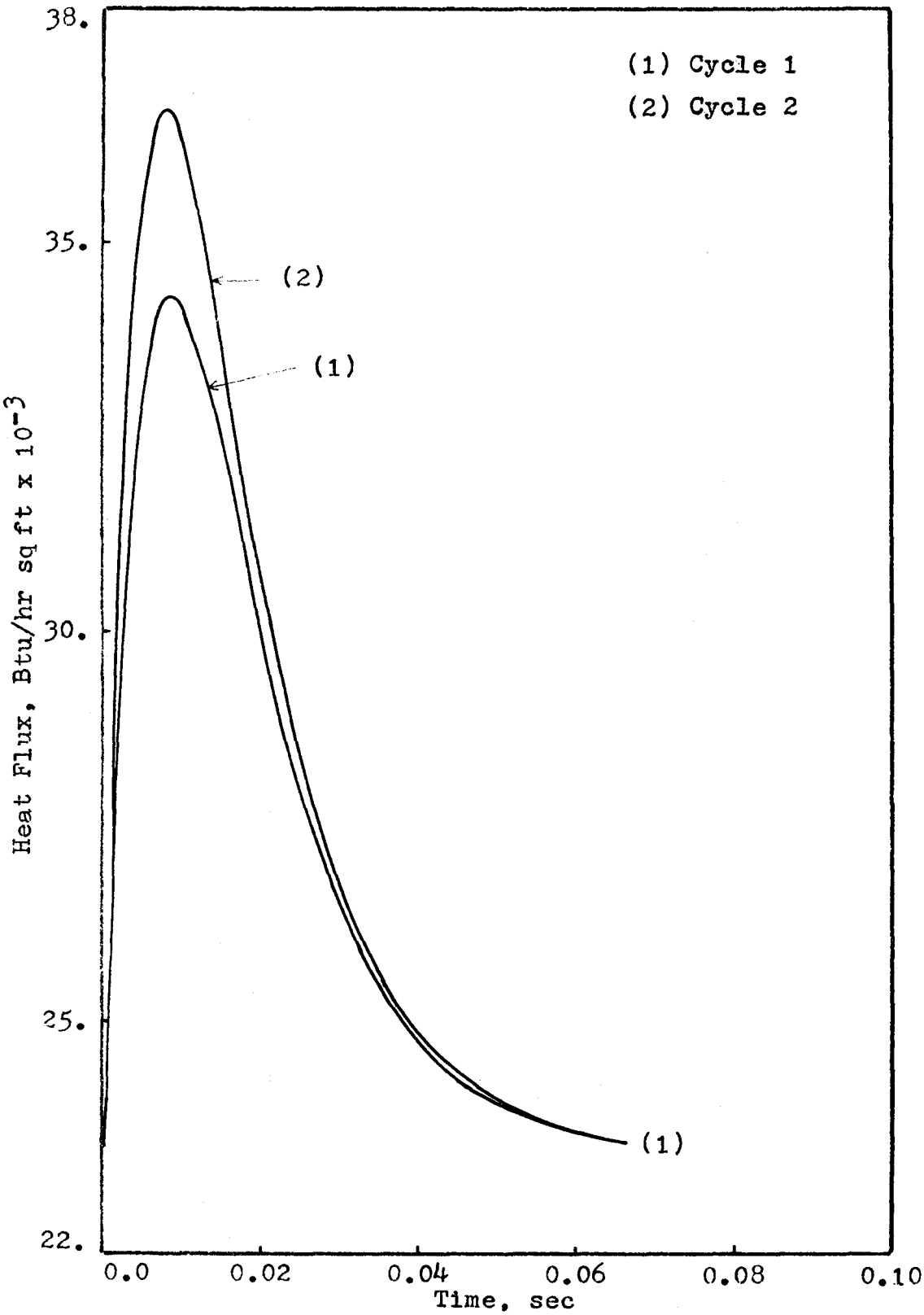

Fig. 5-9

Cycle Difference in Heat Flux

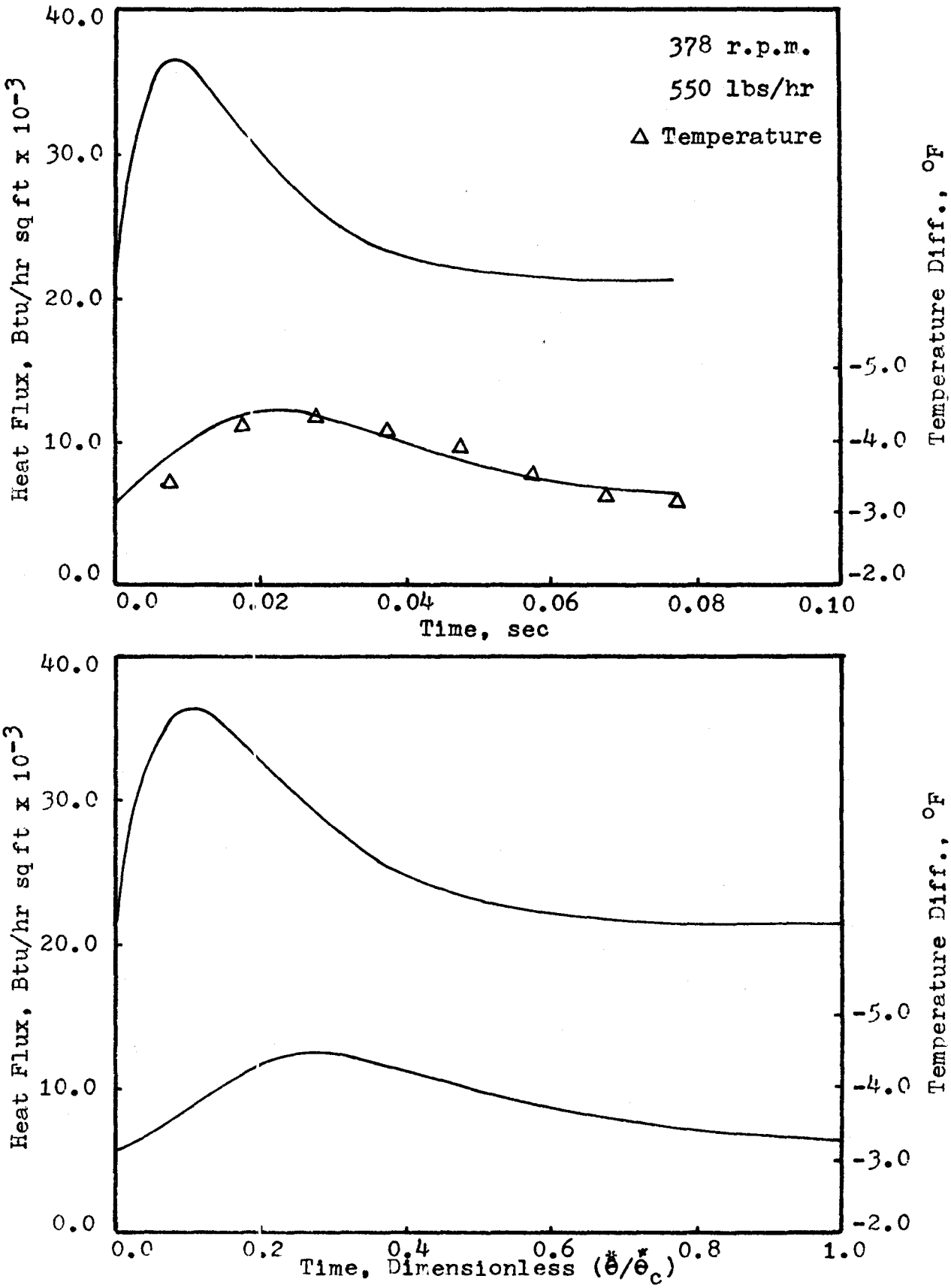

Fig. 5-10

Instantaneous Heat Flux

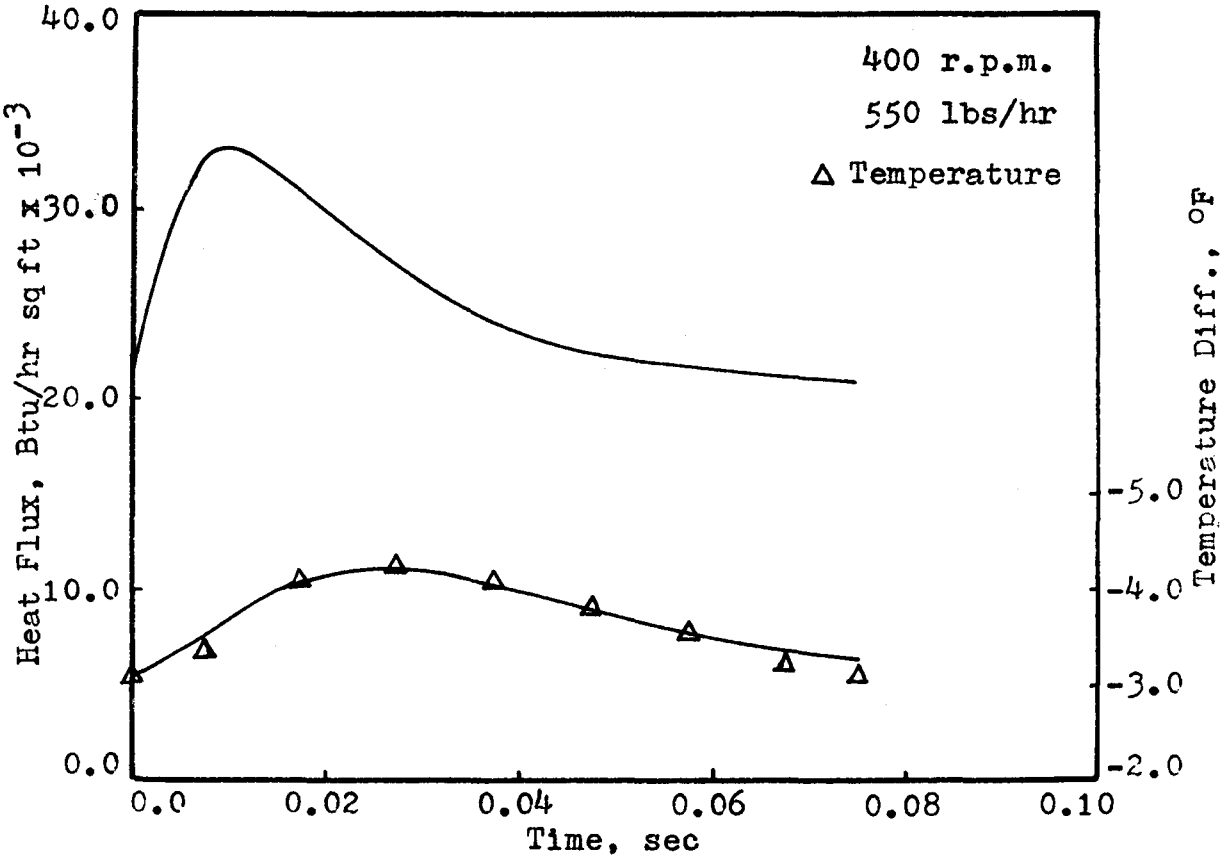

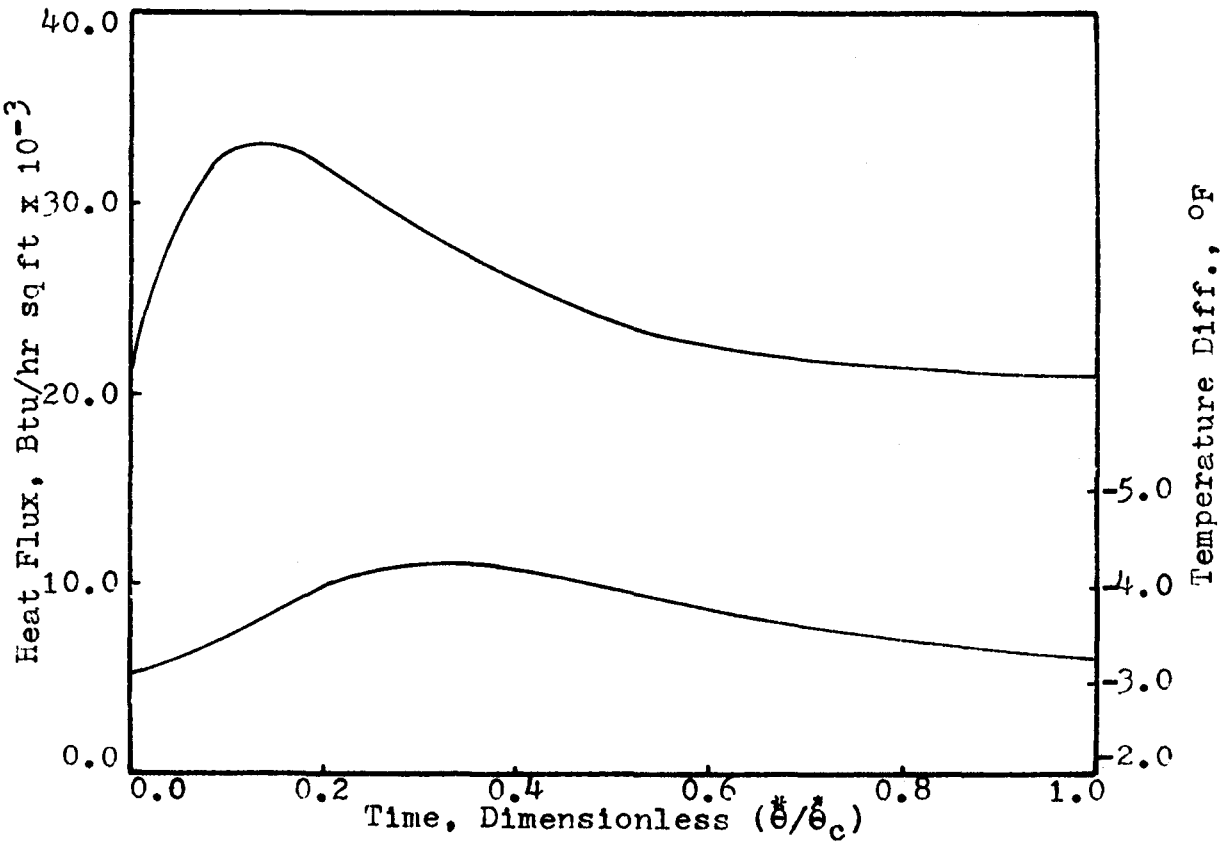

Fig. 5-11

Instantaneous Heat Flux

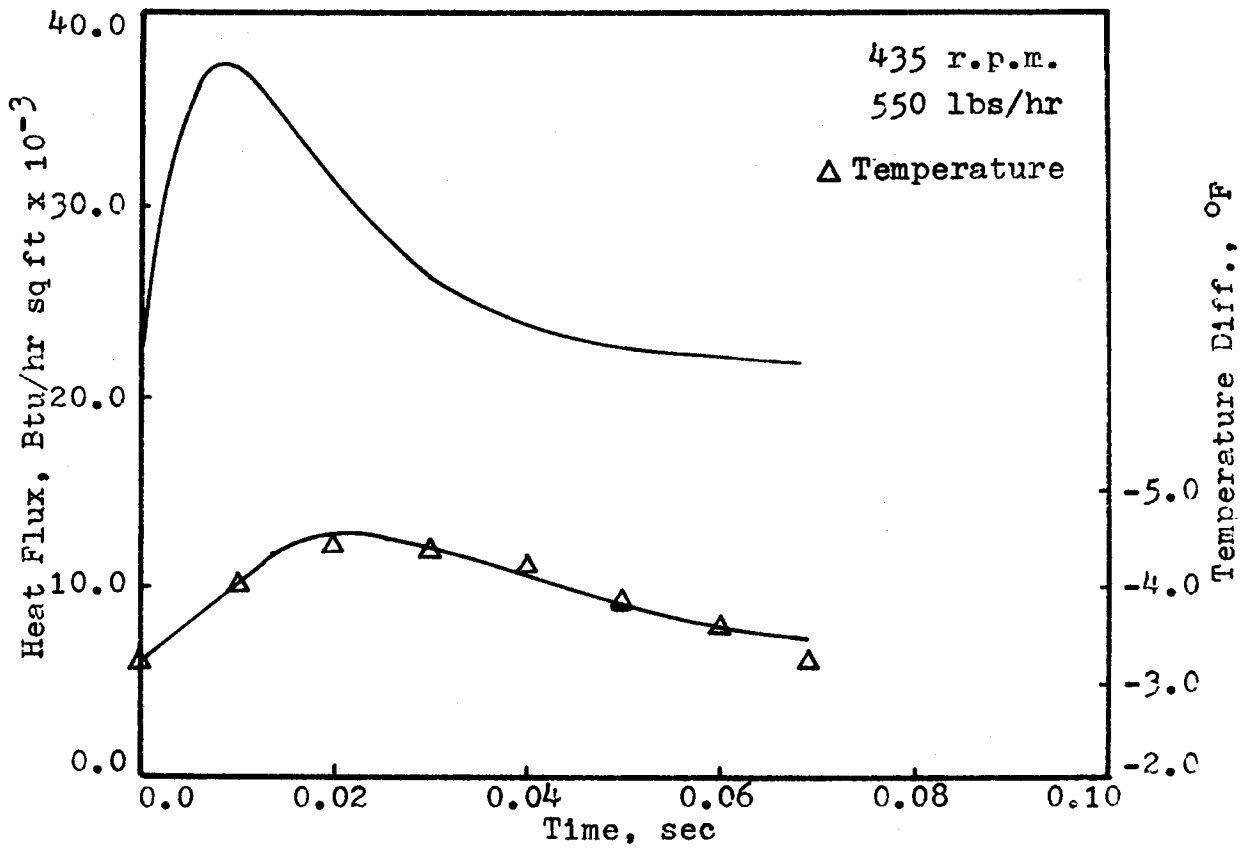

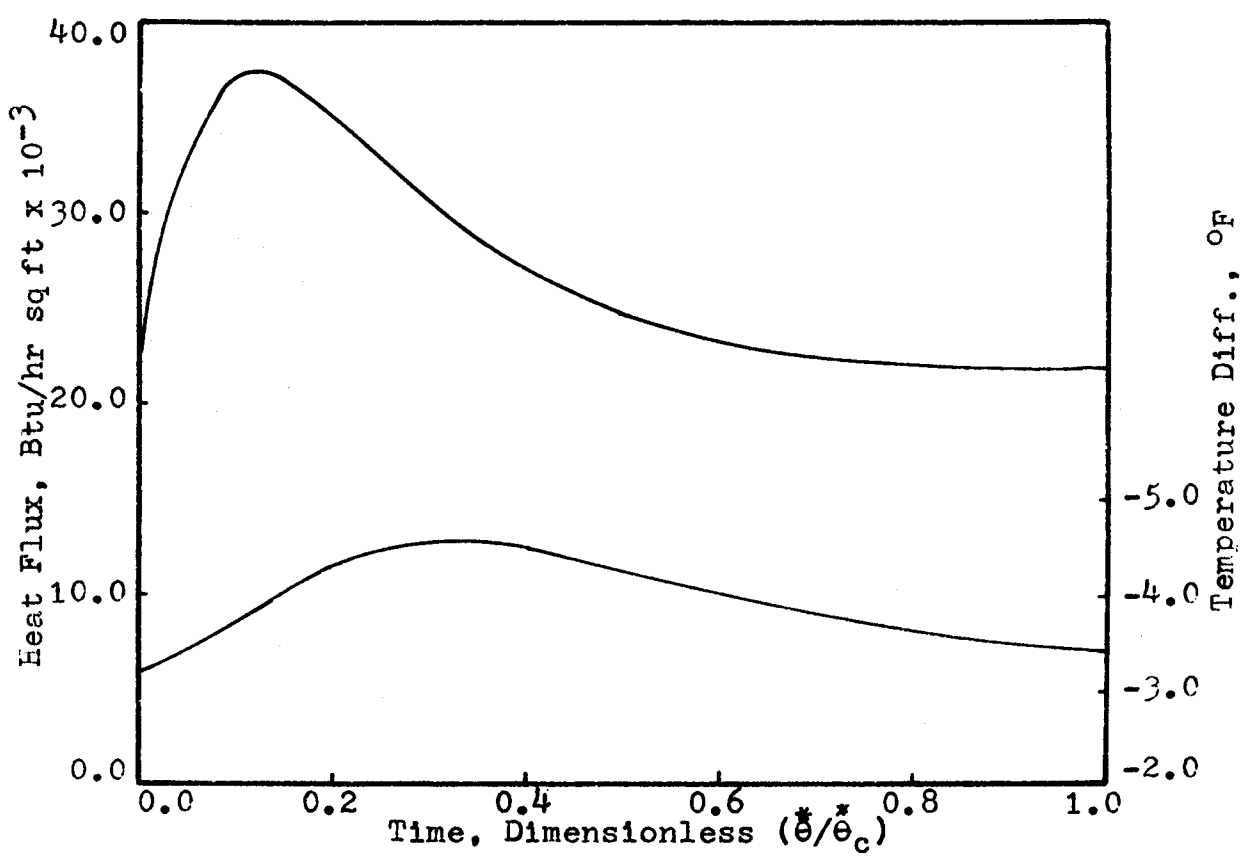

Fig. 5-12

Instantaneous Heat Flux

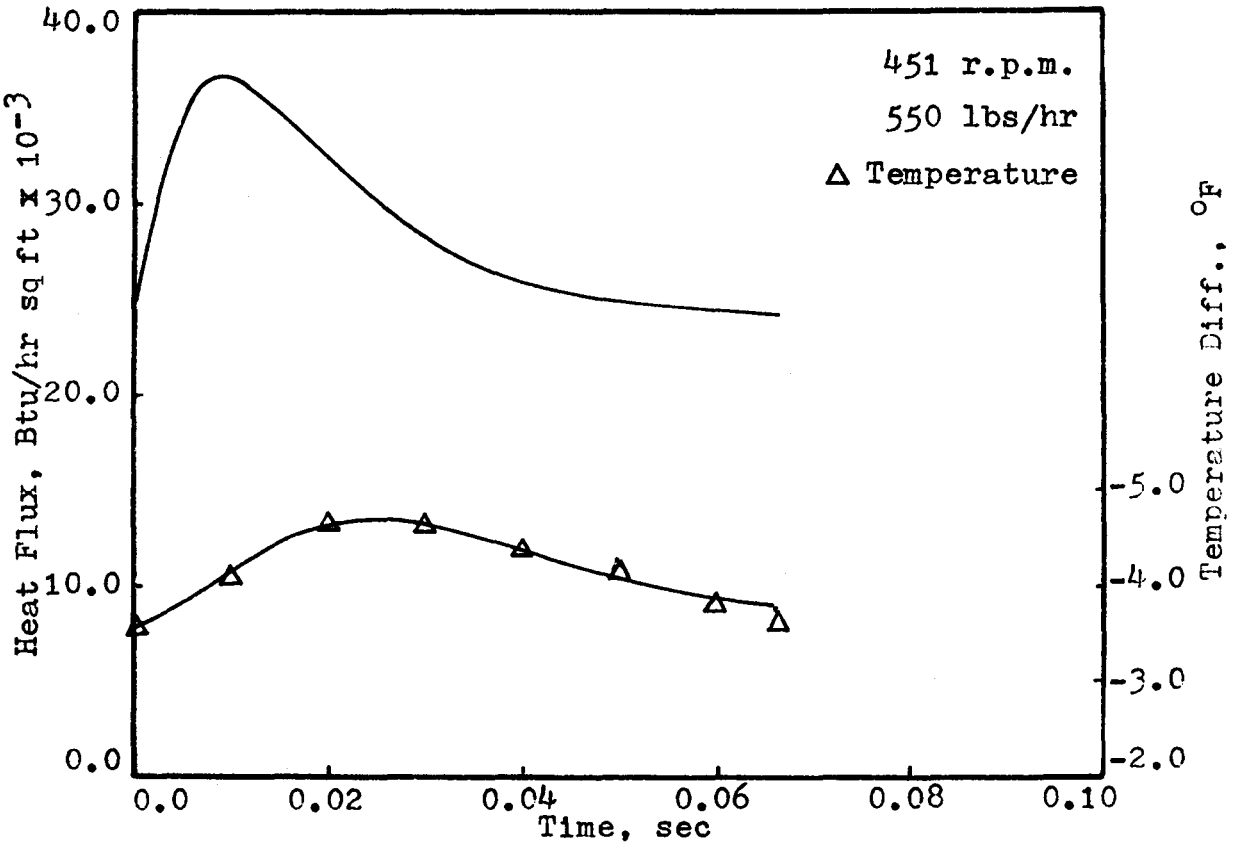

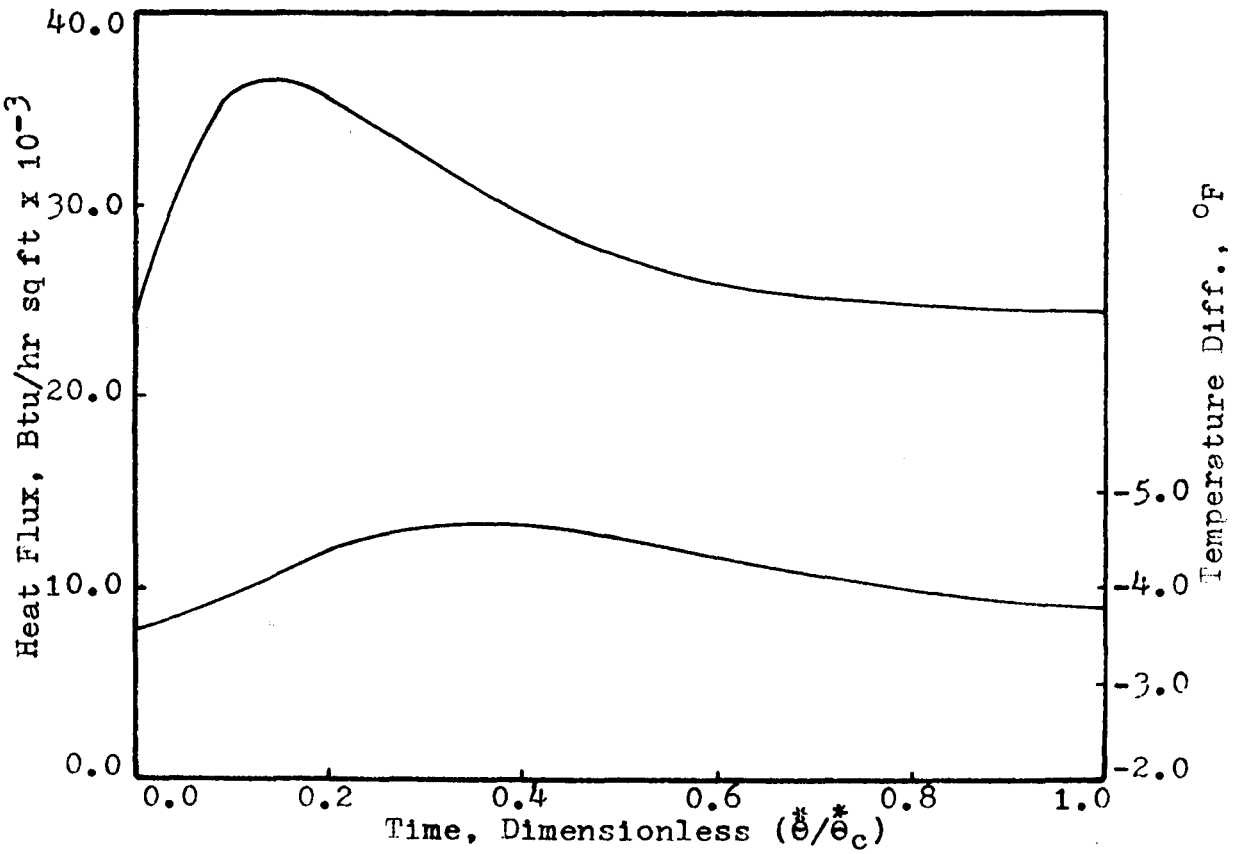

Fig. 5-13
Instantaneous Heat Flux

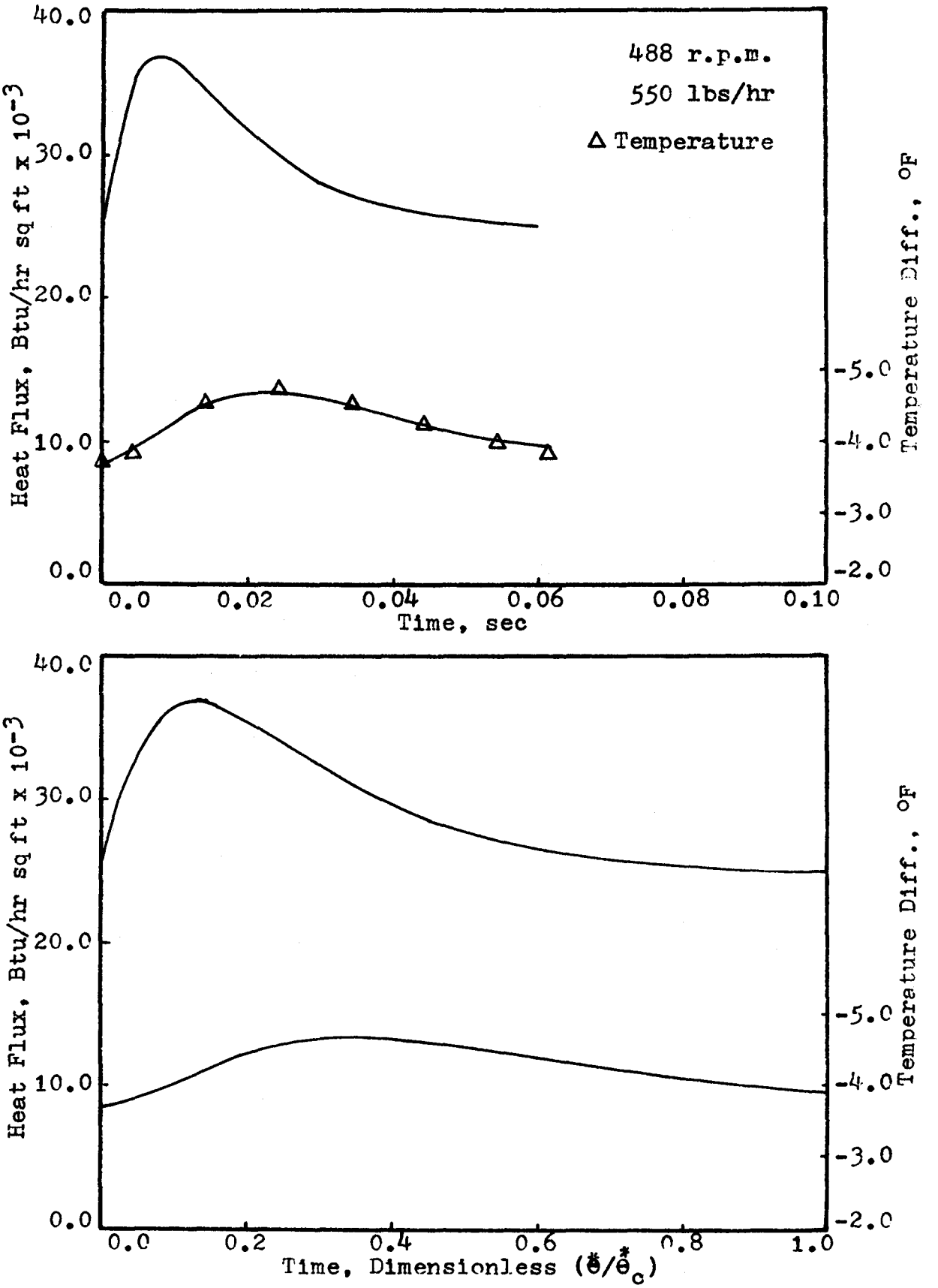

Fig. 5-14

Instantaneous Heat Flux

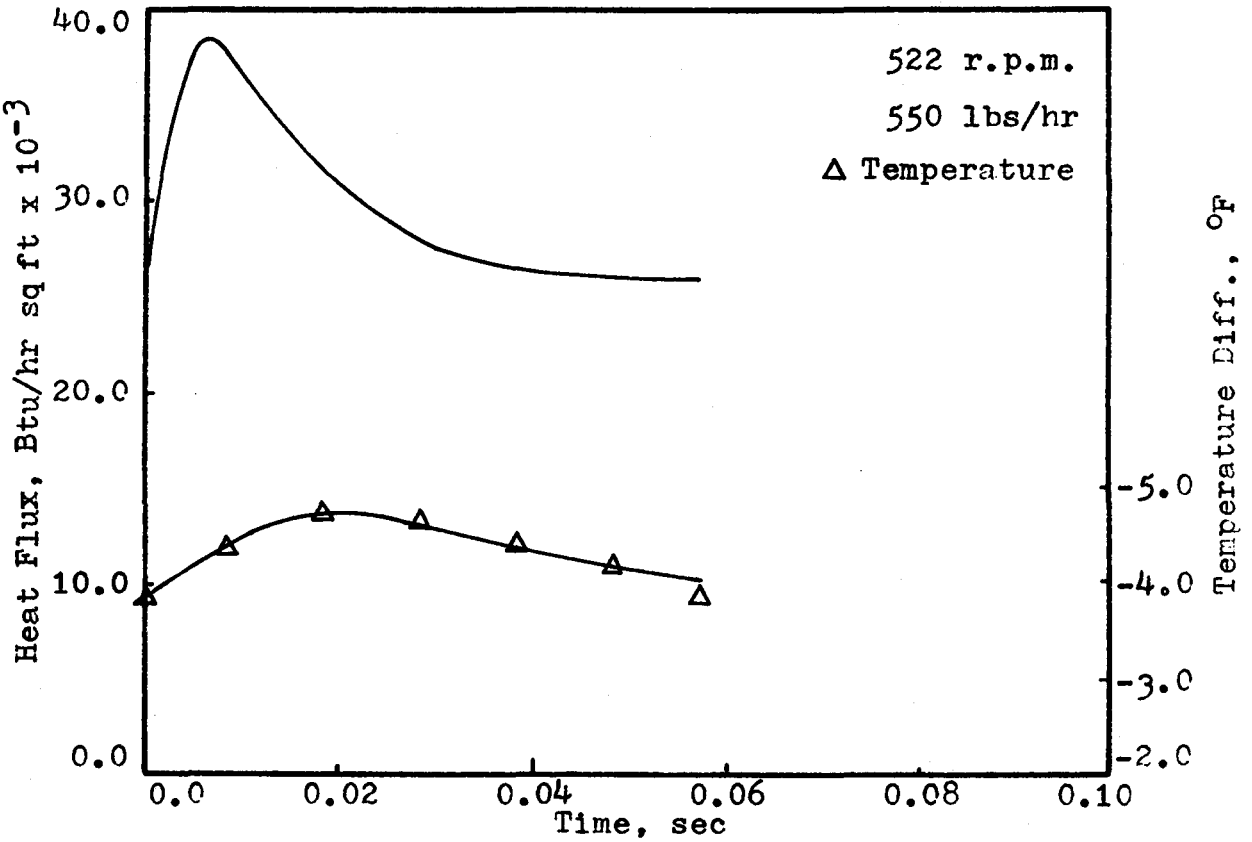

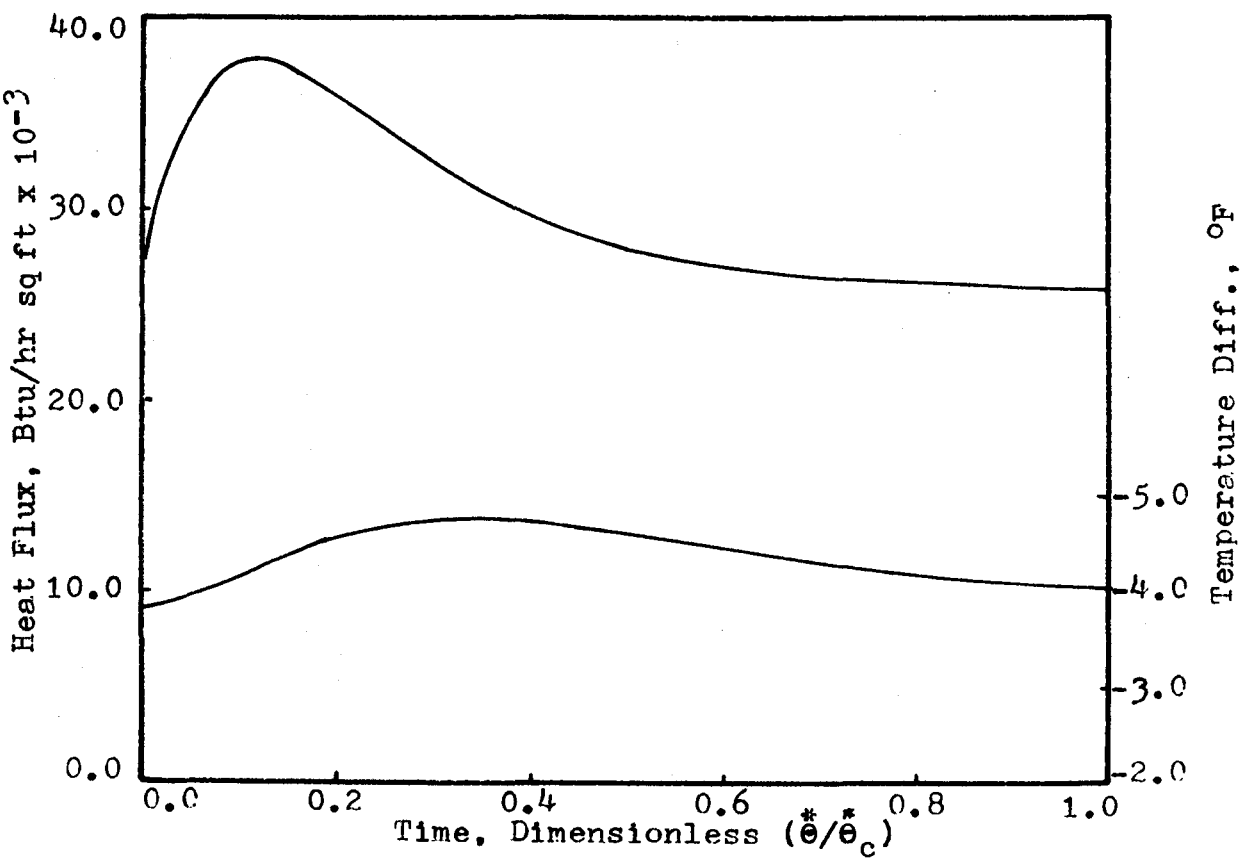

Fig. 5-15
Instantaneous Heat Flux

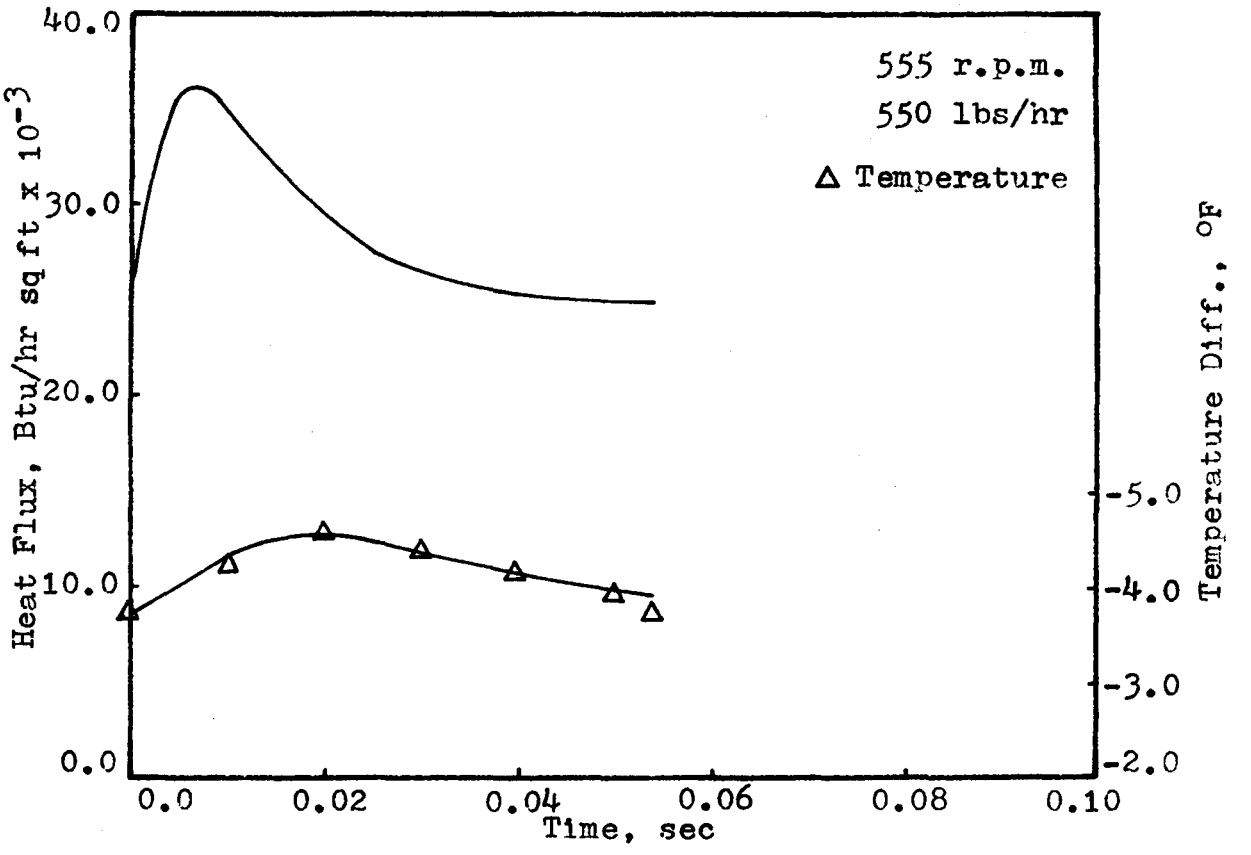

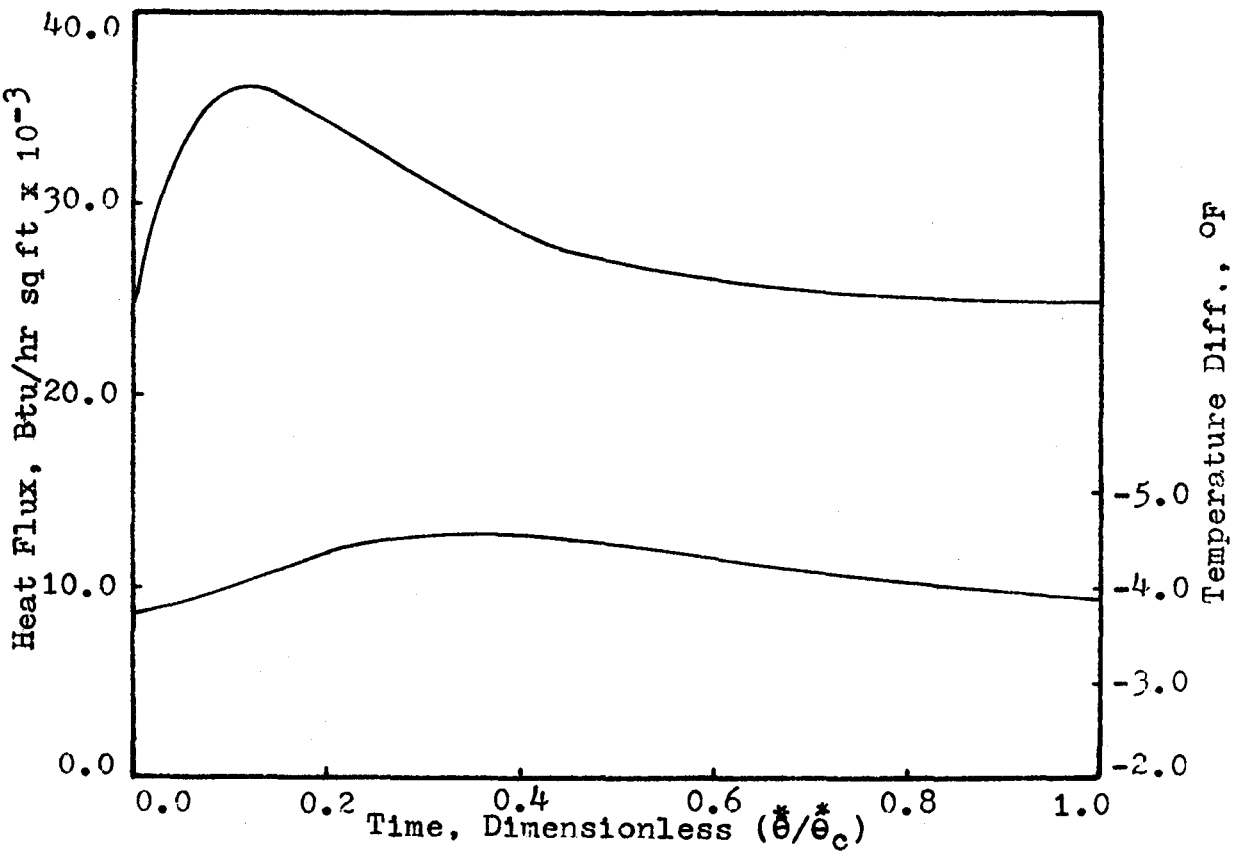

Fig. 5-16
Instantaneous Heat Flux

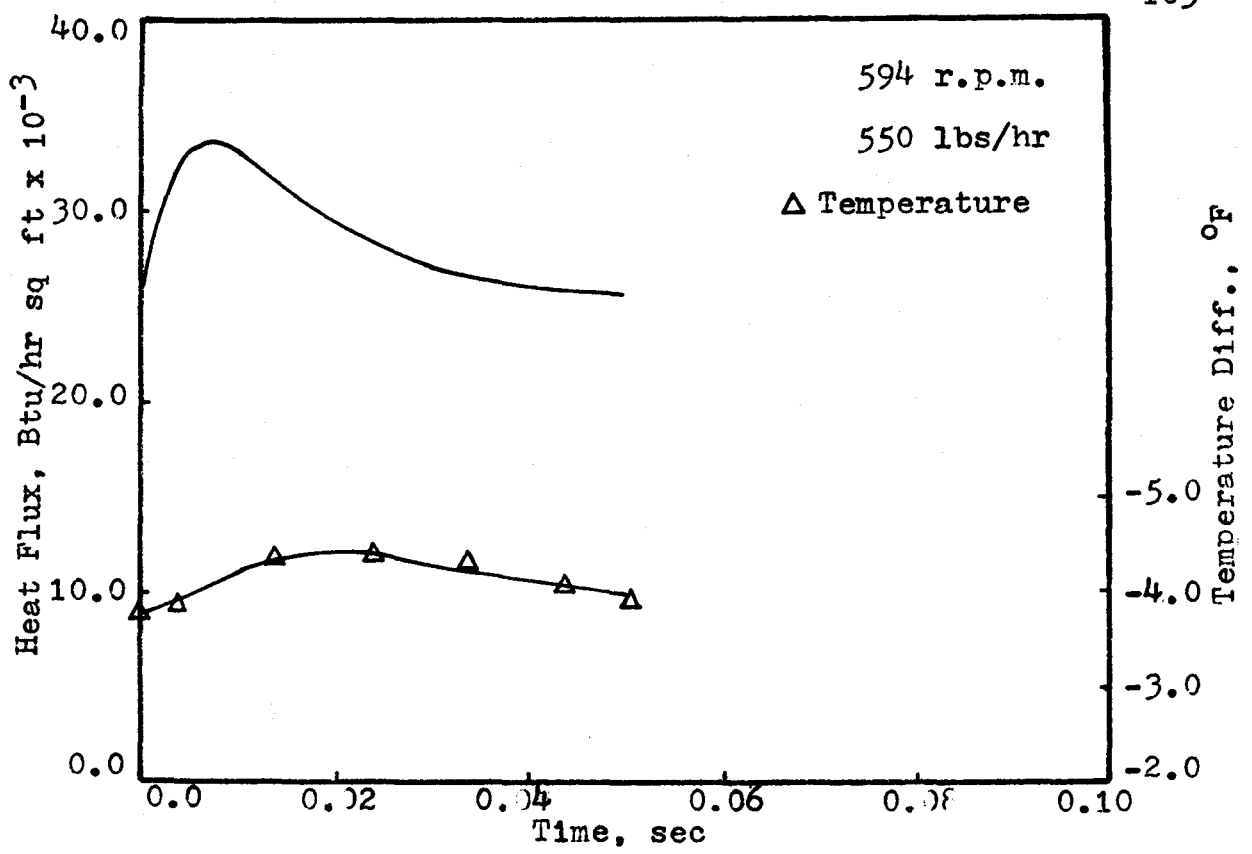

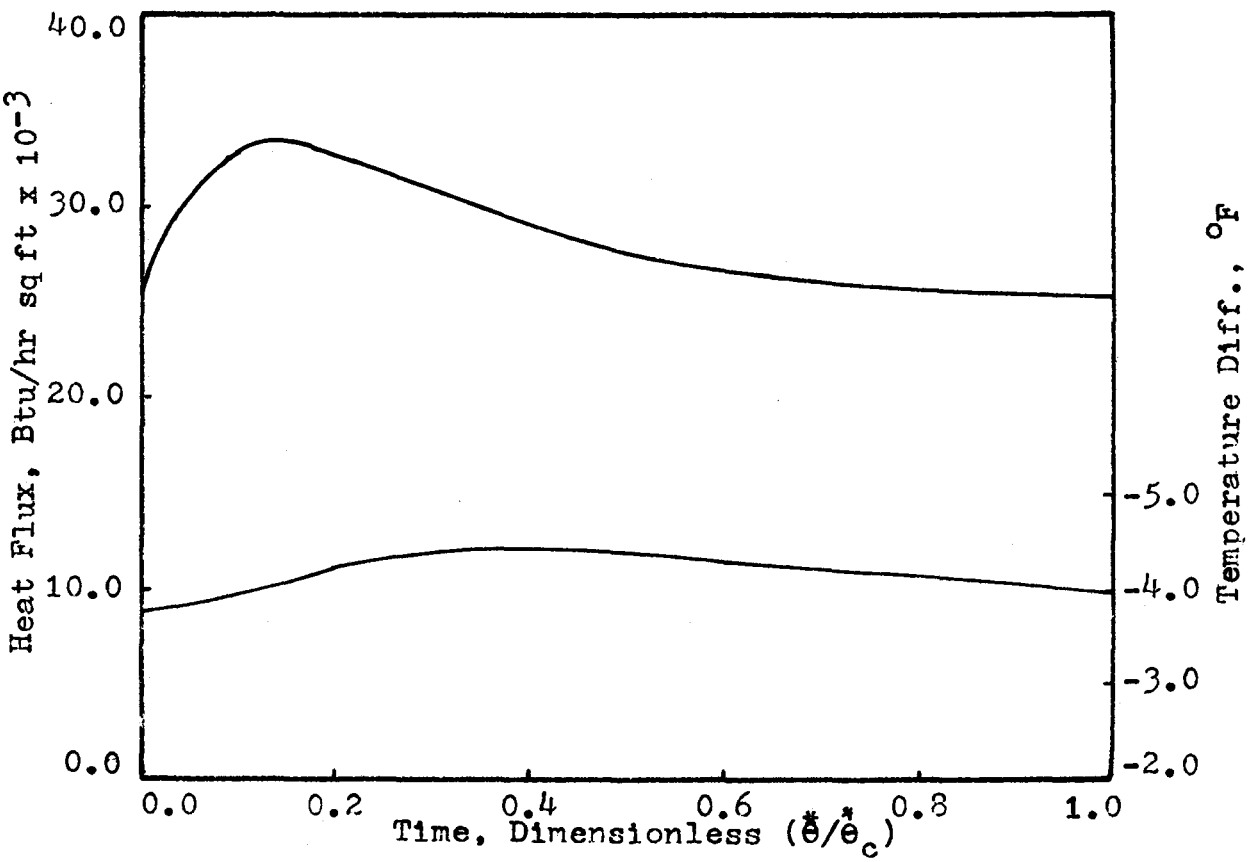

Fig. 5-17

Instantaneous Heat Flux

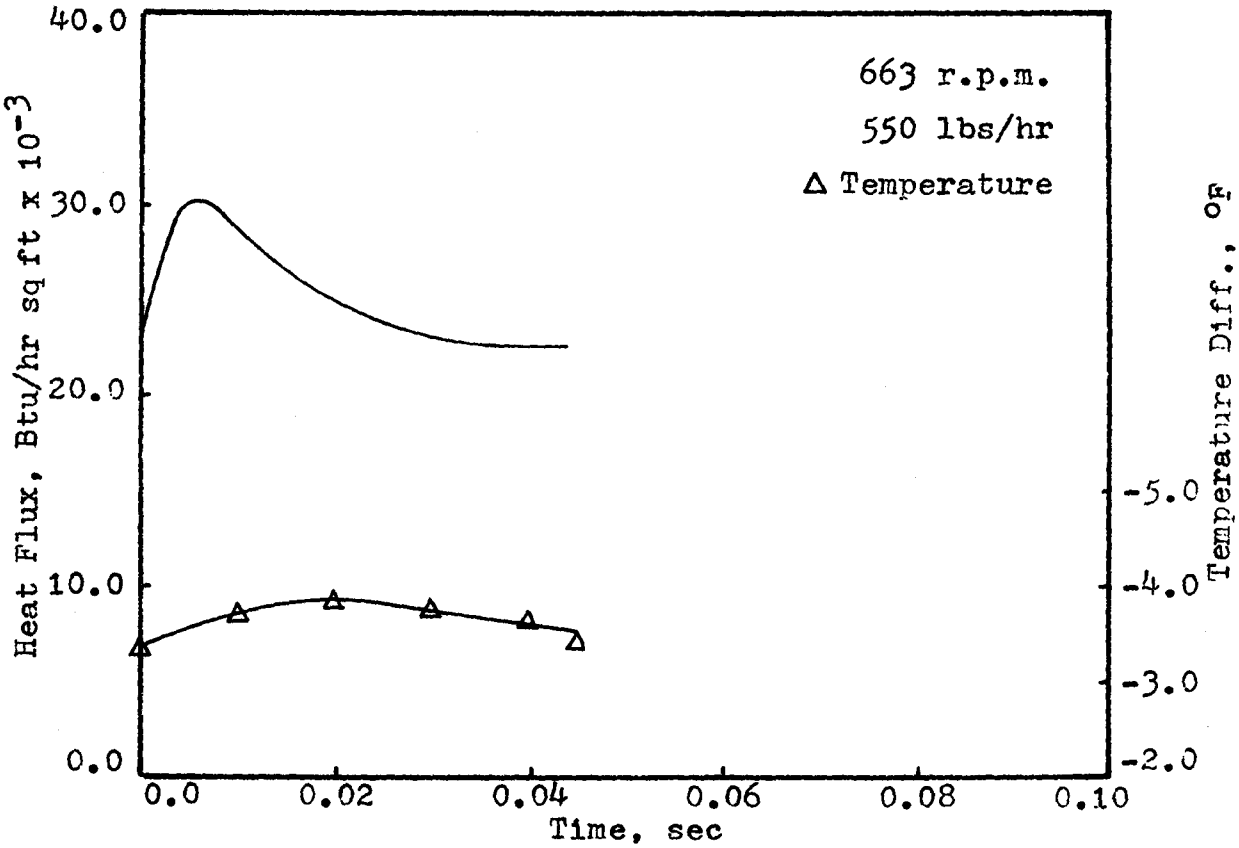

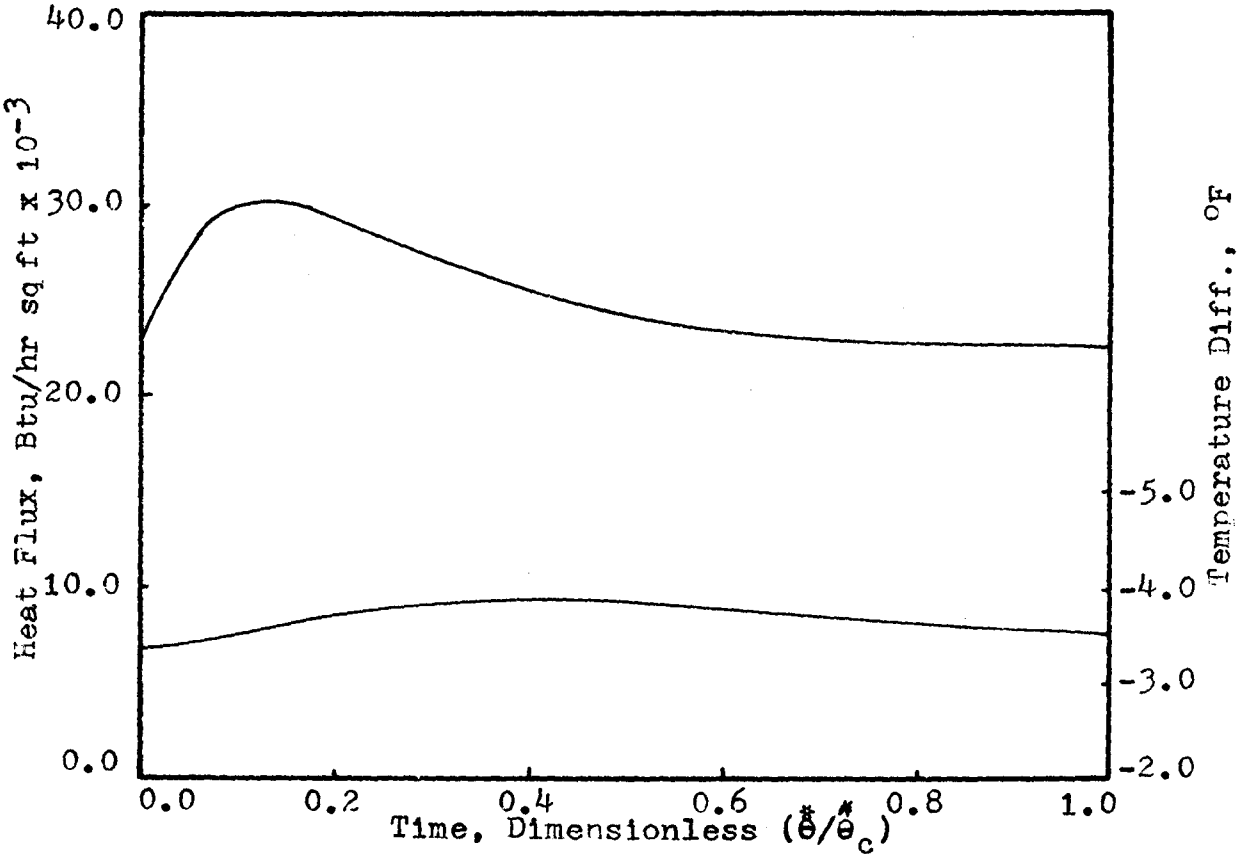

Fig. 5-18

Instantaneous Heat Flux

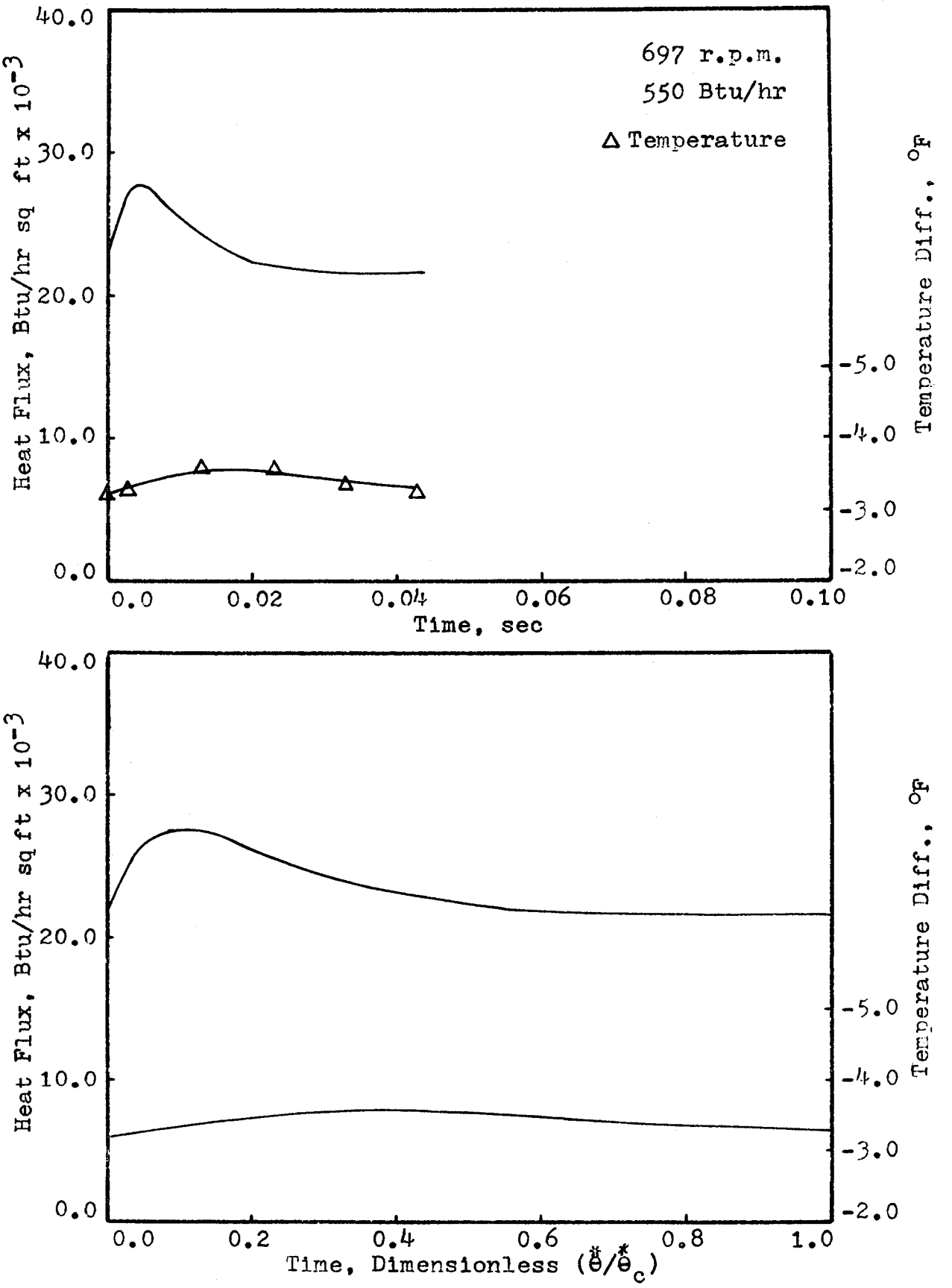

Fig. 5-19

Instantaneous Heat Flux

5.7 INSTANTANEOUS LOCAL HEAT TRANSFER COEFFICIENTS

The instantaneous, point heat transfer coefficient was obtained from the instantaneous local heat flux based on the definition of the coefficient, viz:

$$(q/A) = h\,\Delta T \qquad (5\text{-}14)$$

where ΔT is the temperature difference between the wall and the cup-mixed temperature of the liquid assuming plug flow. In Fig. 5-20 local coefficients corresponding to the local heat fluxes in Fig. 5-10 to 5-19 are plotted against dimensionless time with rotational speed as parameter.

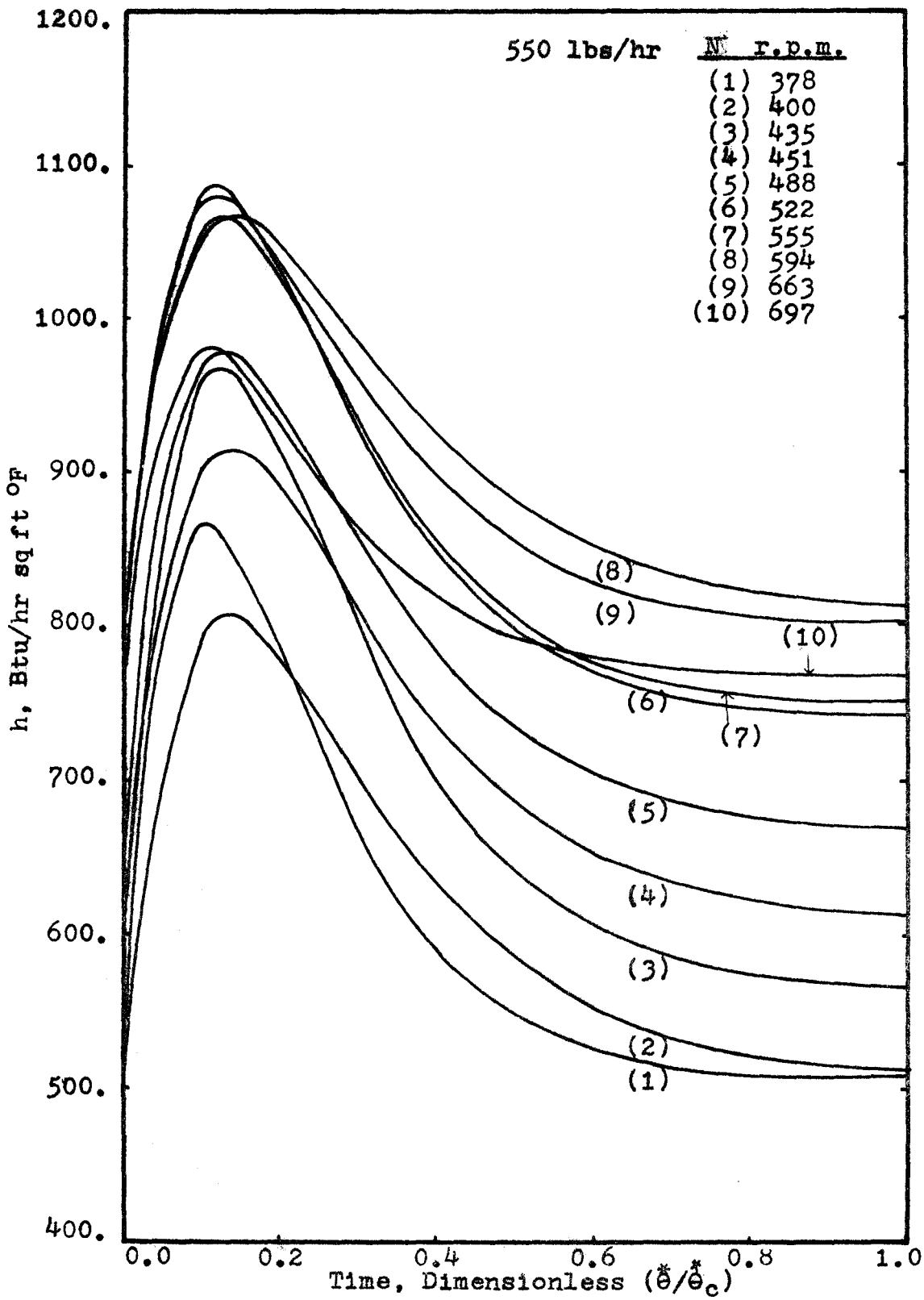

Fig. 5-20
Instantaneous Local Coefficients

6. DISCUSSION

6.1 QUALITATIVE OBSERVATIONS

The flow visualizations studies showed that the fluid travels through mechanically-aided thermal processors on a spiral trajectory. The flow in the azimuthal direction is brought about by the inertia which is imparted to the fluid by the blade. The actual shape of the spiral path would be determined by the gravity, inertial and viscous forces. However, it would be expected that the pitch of the spiral would decrease with rotational speed since the ratio of inertial to gravity forces would increase.

The visual observations of this investigation have shed more light on the complex problem of fluid flow in scraped-surface equipment but no attempt was made to mathematically analyse the phenomenon.

6.2 WALL TEMPERATURE

The wall of a scraped-surface heat exchanger would be expected to be in an unsteady thermal state, because the heat transfer phenomenon from the wall to the fluid is an unsteady state one. In other words, the temperature of the wall would not be constant as the penetration theory assumes but should vary with time (H4). Under unsteady state conditions the wall temperature would remain constant only if the

wall material had an infinite thermal diffusivity. To exemplify, imagine that two semi-infinite solids at temperatures T_W and T_L ($T_W > T_L$) are brought in intimate thermal contact. The moment this is done the temperature of the interface will fall to the value (C3)

$$T_e = T_W - \left(\frac{T_W - T_L}{1 + \frac{k_W}{k_L} \sqrt{\frac{\alpha_L}{\alpha_W}}} \right) \qquad (6\text{-}1)$$

Equation (6-1) shows that the temperature drop at the interface depends on the initial temperature difference and the physical properties of the bodies.

In the experimental work the temperature difference ($T_W - T_L$) at the upper part of the exchanger was of the order of 100°F, which according to equation (6-1) would cause a temperature drop at the interface of about 4°F. Such temperature drops were not observed experimentally. It is likely that the process represented by Eq. (6-1) is not applicable in the present case. As a matter of fact the temperature variation would be governed by the periodic heat flux. No further analysis was made.

The cause of decreasing wall temperature at the upper part of the tube with increasing rotational speed is unknown.

6.3 TIME-AVERAGE HEAT FLUX

The heat-flux distributions given in Sec. 4.4 show that the average heat flux was virtually a linear function

with respect to exchanger length. Only the heat flux over the third section showed deviations from the linear profile. This must have resulted from the scrapers not wiping the wall in that region, which was indeed observed. The non-scraping condition would allow a thin "stagnant" film on the thermal surface which would reduce the transfer rate.

The effect of rotational speed on the heat flux is shown in Fig. 4-21 and 4-26. The latter increased rapidly with rotational speed over the upper part of the exchanger. This trend may have been caused by either better liquid distribution or the more frequent contacts between thermal surface and process liquid from the core under the high driving forces of this region. The heat flux toward the exchanger end did not change much. A two-fold increase in rotational speed increased the heat flux by about 30% at the upper end but only 10% in the lower end.

6.4 TIME-AVERAGE LOCAL COEFFICIENTS

The time-average local heat transfer coefficients obtained in this work do not agree with the coefficients predicted by either the penetration theory model (Eq. (2-5)) or the corrected model proposed by Azoory (Eq. (2-11)). In particular the former gives values greatly higher than the experimental ones while the coefficients from the latter are considerably lower.

The penetration theory model predicts no dependence of the coefficient on the location along the exchanger or the temperature difference. The only variation in the coefficient arises from variation in the physical properties of the fluid. This variation for water as the process fluid would be less than 2.5% for the substantial temperature changes in this work. However, as it can be seen from Fig. 4-27, changes in the coefficient of about 50% were measured. The coefficients have a ΔT dependence so that their dependence on rotational speed cannot be derived from Fig. 4-27. In the experimental work the temperature difference depended on rotational speed, and the two effects could not be separated. The slopes given in Fig. 4-27 are for indicative purposes only.

It should be pointed out the coefficients reported in this thesis might be on the conservative side for they have been calculated with the assumption of plug flow.

6.5 LOCAL NUSSELT AND REYNOLDS NUMBERS

The local Nusselt Numbers given in Fig. 4-28 show the same dependence on the local Reynolds Number as in the penetration theory (Eq. (2-6)) with the exception of those at 7.5 in. from the top of the exchanger. No safe conclusions can be drawn, however, since the Nu_x is a function of ΔT arising from the coefficient dependence on ΔT. The same remarks pertain to the plot of the Nusselt Number for all four locations and all the runs in Fig. 4-29.

6.6 HEAT-FLUX METERS

An examination of the heat-flux meter behaviour under the experimental conditions is appropriate and necessary.

One of the assumptions of the heat-flux meter equations was that of symmetry over the meter disc at all times. This must have been very nearly true except at such times that the blade was over the meter when asymmetries were unavoidable. The arc length spanned by the meter diameter in the tube was 1/20 of the length of the half periphery of the tube which means that the time during which the blade was over the meter was 1/20 of the half-cycle time. Based on this evidence it could be argued that the asymmetries were so short-lived that they would not have a grave effect on the heat flux calculated with the assumption of symmetry.

The unsteady state condition of the wall should not affect the heat-flux meter operation, because the proximity of the two thermocouples would ensure similar transient thermal patterns at the two junctions thus leaving the temperature difference of the meter unaffected. In addition, the condition of constant wall temperature at the edge of the meter was fulfilled since the experimental temperatures at this point were observed to be essentially constant. The observed small temperature fluctuations might have introduced a slight error.

The unsteady state effects of the constantan wire embedded at the center of the copper disc were considered unimportant in view of the small amount of the former.

6.7 INSTANTANEOUS LOCAL HEAT FLUX

The most significant measurements of this investigation were those of the instantaneous local heat flux obtained from the point heat-flux meter although these heat fluxes were lower than those derived from condensation measurements by about 25%.

The heat flux (See Fig. 5-10 to 5-19) increases rapidly at the beginning of the cycle, falls off for some time-interval and changes little for the remaining part of the cycle. The local heat flux starts increasing before the blade reaches the meter and shows a maximum at such time that the blade was approximately over the detector. This observation is in antithesis to the penetration theory prediction that the heat flux is infinite at the beginning of the cycle. This could not be explained by taking into account the wall as discussed in Sec. 6.2 for even this analysis would predict infinite heat flux at time zero. Based on this argument it is reasonable to assume that the drastic difference in heat flux at the beginning of the cycle is caused by the different hydrodynamic and thermal conditions established by the liquid fillet, the presence of which is not taken into account by the penetration theory.

6.8 INSTANTANEOUS LOCAL HEAT TRANSFER COEFFICIENT

The instantaneous point heat transfer coefficients obtained in this work (See Fig. 5-20) show a maximum early

in the cycle as the heat flux does. The time at which this maximum occurs varies a little from run to run. The experimental instantaneous coefficients were obtained at the lower end of the exchanger. At this location the average coefficients were closer to the penetration theory predictions but still lower. The same trend is exhibited by the instantaneous coefficients although again contrary to theory, they are finite at the beginning of the cycle.

7. CONCLUSIONS

The following conclusions can be drawn from the present work:

I. The point heat-flux meter with the mathematical analysis of this study can be used in the investigation of dynamic processes in heat transfer work, provided that the uncertainty of the conduction along the wire of the centre thermocouple is eliminated or minimized.

II. A three-parameter heat flux model was found that made possible the estimation of instantaneous local heat flux from the experimental measurements of heat flux with a thin disc heat-flux meter using known parameter estimation techniques.

III. The heat flux at the beginning of the cycle in scraped-surface equipment was found to be finite contrary to the predictions of the penetration theory.

IV. The time-average local heat transfer coefficients of this work were not in agreement with the penetration model or its corrected form.

V. The local coefficient was found to depend greatly on location contrary to the penetration theory.

VI. The flow visualizations studies showed that the fluid travels through the exchanger on a spiral path.

8. RECOMMENDATIONS

I. The problem of heat conduction along the thermocouple wire could be minimized by using thinner wire and/or embedding the wire in the wall which would reduce the temperature gradient. The latter should be more useful since there is a practical limit in the wire diameter.

II. The lengthy development work of this study led to a fairly safe procedure in constructing the heat-flux meter. However, it would be advisable to extend the development work in order to ensure their proper and reliable operation.

III. The analysis of the heat-flux meter differential emf of this investigation was carried out with the nominal disc thickness. However, it is deemed that this is not sufficient. The thickness should be determined as accurately as possible. To this end, steady state heat transfer experiments could be undertaken that would allow its indirect determination or else γ-rays could be used to directly determine it.

IV. The centre wire should be installed at the centre of the disc as accurately as possible, while the edge one might be installed just off the disc in the hope of avoiding the small temperature fluctuations observed during this work.

V. The heat-transfer investigation in scraped-surface equipment should be extended to include heat transfer to liquids other than water.

VI. In future work in scraped-surface heat exchangers the residence-time distribution technique should be used to ascertain the effect of backmixing on local heat transfer coefficients.

9. NOMENCLATURE

$A_1 - A_4$	constants	
C, C_p	heat capacity	Btu/lb °F
D	diameter	ft
f	correction factor	dimensionless
$\bar{F}$	theoretical time-average heat flux	Btu/hr sq ft
$\bar{h}$	time average heat transfer coefficient	Btu/hr sq ft °F
$\bar{h}'$	heat transfer coefficient from steam jacket to scraping plane	Btu/hr sq ft °F
h	instantaneous heat transfer coefficient	Btu/hr sq ft °F
H_c	latent heat of vaporization	Btu/lb
H'	liquid hold-up per unit length per blade	ft^2
k	thermal conductivity	Btu/hr ft °F
L	exchanger length	ft
n	number of blades	
N	rotational speed	rev/min
Q, P	heat flux model parameters	Btu/hr sq ft
$(\overline{q/A})$	time-average heat flux	Btu/hr sq ft
(q/A)	constant or instantaneous heat flux	Btu/hr sq ft
$\bar{q}$	heat input rate	Btu/hr
R	tube radius	ft
R_o	heat-flux meter radius	in.

$\overset{*}{r}$, $\overset{*}{z}$	dimensional coordinates	
r, z	dimensionless coordinates	
s	blade spacing $(=\pi D_t/n)$	ft
t	heat-flux meter thickness	in.
T	temperature	°F
T_{in}, T_{out}	inlet and outlet liquid temperature	°F
ΔT	temperature difference	°F
$\Delta T^{(t)}$	theoretical temperature difference in heat-flux meter	°F
U	overall heat transfer coefficient	Btu/hr sq ft °F
v	mean axial velocity	ft/sec
w	volumetric flow rate	ft^3/hr
w'	volumetric flow rate per blade	$(ft^3/sec$ blade)
W	condensation rate	lbs/hr

Greek letters

α	thermal diffusivity	in^2/sec, ft^2/sec
γ	heat flux model parameter	
δ	film thickness	ft
$\overset{*}{\theta}$	real time	sec, hr
θ	dimensionless time	
λ	eigenvalue	
μ	viscosity	lb/ft sec
ν	kinematic viscosity	ft^2/sec
ρ	density	lb/hr

τ	mass flow rate per unit length	lb/ft hr
ϕ	parameter	
ψ	parameter	

Subscripts

B	bulk
c	cycle
C	heat-flux meter center
i	index
s	shaft or agitator
ss	steady state
t	transient state, tube or turbulent
w	wall
W	heat-flux meter edge

Superscripts

L	liquid, experimental
l	liquid, regression
w	wall experimental

Dimensionless Groups

Bo	Bodenstein Number	$\left(\frac{vL}{\alpha_t}\right)$
Pr	Prandtl Number	$\left(\frac{C_p\mu}{k}\right)$
Re_r	Rotary Reynolds Number	$\left(\frac{D_t^2 N\rho}{\mu}\right)$
S	Group from Kool's model	$\left[h'\left(\frac{\ddot{\theta}_c}{kC_p\rho}\right)^{1/2}\right]$

10. BIBLIOGRAPHY

A1 AZOORY, S. Ph.D Thesis, The University of Birmingham (1967).*

B1 BORG, E.L., PROVOST, R.L., and BAWN, C.V. "The Concentration of GR-S Latex in a Turbulent-film Evaporator", Chem. Eng. Progr., 51, 278 (1955).

B2 BRESSLER, R. Forshungsbericht No. 770, Kultusminiberium Nordrhein, Westfalen, Cologne (1960).

B3 BOTT, T.R., ROMERO, J.J.B. "Heat Transfer Across a Scraped Surface", Can. J. Chem. Eng., 41, 213 (1963).

B4 BOTT, T.R., SHEIKH, M.R. "Effect of Blade Design in Scraped Surface Heat Transfer", Brit. Chem. Eng., 9 (1964).

B5 BOTT, T.R., ROMERO, J.J.B. "The Characteristic Dimension in Scraped Surface Heat Transfer", Can. J. Chem. Eng., 44, 226 (1966).

B6 BOTT, T.R., AZOORY, S., PORTER, K.E. "Scraped-Surface Heat Exchangers. Part I—Hold-up and Residence Time Studies", Trans. Instn. Chem. Engs., 46, T33 (1968).

B7 BLAISDELL, J.L., ZAHRADNIK, J.W. "Longitudinal Temperature Distribution in a Scraped-Surface Heat Exchanger", Food Tech., XIII, 659 (1959).

B8 BRAGINSKII, L.N., BEGACHEV, V.I. "Heat Transfer in Heat Exchangers with Scraper Stirrers", Theoretical Foundations of Chem. Eng., 3, (2), 201 (1969).

B9 BOTT, T.R., AZOORY, S., PORTER, K.E. "Scraped-Surface Heat Exchangers. Part II—The Effects of Axial Dispersion on Heat Transfer", Trans. Instn. Chem. Engs., 46, T37 (1968).

B10 BADGER, W.L., BANCHERO, J.T. Introduction to Chemical Engineering. (1955) McGraw-Hill, Kogakusha.

---

*Birmingham, England, U.K.

C1 CHURCHILL, S.W., WHITE, R.R. "Experimental Foundations of Chemical Engineering", A.I.Ch.E.J., 5, 358 (1959).

C2 CHURCHILL, R.V. Operational Mathematics. (1958) McGraw-Hill.

C3 CARSLAW, H.S., JAEGER, J.C. Conduction of Heat in Solids. (1959) Oxford at the Clarendon Press.

D1 DANCKWERTS, P.V. "Significance of Liquid-film Coefficients in Gas Absorption", Ind. Eng. Chem., 43, 1460, (1951)

D2 DARNEDDE, E. M.Eng. Thesis, McMaster University (1966).*

G1 GUDHEIM, A.R., DONOVAN, J. "Heat Transfer in Thin-film Centrifugal Processing Units", Chem. Eng. Progr., 53, 476 (1957).

G2 GREEN, S.J. "Agitation in Process Design", Trans. Instn. Chem. Engrs., 31, 327 (1953).

G3 GARDON, R. "A Transducer for the Measurement of Heat Flow Rate", J. Heat Transfer, 82, 396 (1960).

H1 HIGBIE, R. "The Rate of Absorption of a Pure Gas into a Still Liquid During Short Periods of Exposure", Trans. Am. Inst. Chem. Engrs., 31, 365 (1935).

H2 HARRIOTT, P. "Heat Transfer in Scraped-Surface Heat Exchangers", Chem. Eng. Progress Symp. Series, 55, 137 (1959).

H3 HOULTON, H.G. "Heat Transfer in the Votator", Ind. Eng. Chem., 36, 522 (1944).

H4 HOFFMAN, T.W. Private Communication. McMaster University, Hamilton, Ontario (1970).

J1 JEPSON, C.H. "Future Extrusion Studies", Ind. Eng. Chem., 45, 992 (1953).

K1 KERN, D.Q., KARAKAS, H.J. "Mechanically Aided Heat Transfer", Chem. Eng. Progress Symp. Series, 55, 141 (1959).

---

*Hamilton, Ontario, Canada.

K2 KOOL, J. "Heat Transfer in Scraped Vessels and Pipes Handling Viscous Materials", Trans. Instn. Chem. Engrs., 36, 253 (1958).

L1 LATINEN, G.A. Chem. Eng. Sci., 9, 263 (1959).

L2 LEVICH, V.G. Physicochemical Hydrodynamics. (1963) Prentice Hall.

M1 MUTZENBURG, A.B. "Agitated Thin-film Evaporators. Part I—Thin-film Technology", Chem. Engng., Sept.13, 175 (1965).

P1 PENNEY, W.R., BELL, K.J. "Close Clearance Agitators. Part 2. Heat Transfer Coefficients", Ind. Eng. Chem., 59, 47 (1967).

S1 SKELLAND, A.H.P. "Correlation of Scraped-film Heat Transfer in the Votator", Chem. Eng. Sci., 7, 166 (1958).

S2 SKELLAND, A.H.P., OLIVER, D.R., TOOKE, S. "Heat-Transfer in a Water-Cooled Scraped-Surface Heat Exchanger", Brit. Chem. Eng., 7, 346,(1962).

U1 UHL, V.W. Mixing, I, (1965) Academic Press.

U2 UHL, V.W., ROOT, W.L. "Heat Transfer to Granular Solids in Agitated Units", Chem. Eng. Progr., 63, 81 (1967).

APPENDIX I

CALIBRATION OF VISICORDER GALVANOMETERS

The galvanometers were calibrated using two constant temperature baths and a copper-constantan thermocouple. The arrangement is shown in Fig. I-1.

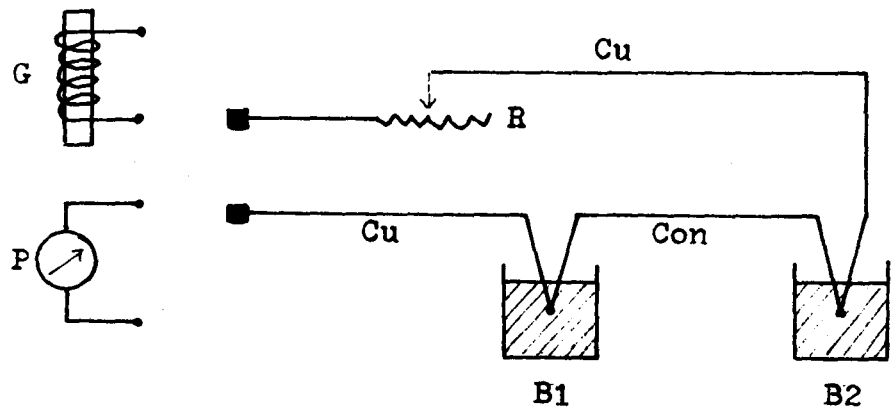

Fig. I-1
Galvanometer Calibration

A variable resistance, R, was used to set the impedance of the source at a fixed known value. G is a visicorder galvanometer, P is a potentiometer. The procedure followed for the calibration of the galvanometer is given below.

The temperatures of the baths were set at about 85° with B_2 slightly higher than B_1. After steady state had obtained the circuit was connected to the potentiometer whose reading was recorded. The circuit was then connected to the galvanometer and a record was taken from the visicorder. The procedure was repeated for each step change (1 - 2°F) in

the temperature of both B_2. Six measurements were made for each impedance level. Table I-1 gives the calibration points for the 33Ω impedance used in this experimental work.

Table I-1

Deflection (recorder divisions)	Voltage (mV)
16.75	0.000
18.5	0.061
19.75	0.100
20.3	0.114
21.8	0.164
22.9	0.201

To these points a least-squares line was fitted, which was used for the conversion of data in deflection units to data in millivots.

APPENDIX II

SOLUTION OF THE HEAT FLUX METER EQUATIONS

The partial differential equation (6-7.a) was solved by the Laplace transformation method.

The transformed P.D.E. and initial and boundary conditions are:

$$s\bar{T} = \frac{\partial^2 \bar{T}}{\partial r^2} + \frac{1}{r}\frac{\partial \bar{T}}{\partial r} + \left(\frac{R_o}{t}\right)^2 \frac{\partial^2 \bar{T}}{\partial z^2} \qquad \text{(II-1.a)}$$

$$r = 0 \quad \forall\, z \quad \frac{\partial \bar{T}}{\partial r} = 0 \qquad \text{(II-1.b)}$$

$$r = 1 \quad \forall\, z \quad \bar{T} = 0 \qquad \text{(II-1.c)}$$

$$z = 0 \quad \forall\, r \quad \frac{\partial \bar{T}}{\partial z} = 0 \qquad \text{(II-1.d)}$$

$$z = 1 \quad \forall\, r \quad \frac{\partial \bar{T}}{\partial z} = -\frac{t}{k}\, g(s) \qquad \text{(II-1.e)}$$

where $\bar{T} = \int_o^\infty e^{-s\theta} T_t d\theta$

and $g(s) = \int_o^\infty e^{-s\theta} G(\theta) d\theta$

The method of separation of variables was used in solving the transformed P.D.E. (II-1.a). Let

$$T = R(r)\, X(z) \qquad \text{(II-2)}$$

Upon substitution of Eq. (II-2) into Eq. (II-1.a) and manipulation of the result one obtained:

$$\frac{d^2R}{dr^2} + \frac{1}{r}\frac{dR}{dr} + \lambda^2 R = 0 \qquad \text{(II-3)}$$

$$\frac{d^2X}{dz^2} - (s+\lambda^2)\left(\frac{t}{R_o}\right)^2 X = 0 \qquad \text{(II-4)}$$

where the eigenvalue was set equal to $-\lambda^2$. The solutions of O.D.E. (II-3) and (II-4) are

$$R = A_1 J_o(\lambda r) + A_2 Y_o(\lambda r) \qquad \text{(II-5)}$$

$$X = A_3 \sinh \phi z + A_4 \cosh \phi z \qquad \text{(II-6)}$$

where $\phi^2 = (s+\lambda^2)\left(\frac{t}{R_o}\right)^2$

From boundary condition (II-1.b) $A_2 = 0$, and from (II-1.d) $A_3 = 0$, whereupon

$$\bar{T} = A J_o(\lambda r) \cosh \phi z \qquad \text{(II-7)}$$

Boundary condition (II-1.c) resulted in

$$J_o(\lambda) = 0 \qquad \text{(II-8)}$$

from which the eigenvalues λ_m were obtained. The solution of P.D.E. (II-1.a) is therefore given by an infinite summation, i.e.,

$$\bar{T} = \sum_{m=1}^{\infty} A_m J_o(\lambda_m r) \cosh \phi_m z$$

where $\phi_m^2 = (s+\lambda_m^2)\left(\frac{t}{R_o}\right)^2$

Boundary condition (II-1.e) gave

$$\sum_{m=1}^{\infty} A_m \phi_m J_o(\gamma_m r) \sinh \phi_m = - \frac{t}{k} g(s) \qquad \text{(II-10)}$$

The constants A_m were obtained from Eq. (II-10) by using the orthogonality properties of the Bessel functions, i.e.,

$$\int_o^1 J_o(\gamma_m r)\, J_o(\gamma_n r) r\, dr = 0 \qquad \text{(II-11)}$$

$$\int_o^1 J_o(\gamma_m r)^2 r\, dr = \frac{1}{2} J_1^2(\gamma_m) \qquad \text{(II-12)}$$

The result was:

$$A_m = \frac{2(\frac{t}{k})\, g(s)}{\gamma_m \phi_m \sinh \phi_m J_1(\gamma_m)} \qquad \text{(II-13)}$$

The Laplace transform of the temperature then is:

$$\bar{T} = -\sum_{m=1}^{\infty} \frac{2t J_o(\gamma_m r)}{k \gamma_m J_1(\gamma_m)} \frac{g(s) \cosh \phi_m z}{\phi_m \sinh \phi_m} \qquad \text{(II-14)}$$

Transform (II-14) is general in the sense that it can be used for any heat flux that is a function of time, provided that this function has a Laplace transform.

In the present investigation the inverse of Eq. (II-14) was to be found for a heat flux of the form

$$G(\theta) = P\theta \exp(-\gamma\theta) \qquad \text{(II-15)}$$

whose Laplace transform is

$$g(s) = P \frac{1}{(s+\gamma)^2} \qquad \text{(II-16)}$$

Substitution of Eq. (II-16) in Eq. (II-14) resulted in

$$\bar{T} = -\sum_{m=1}^{\infty} \frac{2Pt\, J_o(\lambda_m r)}{k\lambda_m J_1(\lambda_m)} \frac{\cosh \phi_m z}{(s+\gamma)^2 \phi_m \sinh \phi_m} \qquad \text{(II-17)}$$

The inverse of Eq. (II-17) was obtained by the method of convolution (C2):

$$\int_o^{\theta} P(\theta - \tau)\, H(\tau)\, d\tau$$

where $P(\theta) = \theta \exp(-\ 0)$

and $H(\theta) = \mathcal{L}^{-1}\left[\sum_m \frac{\cosh \phi_m z}{\phi_m \sinh \phi_m}\right]$

The final solution is:

$$T_t = \mathcal{L}^{-1}\, \bar{T} =$$

$$= -\sum_{m=1}^{\infty} \frac{2PR_o J_o(\lambda_m r)}{kt\lambda_m J_1(\lambda_m)} \left[\frac{\exp(-\lambda_m^2\theta) + \left[(\lambda_m^2 - \gamma)\theta - 1\right]\exp(-\gamma\theta)}{(\lambda_m^2 - \gamma)^2}\right]$$

$$-\sum_{m=1}^{\infty}\sum_{n=1}^{\infty} \frac{4PR_o^2(-1)^m \cos(m\pi z) J_o(\lambda_m r)}{kt\lambda_m J_1(\lambda_m)}$$

$$\left[\frac{\exp(-\psi_{m,n}^2\theta) + \left[(\psi_{m,n}^2 - \gamma)\theta - 1\right]\exp(-\gamma\theta)}{(\psi_{m,n}^2 - \gamma)^2}\right] \qquad \text{(II-18)}$$

where $\psi_{m,n}^2 = \lambda_m^2 + \frac{n^2\pi^2 R_o^2}{t^2}$

APPENDIX III

FITTING THE TEMPERATURE DIFFERENCE MODEL

The computer programme that was written for the estimation of the parameters Q, P and γ of the model started with the raw heat-flux meter data and initial guesses Q_o, P_o, γ_o for the parameters and ended with the estimated optimal values, $\overset{*}{Q}$, $\overset{*}{P}$, and $\overset{*}{\gamma}$, of the parameters. The raw meter data consisted of the differential emf points in deflection units (= distance between two adjacent grid-lines of the recording paper) and the absolute emf, E_w, at the edge of the meter.

The raw differential emf points were converted into differential emf ones, ΔE_i, by means of the galvanometer calibration curve. The absolute emf points, E_i, at the centre of the meter were obtained from equation (III-1)

$$E_i = E_w - \Delta E_i \qquad \text{(III-1)}$$

The absolute emfs E_i and E_w were converted to temperatures, T_{ci} and T_w respectively, through use of a table look-up from which the temperature difference points were obtained, equation (III-2)

$$\Delta T_i = T_{ci} - T_w \qquad \text{(III-2)}$$

To these points the temperature difference model was fitted

as discussed in Sec. 6.3. The algorithm of the computer programme is shown in Fig. III-1.

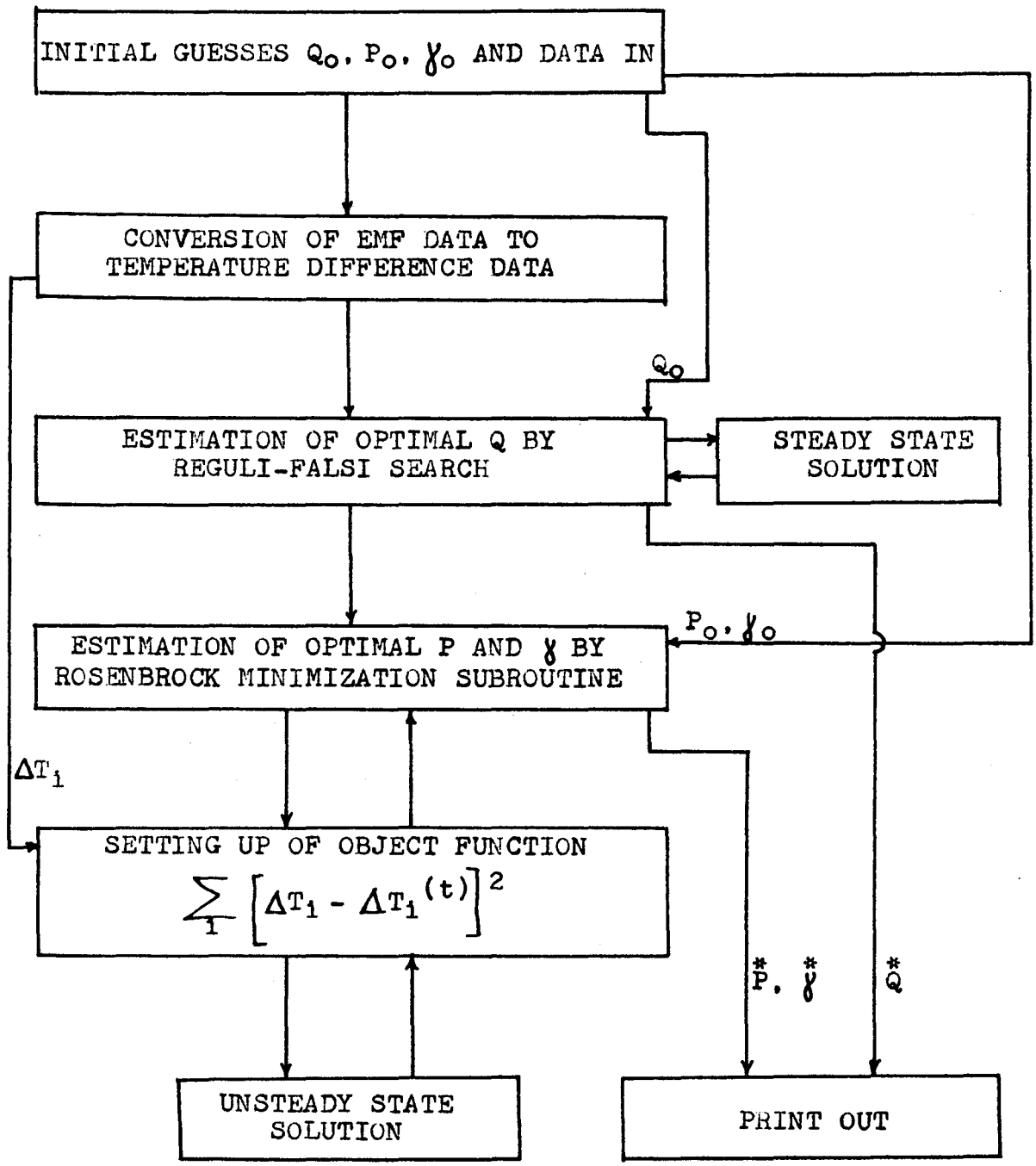

Fig. III-1

Algorithm of Parameter Estimation Programme

APPENDIX IV

THERMAL BALANCES AND DERIVED QUANTITIES

IV.1 JUSTIFICATIONS OF ASSUMPTIONS AND ERRORS

The instantaneous local heat flux is a function of the azimuthal, axial and time coordinates. Assuming that each point along the circumference experiences the same heat flux variation with time the dependence of the instantaneous point heat flux on the azimuthal coordinate is eliminated. Based on this assumption the time integral of the instantaneous point heat flux will be a function of the axial coordinate, i.e., exchanger length and symmetric with respect to tube axis.

For a heat flux distribution that is linear or has a small curvature over a ring-to-ring length the spatial average of the heat flux will lie on or very close to the mid-point of this region. This is the argument justifying assumption (b) in Sec. 4.4.

The justification of the third assumption in Sec. 4.4 results from the following argument: The average heat input rate over a ring-to-ring region for the experiments carried out was of the order of 8000 Btu/hr. Assuming a 10^{o}F temperature difference over a distance of 3 in. along the exchanger, the heat conducted along the wall would be:

$$\pi D_t \Delta r k \frac{\Delta T}{\Delta x} = (3.1)(\frac{7}{32})(\frac{1}{144})(220)(\frac{10}{3})(\frac{1}{12}) = 13.2 \text{ Btu/hr}$$

or percentage-wise

$$\frac{13.2}{8000} (100) = 0.16\%$$

of the heat input due to condensation. Therefore, the contribution to condensation because some of the heat is conducted to another ring is negligible and the condensate collected by one ring corresponds to the heat transferred over the section upstream of it.

The plug flow assumption was not based on evidence obtained in this investigation. It was based on the findings of Bott et al. (B9) with regard to axial dispersion.

The steam was found to have a superheat of about 15°F. The sensible heat of this superheat is about 0.7% of the heat of condensation. Because the superheat was negligible, it was tolerated as error, and the steam was considered saturated. It was further assumed that the condensate left the exchanger at saturation temperature. Heat loss experiments showed that very little heat was lost to the environment from the sections whose condensate was collected. This loss was also tolerated as error. Hence, the assumption of no heat loss. The errors arising from the superheat of steam and the heat loss should be included in the error of condensate collection.

The error in the condensate collection was estimated by reproducibility tests to have an average value of ±1.5%.

To this an error of ±1.5% was added to account for the heat loss, the conduction along the wall and the steam superheat, resulting in a total error for the heat input rates of ±3%. An error of ±1% was estimated for the mass flow rate. The error for the bulk liquid temperature increase across a ring-to-ring section would therefore be of the order of ±4%.

The accuracy of the coefficients obtained in this work varies from one location to another. This arises from the fact that the temperature difference between wall and liquid bulk temperature decreases substantially along the exchanger which results in increasing relative errors. The coefficients are most accurate at 4.5 in. from the top with a relative error of ±5% based on a ΔT error of ±1% and least accurate at 14.5 in. with a relative error of less than ±15% based on a ΔT error of about ±10%.

IV.2 CALCULATION PROCEDURE

Average heat input rates and heat fluxes over a ring-to-ring region were calculated from the condensate collected, the latent heat of vaporization, and the geometrical dimensions of the exchanger (See Fig. IV-1):

heat input rates:

$$\bar{q}_i = H_o W_i \qquad i = 1, 2, 3, 4, 6 \qquad \text{(IV-1)}$$

heat fluxes:

$$(\bar{q/A})_i = \frac{\bar{q}_i}{A_i} = \frac{\bar{q}_i}{\pi D \Delta x_i} \qquad i = 1,2,3,4,6 \qquad \text{(IV-2)}$$

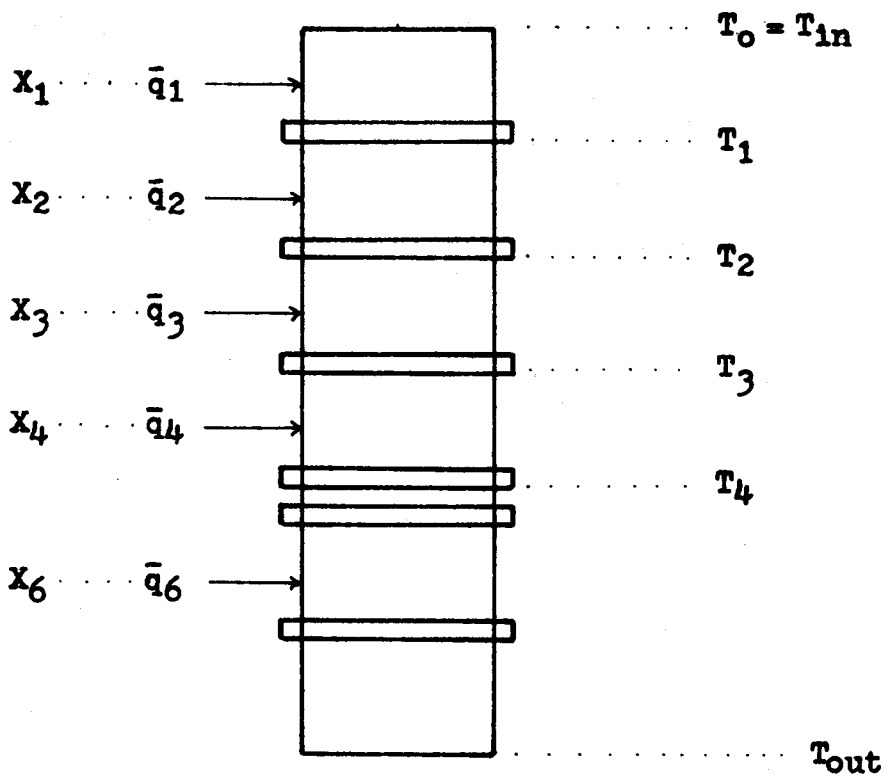

Fig. IV-1

Liquid Temperature Nomenclature

The temperature increase of the process liquid across a section was obtained from the heat input rate and the mass flow rate of the process liquid:

$$\Delta T_i^L = T_i^L - T_{i-1}^L = \frac{\bar{q}_i}{W_L} \qquad i = 1 \text{ to } 4 \qquad \text{(IV-3)}$$

The temperature profile resulted from Eq. (IV-4), and the inlet and outlet

$$T_i^L = T_{i-1}^L + \quad T_i^L \qquad i = 1 \text{ to } 4 \qquad \text{(IV-4)}$$

temperatures. To all the points but the one for the inlet temperature a quadratic least-square curve was fitted, from which the liquid bulk temperatures were obtained at the mid-points of regions 2, 3, 4 and 6, that is

$$T_i^l = A_o X_i^2 + A_1 X_i + A_2 \qquad i = 2,3,4,6 \qquad \text{(IV-5)}$$

The time-average local heat transfer coefficients resulted from Eq. (IV-6)

$$\bar{h}_i = \frac{(\overline{q/A})_i}{T_i^W - T_i^l} \qquad i = 2,3,4,6 \qquad \text{(IV-6)}$$

where T_i^W are the local wall temperatures taken as discussed in Sec. 5.2.

The local Nusselt $\left(Nu_i = \frac{h_i D_t}{k}\right)$ and rotary Reynolds $Re_{ri} = \left(\frac{D_t N^2 \rho}{\mu}\right)$ were evaluated at the same locations as the coefficients. The physical properties of the process liquid were taken at the local temperature, T_i^l, as given by Eq. (IV-5).

They were obtained from regression curves of the properties versus temperature. The data for the regression were taken from the literature (B10).

APPENDIX V

EXPERIMENTAL DIFFICULTIES

The main experimental difficulties in this investigation were the condensate collection and the construction of rugged heat-flux meters. The former presented the problem of mechanically separating the condensate from steam. Development work led to the collection system that is described in the main body of this thesis. The latter involved the construction of heat-flux meters whose electrical wiring would endure the experimental conditions. The development work to this end is detailed below.

Originally, twelve heat-flux meters of various thicknesses were made in the tube. Two constantan wires 0.005 in. diameter were soft-soldered in each of them. The recesses were filled with epoxy resin. After a short usage of the apparatus the heat-flux meter circuits failed. The apparatus, upon inspection, showed that the resin had not endured the steam temperature. It was assumed that the deterioration of the resin caused the breakdown of the wires. New wires were soft-soldered in the discs and Saureisen cement was used as insulating material. The same failure of the wires occurred; this failure again could be traced to the cement used. A silicone-rubber adhesive was tried next; although the life of the meters was longer, they did fail in

the end. Upon inspection, it was found that the adhesive plugs did not stick to the inner walls of the meter recess, although the rubber showed no deterioration in the steam environment. This problem was overcome by careful cleaning of the recess. The operation was repeated with one exception. Four of the twelve heat-flux meters were fitted with 0.015 in. diameter constantan wires. Again all meters failed. The heat-flux meters made with thick wires were carefully dug out and examined under a microscope. It was found that corrosion had eroded the soft-solder and the corrosion products insulated the wire from the copper disc. This led to the use of silver solder.

Four new heat-flux meters were made. The first time that silver-soldering was attempted the job was badly oxidized. The second time oxidation was reduced, but the job did not come up to temperature. The third time when the copper screen was used to remove oxygen in the incoming nitrogen oxidation was not observed at all and the wires were securely soldered in the disc. The repeated high temperature treatment of the tube was likely the cause of the following deformities:

(a) the disc of the heat flux meter I looked like it had been displaced to a few thousands of an inch from the inner surface of the shell, and

(b) the other heat-flux meters showed an inward buckling.

There was no remedy for the former. The latter was remedied by honing using fine grade emery paper on a wooden, tapered plug.

After rugged heat-flux meters had been constructed, some interesting observations were made. While the heat-flux-meter recesses were filled with the silicone rubber, what could be called "thermal inertia" effects were observed under step-changes in heat flux. These effects were attributed to the thermal capacity of the insulating material (H4). Thus the adhesive was eliminated and the metallic caps installed. This alteration remedied the inertial effects. The observations reported in this thesis were made with these heat-flux meters.